REGENERATIVE SUSPENSION SYSTEM MODELING AND CONTROL

A Dissertation

by

ABDULLAH AYEDH B. ALGETHAMI

Submitted to the Office of Graduate and Professional Studies of
Texas A&M University
in partial fulfillment of the requirements for the degree of

DOCTOR OF PHILOSOPHY

Chair of Committee,	Won-jong Kim
Committee Members,	Mehrdad Ehsani
	Alan Palazzolo
	Steve Suh
Head of Department,	Andreas A. Polycarpou

December 2017

Major Subject: Mechanical Engineering

ABSTRACT

Many energy indicators show an increase in the world's energy deficit. Demand for portable energy sources is growing and has increased the market for energy harvesters and regenerative systems. This work investigated the implementation of a regenerative suspension in a two-degree-of freedom (2-DOF) quarter-car suspension system. First, an active controller was designed and implemented. It showed 69% improvement in rider comfort and consumed 8 – 9 W of power to run the linear motor used in the experiment.

A regenerative suspension system was then designed to save the energy normally spent in active suspensions, approximately several kilowatts in an actual car. Regenerative suspension is preferable because it can regenerate energy. Experimental investigations were then conducted to find generator constants and damping coefficients. Additionally, generator damping effects and power regeneration in the quarter-car test bed were also investigated. The experiments showed that a linear regenerative damper can suppress up to 22% of vibrations and harvest 2% of the disturbance power. Since both harvesting and damping capabilities were noticeable in this test bed, it was used to implement regenerative suspension, and a regenerative controller was developed to provide riders with additional comfort.

To implement this regenerative controller, an electronic interface was designed to facilitate controlling the regenerative force and storing energy after the rectification process. The electronic interface used was a symmetrical-bridgeless boost converter (SBBC) due to its few components and even fewer control efforts. The converter was then

modeled in a manner that made the current and voltage in phase for the maximum power factor. The converter control allowed the motor's external load to be presented as of variable resistance with the unity power factor. The generator was then considered a voltage source for energy regeneration purposes.

The controller was designed to control regenerative force at a frequency of 20 kHz. This frequency was sufficient to enable another controller to manipulate the desired regenerative damping force, which was chosen to be 1 kHz. The input to this controller was the generator voltage used to determine the polarity of pulse-width modulation (PWM). Therefore, a combination of converter and controller was able to take the place of an active controller. A different controller was then designed to manipulate the desired damping force.

This regenerative controller was designed in a manner similar to that of a semi-active controller. It improved vibration suppression and enhanced harvesting capabilities. The regenerative suspension showed better results than a passive suspension. The improvements are minimal at this time, but there is the potential for greater improvement with a more efficient controller. The harvested energy was so small in this experiment because the damper was inefficient. In practice, the damper's efficiency should be improved. A regenerative damper will be more economical than a passive damper, and suppress more vibration at the same time. The active suspension system showed superior performance. Conversely, the regenerative system showed only modest performance but also regenerated energy. However, a regenerative suspension can be combined with an active suspension to enhance the rider's comfort and provide energy regeneration.

CONTRIBUTORS AND FUNDING SOURCES

I would sincerely like to thank my committee chair, Dr. Won-jong Kim, for being my mentor and providing valuable insights and guidance during every step of my research. I would also like to thank my committee members, Dr. Mehrdad Ehsani, Dr. Alan Palazzolo, and Dr. Steve Suh, for their help in completing this work. I am also grateful to Dr. Kim's former students, Mr. Rohit Chintala, Mr. Seungho Lee, Mr. Bryan Murphy, and Mr. Justin Allen, whose efforts helped to form the basis of this research. I would also like to thank my friends in the research lab who made my research experience so enjoyable. Last but not the least, I would like to thank my family for their tremendous support and love.

I would like to thank my Sponsor Taif University for the scholarship of my Ph.D study.

NOMENCLATURE

$R_{e,des}$	Desired Equivalent Resistance
i_i	Generator Current
$i_{i,Avg}$	Average Generator Current
v_i	Input Voltage
v_o	Output Voltage
x_s	Sprung Mass Displacement
$\dot{x}_s$	Sprung Mass Velocity
$\ddot{x}_s$	Sprung Mass Acceleration
z	Relative Displacement
$\dot{z}$	Relative Velocity
d	Duty-Ratio
d_c	Duty-Ratio used for converter control
d_{abc}	Duty-Ratio used for three- phase converter control
$\dot{x}_{us}$	Sprung Mass Velocity
$\ddot{x}_{us}$	Unsprung Mass Acceleration
R_e	Equivalent Resistance
F_{act}	Motor Force
F_d	Actuation/Regenerative Damping Force
M_s	Sprung Mass

M_{us}	Unsprung Mass
c_e	EM Damping Coefficient
c	Damping Coefficient

TABLE OF CONTENTS

Page

LIST OF FIGURES

Page

LIST OF TABLES

Page

CHAPTER I

INTRODUCTION TO REGENERATIVE SUSPENSIONS

1.1 Background

According to the Energy Information Administration, approximately 28% of all energy consumed in the United States goes to transportation [1]. A 70% increase in world energy demand is expected by 2050, as estimated by the International Energy Agency in 2014 [2]. It is assumed that global energy demand will increase by nearly one-third from 2013 to 2040. Energy indicators show that there continues to be an energy deficit in the world, with almost 1.1 billion people, approximately 15% of the world's population, still living without electricity [2]. Furthermore, there is an increased need for small, portable energy sources that can be used as energy harvesters. Long-term studies should be conducted that focus on control strategies and power electronics interface topologies that will improve energy utilization in these harvesters. Research has estimated that the amount of power lost in a car suspension system can reach 30% of the total power [3]. Most work on suspensions has dealt with energy estimation and the design of electromagnetic actuators. However, electronic power conversion and controlling systems require more investigation.

The field of regenerative vibration damping or, more specifically, the process of recovering energy from damped, vibrating systems is growing. This doctoral dissertation addresses the design and control of regenerative suspension systems. The results presented were tested in a quarter-car suspension testbed. The main research objective is to

determine the performance of regenerative damping in relation to vehicle suspension systems.

1.2 Review of Prior Art

1.2.1 Energy Dissipation and Suspension Systems

Energy harvesting captures and stores ambient energy, and then supplies it to a load. Ambient energy comes in various forms, such as mechanical, chemical, electromagnetic, and thermal. Converting energy from other sources to the electric form is one of the most prevalent harvesting methods. Energy in the mechanical form is found everywhere and of greater use than that gathered from other sources [4].

Mechanical energy is primarily derived from vibrations that occur in systems. There are a variety of sources of vibrational energy, such as ocean waves, movements in large structures, and even the motions of small microsystems. These all share the same common underlying principles and challenges. In one study conducted to harvest structural vibration energy using a linear electromagnetic (EM) damper connected with various circuits, several milliwatts were harvested while simultaneously damping the structure's vibrations [5]. In another study designed to harvest energy from human motion using a linear permanent magnet (PM) energy-harvesting device, the electric power of 674 mW was generated [6]. However, as yet there has been no study of the damping forces generated in the optimal harvesting case.

There are many subsystems in the automobile industry that harvest and reuse energy, such as regenerative braking. Suspension systems have the potential to be another such

energy source. A suspension system's main function is to stop vibrations from transferring to the rider. Traditionally, this energy is dissipated in the suspension system through a passive damper. The main function of a car's suspension system is to isolate the rider from road roughness. Historically, the damper wasted energy because of friction. Many previous studies investigated the amount of energy wasted in a car's suspension. Theoretical investigations have been carried out to analyze the mechanism supporting a vehicle's rolling resistance and dissipation [7]. In this survey, only the experimental investigation was documented.

Browne and Hamburg [8] concluded that the power of 40–60 W was dissipated in a test truck. The authors suggested that this small amount of energy could be stored and used for amenities not accessed on a regular basis, such as windshield wipers and defrosters. In a study using hybrid electric vehicles (EVs), the power of 68 W was harvested on a smooth road [9]. Other studies have estimated the power wasted by a suspension system to range from 100 to 400 W for medium-sized cars running at 60 mph [10]. An active damper achieves better vibration suppression than other types of dampers. This translates to a more comfortable ride, but it consumes a significant amount of energy. Previous studies indicated that a fully active suspension consumes 10% of the engine's power [3].

1.2.2 Electronic Interface

The literature on electronics is very rich. Therefore, a short survey of only the most pertinent pieces is listed below. Electric interfaces can have a number of functions, such

as rectifying AC signals to utilize the harvested power or store it for control purposes. Because most harvesters deal with small AC signals, these signals need to be boosted to the level of the storage voltage threshold. Numerous methods have been proposed to overcome this obstacle, such as the synchronous switching doubler deployed for energy harvesting applications [11]. This type of converter is used to step up the voltage without any capacitor or inductor, as shown in Figure 1. However, it is expensive to employ.

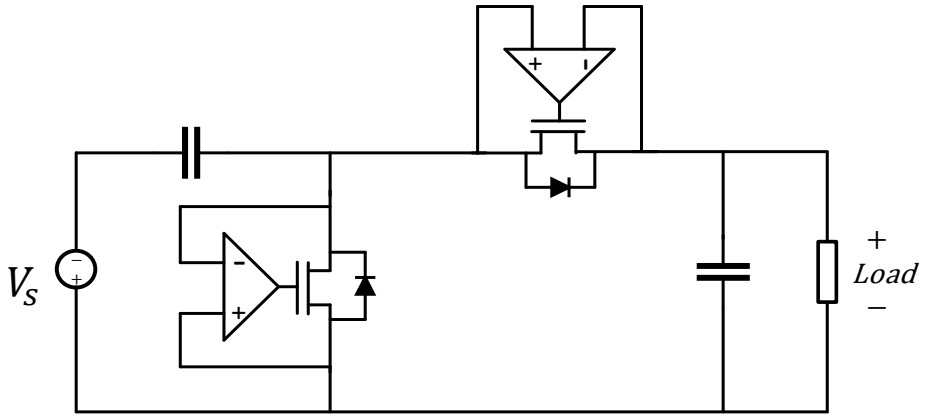

Figure 1. Synchronous voltage doubler [11].

Another voltage regulator, shown in Figure 2, uses hysteretic controls. A critical conduction mode is employed with an upper band so that the current can reach twice the level of the theoretical optimal current. The current's lower band is set to zero. This converter works well when the output voltage varies at frequencies lower than 60 Hz [12].

A buck-boost converter is commonly used to harvest energy. In this study, this type of converter was used with a cantilever-based piezoelectric harvester, as shown in Figure 3. The piezoelectric generator had limited output power. Therefore, a converter modeled in discontinuous mode (DCM) and at a fixed duty cycle was used to control the pulse-width

modulation (PWM) generator that drove the switch, so that the equivalent resistance of the buck-boost converter in DCM mode equaled that of the internal impedance of the piezoelectric generator. A buck-boost converter can be used for efficient maximum power extraction for input voltages ranging lower and possibly higher than the voltage of a battery load. Because of the limited power generated by the piezoelectric generator in the buck-boost design, the experimental results showed that the DC-DC converter efficiency was 64% [13].

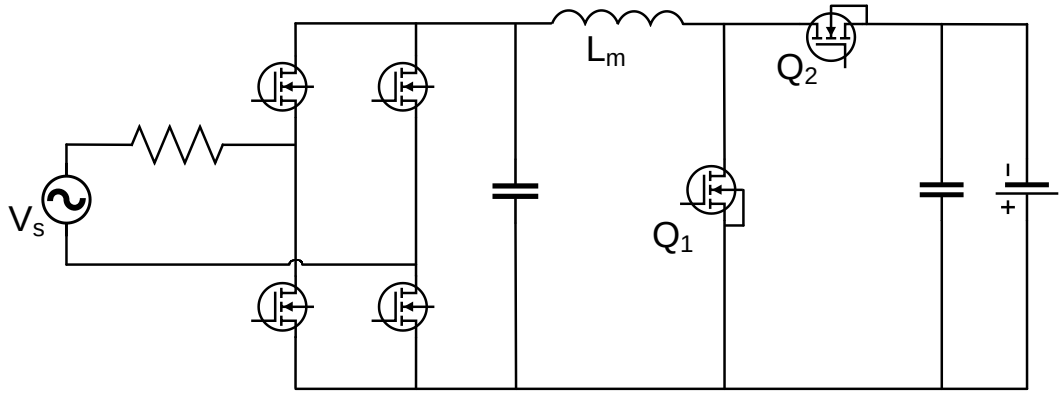

Figure 2. Synchronous boost converter [12].

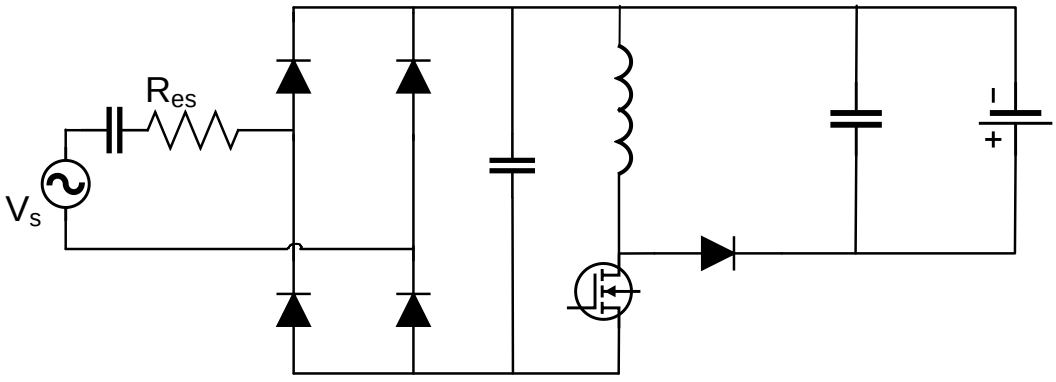

Figure 3. Buck-boost converter.

Another study examined a control piece for a self-tuning duty cycle proposed for a buck converter in DCM, as shown in Figure 4. This controller could vary the duty ratio to maximize the output power. The controller was tested with a piezoelectric generator, and maintained a maximum power transfer while slightly perturbing the duty cycle after the initial tracking [14].

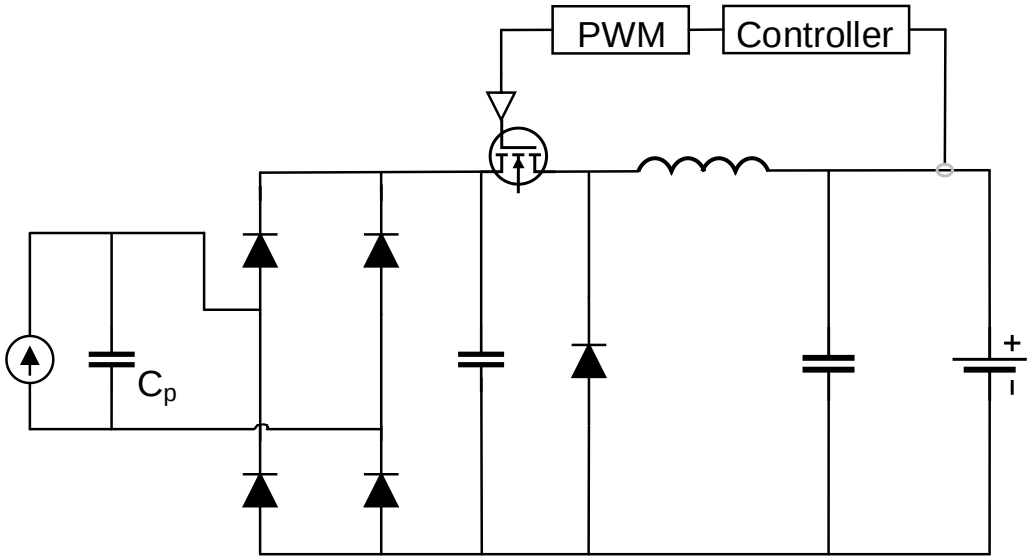

Figure 4. Buck converter with an adaptive controller.

The researchers in [15] proposed a converter that would achieve maximum output power for a linear generator, using a current control. This was deployed in an ocean wave energy harvester. The converter output voltage was fixed at 720 V. According to the simulation, the converter could extract maximum output power and follow a reference current. However, this design's hardware required more testing.

1.2.3 Literature Review of Regenerative Interfaces

A passive rectifier interface, as shown in Figure 5, does not need a controller. Rather, it has a fixed impedance so is not efficient for harvesting or damping.

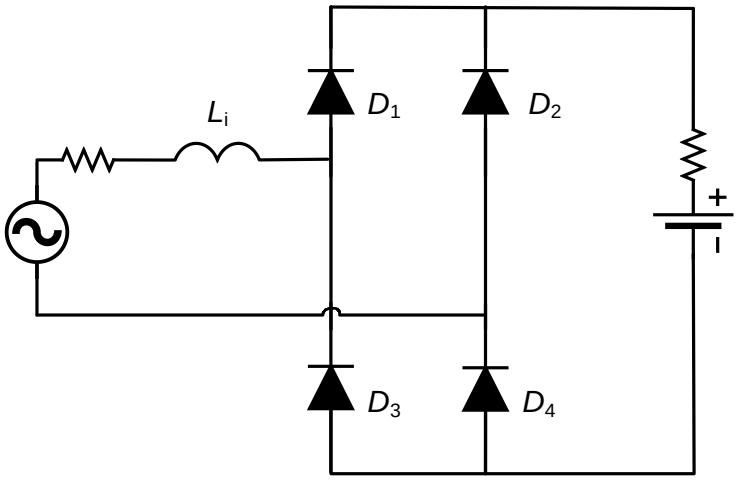

Figure 5. Passive rectifier interface.

In his doctoral dissertation, the author of [16] used a full-bridge boost converter (FBBC) in a continuous conduction mode (CCM) of operation (see Figure 6). He investigated FBBC topology for rectification and boosting. However, this topology required more control effort and a power driver for the two upper-half metal-oxide-semiconductor field-effect transistors (MOSFETs).

A diode rectifier was used as opposed to a synchronous rectifier to reduce control losses [17]. The unidirectional power converter was sufficient to implement static admittance (SA) and a performance-guaranteed (PG) controller, whereas linear quadratic Gaussian (LQG) controllers required bidirectional converters [18].

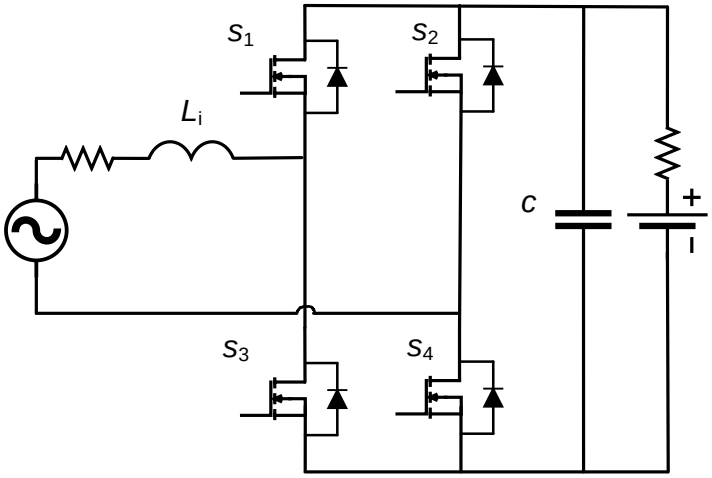

Figure 6. Full bridge boost converter (FBBC) for rectification and boost.

A symmetrical-bridgeless boost converter (SBBC) was used in [19] to develop a controller for pseudo-resistive behavior (see Figure 7). It showed promising performance, but should have been applied in a quarter-car suspension to check the performance with external disturbances. This topology was adapted for this work because it has the same specifications for the FBBC, without the effort required to control more than two MOSFETs. SBBCs are briefly discussed below, among other topologies in [20].

Buck-boost and FBBC converters, as shown in Figure 8, are commonly used in energy harvesting from structural vibrations [18]. However, in suspension systems the vibrations are at a higher frequency and much lower amplitude than in structures. Therefore, the voltage generated from automobile suspensions tends to be less and requires boosting to the level of car battery voltages.

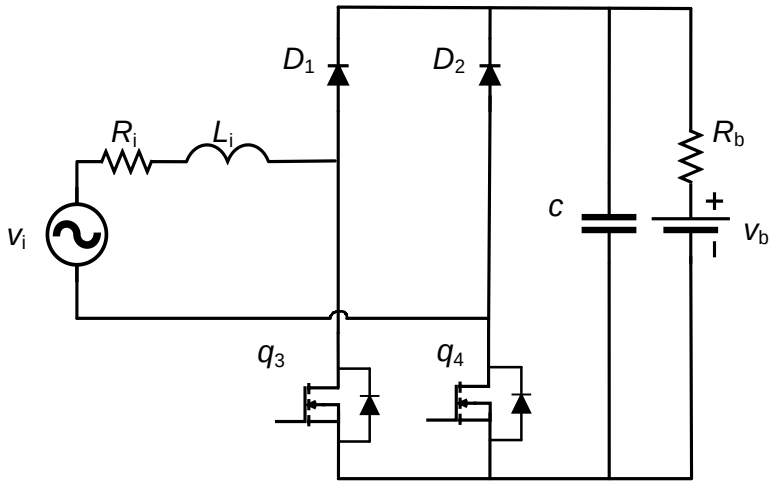

Figure 7. Symmetrical-bridgeless boost converter (SBBC).

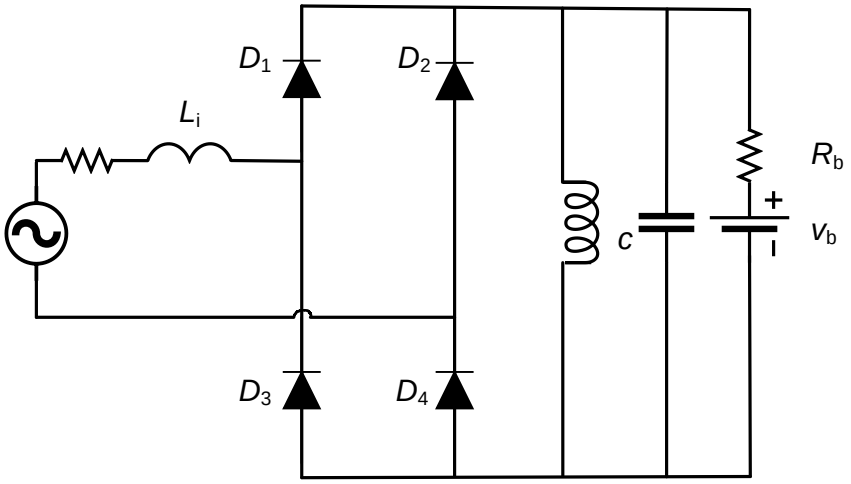

Figure 8. FBBC and buck boost used in a structural regenerative damper.

1.2.4 Types of Suspension Systems

This section provides an overview of suspension types and a short history of how these suspensions function, as well as more detail on regenerative suspensions. Suspensions are mechanical systems used mainly to suppress rider vibrations and maintain safe tire deflection. In other words, they act as low-pass filters used to attenuate road irregularities and roughness. They consist of spring and damping elements, as shown in Figure 9. The

springs or elastic elements carry static loads and store the potential energy input for the systems. Damper elements provide power dissipation through which dynamic energy such as heat is passed. The damper is a crucial factor in the dynamic transient behavior of a suspension system [21].

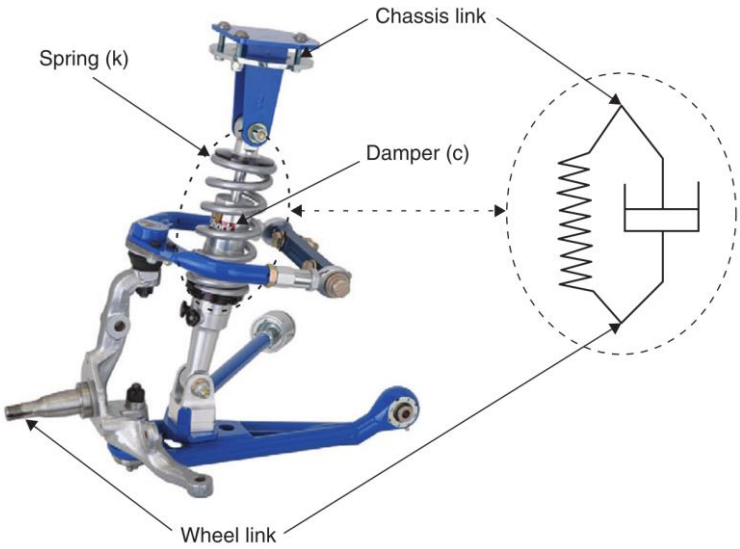

Figure 9. Suspension system [21].

At first, early vehicles were designed for low speeds, which meant there was no need for suspension systems. After the invention of an internal combustion engine, the spring suspension came into existence. Different springs were produced, such as with leaf or coil structures. Later, the independent suspension, which allows each wheel to vibrate vertically without connection to the other wheels, was adapted and implemented in vehicles. Due to advancements in electronics in 1960, online electronics-controlled suspensions were also investigated. The idea of a fully active suspension was attractive to automobile manufacturers.

Due to some disadvantages in active suspensions such as high cost, high power consumption, and certain safety issues, they have become unpopular in mass-market car production. By 1990, variable damping suspensions described as semi-active in the industry were developed as a best compromise between cost and performance [21]. Researchers continue to take an interest in using advanced technology to make suspensions safer and more energy efficient. Regenerative suspensions, for instance, have been in investigated and in continued development for more than two decades.

1.2.4.1 Passive suspensions

Passive suspensions are comprised of a spring (either leaf or coil) and a viscous damper. This type of suspension has the simplest structure and is of the lowest cost. Passive suspension parameters (k, c) are not tunable, which means that they can only be optimized for certain operating conditions. If the suspension is operated outside of this operating condition, the performance is degraded [21].

1.2.4.2 Semi-active suspensions

Semi-active suspensions are used in small, externally-powered machines to alter the damping coefficient. This coefficient changes according to road roughness. The damper is generally either an orifice or magnetorheological (MR) fluid-based damper. The orifice type can change the flow of oil by using an actuator to open or close a hole. MR-based suspensions depend on changing the fluid viscosity using a magnetic field. The semi-active form can generally achieve a reasonable level of performance and is fail safe. The

energy required to modify the hydraulic orifices and the fluid viscosity is low. However, it has limitations because the MR type can worsen over time and in the presence of high temperature. Also, this type can see some sealing leakage problems [21].

1.2.4.3 Active suspensions

An active suspension is much like a passive one in its elements, except the passive damper is replaced by an active element. This active element is an actuator (hydraulic, pneumatic, or electromechanical) used to input controlled force into the system. An active suspension requires an external source of energy. It relies on a closed-loop control with feedback signals. Active suspensions have outstanding performance compared with other types. However, they exhibit a high level of power consumption and are expensive. Figure 10 depicts typical models of the above three types of suspension systems [21].

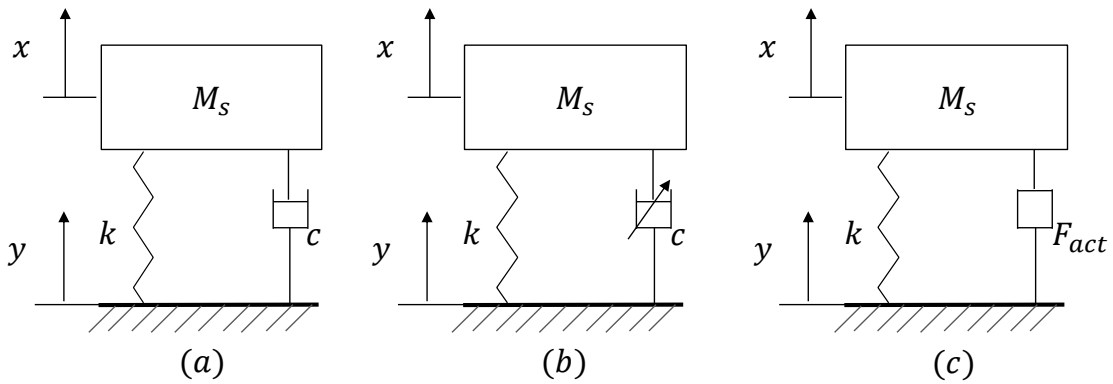

Figure 10. Model of different types of suspension: a) passive, b) semi-active, and c) active.

1.2.5 Regenerative Suspensions

Due to the increase in transportation-related energy consumption, the automobile industry is regularly looking for ways to become more fuel efficient. One outcome of this effort is the electric vehicle. Car manufacturers now consider power consumption to be one of the main product performance indices. Thus, the idea of recycling vehicle waste energy has attracted many researchers. Approximately 65% of a car's propulsion can be regenerated [22]. Road disturbances represent wasted energy in passive, semi-active, and active suspensions. Consequently, the principle of an energy regenerative suspension is key to restoring wasted energy for later use.

The level of regenerated energy is small, but the amount can still be useful since it can increase the car's overall efficiency. A regenerative shock absorber converts vibrations into useful energy such as electricity. This conversion uses either a linear or rotary motor instead of a linear damper. Below is provided a short survey of the work done to recover waste energy using regenerative suspension. There are many areas within the category of regenerative suspension studies. However, in this survey the following will be considered:

- Regenerative vibration systems
- EM dampers, both linear and rotary
- EM semi-active and active suspensions
- Self-powered active suspensions

Karnopp examined the feasibility of using a linear EM motor as a suspension dissipation element, wherein the gained energy was dissipated in internal (e.g., motor

coils) and external resistances [23]. In another study, rotary EM dampers and a skyhook control principle were used [24]. The concept of using a hybrid control has also been proposed, including using a regenerative active suspension with a linear DC actuator [25]. Other studies have suggested that regenerative suspensions should use linear DC motors [26-29]. Suda et al. [30] considered two linear motor mechanisms, using one as an actuator and the other as a generator. Martins et al. [31, 32] designed a prototype of a PM linear actuator and analyzed its dynamic performances at different excitation frequencies.

In Graves's dissertation [16], an electromagnetic damper was subjected to a sinusoidal disturbance within a 1-DOF dynamic system. The electromagnetic damper was connected to a tacho-generator and controlled via an interface card from a personal computer. A software algorithm converted the tacho-generator voltage into a duty cycle and polarity output signals. The scale of the testbed was small compared to a real suspension (the spring force was less than 100 N. The author used a full-bridge regenerative circuit due to the bidirectional damper velocity. However, a bidirectional feature was not used. The internal current conduction mode was assumed to be continuous, which is not always the case, especially with a small inductor. Although damping forces were estimated at various displacement amplitudes and frequencies, sprung mass acceleration was not shown. While a self-powered suspension system suppresses vibrations to a lesser extent than does an active suspension system, it is still better than a passive system. However, the consumption of a self-powered active suspension system was not shown [33].

The self-powered active suspension was improved by replacing the two motors with a single actuator. The actuator worked as a generator at high-frequency excitation and as a

motor at low-frequency excitation [33]. Linear and rotary motors were investigated experimentally on a small all-terrain vehicle [34, 35]. Also, a rotary DC motor with planetary gears and a ball crew used to convert linear motion was proposed to improve ride comfort without using any external power [36]. An EM damper is shown in Figure 11.

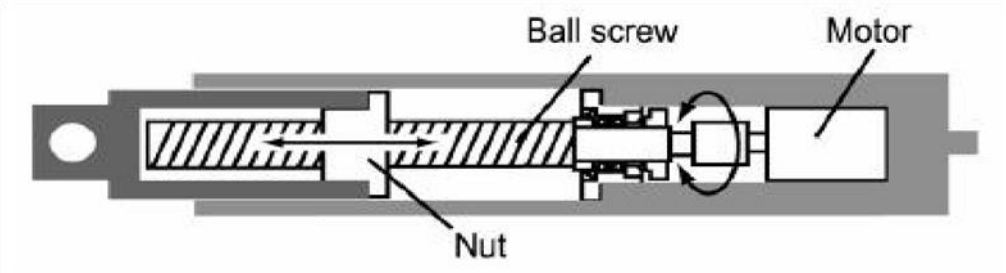

Figure 11. Electromagnetic (EM) damper using a ball screw and nut [37].

Jones introduced a system that included a linear electromagnetic actuator and power amplifier at each suspension as a means of reducing roll and forward dipping during braking [38]. An EM rotary damper was also shown to harvest more energy [39]. However, using the rotary EM damper increased the complexity of the system and was inefficient at high frequencies [40].

Another study used a linear AC actuator to regenerate energy using H_∞control [41]. The energy balance frequency characteristics of the regenerative actuator have also been analyzed [39]. The experimental verification was done in subsequent investigations [40, 42]. Wang et al. studied rotary damper equipment with a rack-pinion mechanism, as well as a linear generator [43]. Another study designed an EM damper and added a PM harvester [44]. The authors in [45] proposed using a linear EM damper as a regenerative

actuator, based on the eddy current effect. Another study estimated that 5% to 10% of a vehicle's power consumption could be restored by using a regenerative suspension employing a linear generator [46].

In his dissertation [47], Cassidy derived an analytical expression for generated average power. The forces required to move the motor were in the order of 100 N. This was much higher than the suspension forces. The realization of the converter, however, was not easy to reconfigure. In a different study carried out to retrofit a regenerative shock absorber using a rotary PM generator and rack-and-pinion mechanism, the average power of 19 W was harvested when the vehicle was driven at 30 mph [48], as illustrated in Figure 12.

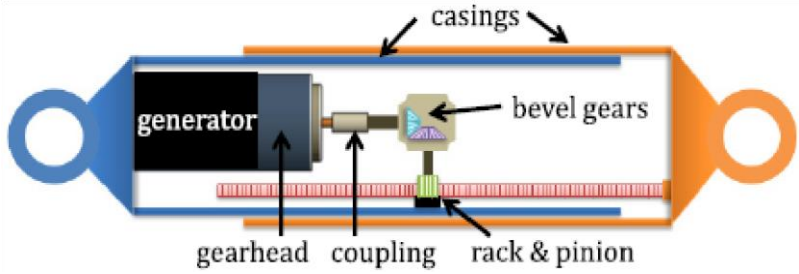

Figure 12. EM shock absorber using a rack-and-pinion mechanism [48].

Another study also examined self-powered active suspension systems [49]. The results showed that the system required zero external power. However, the excitation only used sinusoidal waves. An algebraic screw mechanism was designed in [50] and tested with a rotary motor. This design showed a high level of efficiency in the motion conversion. To use a rotary motor, the linear motion had to be converted into rotational motion. Various motion converters with different efficiencies were used in the literature, such as rack-and-

pinion and ball-screw. In a recent study, an improvement was made in the efficiency of motion conversion by using a two-leg rotary-to-linear mechanism [51].

1.2.6 Literature Review of Regenerative Control

Regenerative control is similar in structure to semi-active suspensions. The following survey was conducted to investigate the various control strategies that can be implemented into a regenerative controller.

A skyhook damper control algorithm was proposed for a vehicle suspension in one of the first examinations of semi-active control [52]. The author verified that the skyhook offered improved performance over a passive system when applied with a single degree of freedom. The skyhook control used a fictional damper connected to an inertial reference line, as shown in Figure 13. This damper was realizable by a feedback-closed-loop control, as illustrated in Figure 14.

The control law used was as follows:

$$F_d = \begin{cases} b\,\dot{x} & \dot{x}\,(\dot{x} - \dot{x}_o) \geq 0 \\ 0 & \dot{x}\,(\dot{x} - \dot{x}_o) < 0 \end{cases} \quad (1)$$

Another author used a skyhook controller with a semi-active suspension [24] (see Figure 15). This type of controller could also be used for a regenerative suspension. The idea of a hybrid suspension, as shown in Figure 16, was introduced in [25]. However, some obstacles were found with regards to this type of system, especially in regenerative mode, due to the small amount of harvested energy and power-electronic converter. The suggestion of a hybrid suspension was tested numerically in [53]. The author proposed a control law and compared it to other controllers.

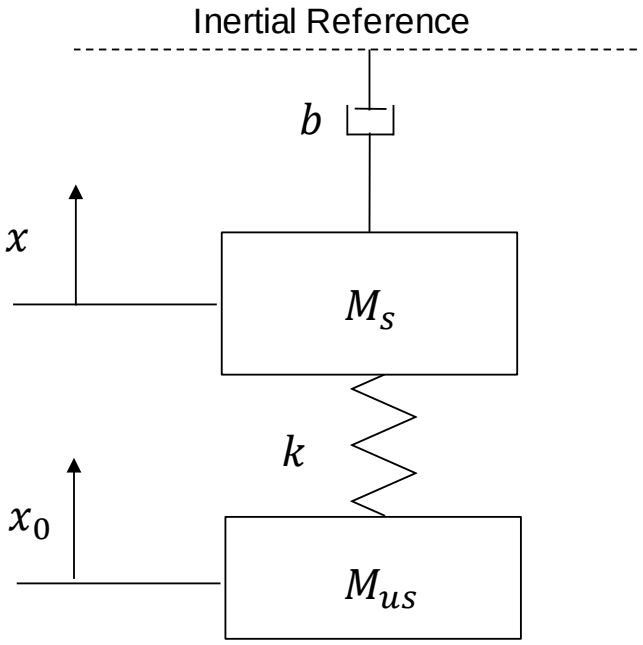

Figure 13. Skyhook control strategy [52].

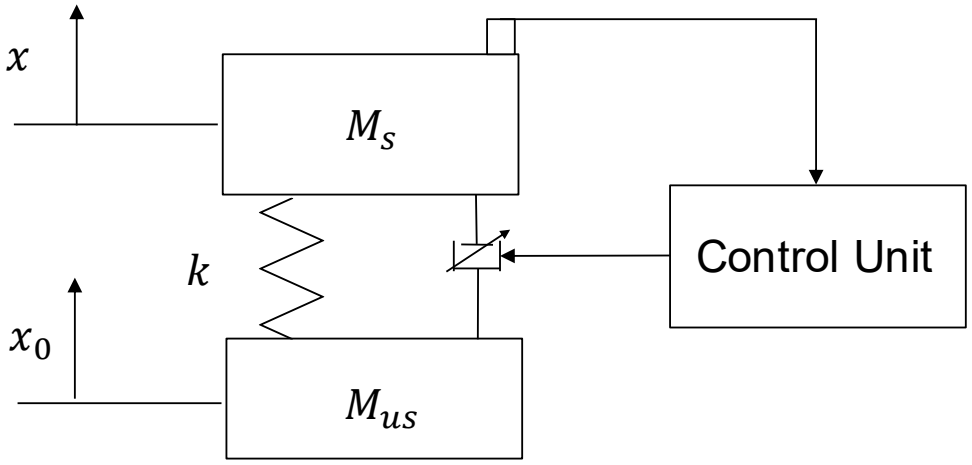

Figure 14. Skyhook control strategy layout [52].

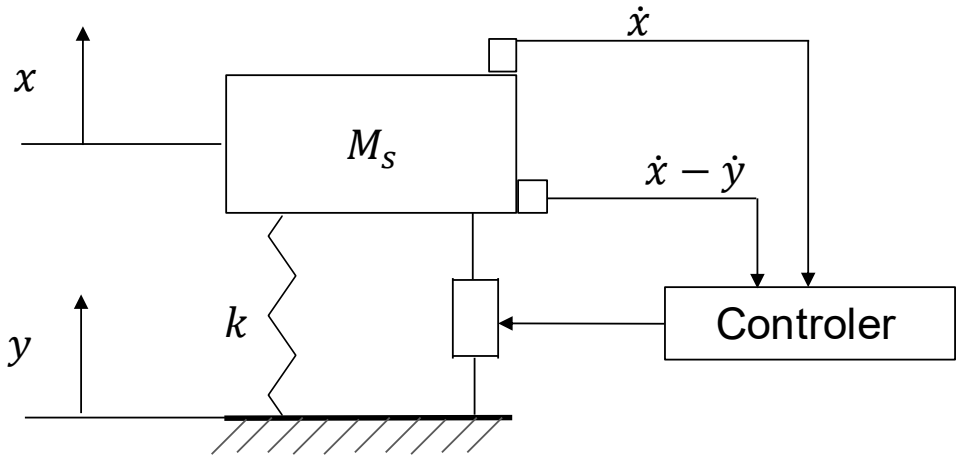

Figure 15. Skyhook control scheme used in a semi-active suspension [24].

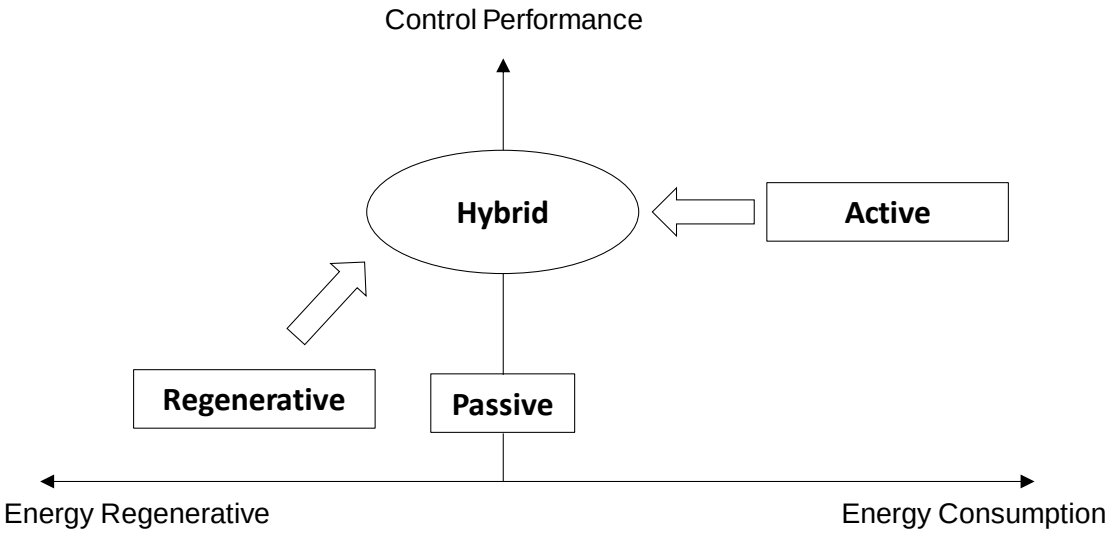

Figure 16. Hybrid suspension proposed by Rebya [25].

Another author who investigated a hybrid control strategy was Okada [29]. He applied an active controller at low frequencies; at high frequencies, the regenerative mode was applied. The controller switched between these modes by checking the induced voltages with the battery voltages. At high frequencies, the induced voltage was greater than the

battery voltage. Thus, the system was in regeneration mode. They reported some disagreement between the experimental and numerical results, which could have been due to the low-efficiency actuator and mechanical relays used in the experiments.

In [29], a combination of groundhooks and skyhooks were implemented, as shown in Figure 17. The skyhooks achieved a better ride with regards to comfort whereas the ground hooks ensured tire-ground contact for improved rider safety. In other research [54], one author followed previous numerical studies [37, 54] for the skyhooks and ground hooks. The simulation results demonstrated that the designed active suspension had the desired performance and energy could be regenerated from road excitation.

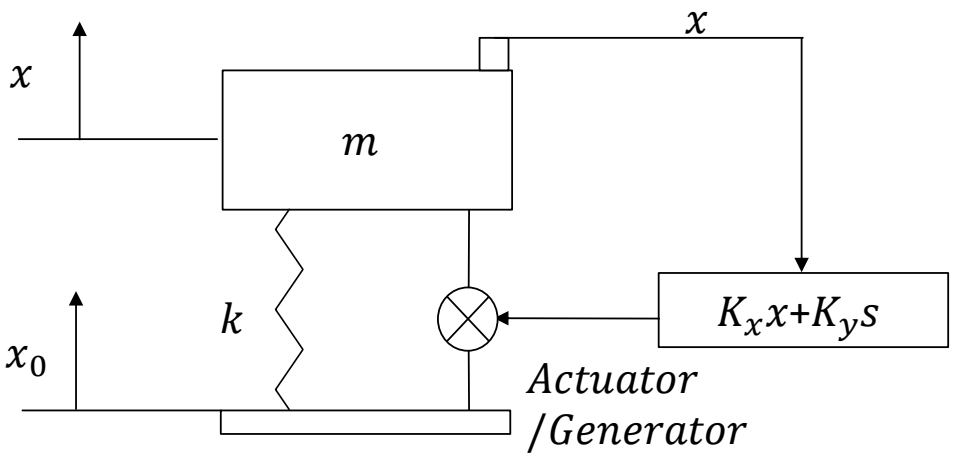

Figure 17. Skyhook control used to control 1-DOF suspension system [29].

1.3 Motivation

Thus far, research in this area has explored the possibility of power recovery from suspension systems. It has lacked a systematic method of actively tuning the system

parameters to achieve the optimum dynamic control or power recovery. Therefore, developing an analytical solution for optimizing system performance metrics is key to the design of efficient energy-harvesting suspension systems.

As noted in the above literature review, the areas in need of further research can be categorized into two main groups. First, improvements to the linear actuator design or redesign of the suspension system to better adopt a rotary motor and minimize drawbacks to the behavior of the system, and second, advancements to the power electronics interface. The controller must also be further developed and tested, and additional work is needed on implementing the regenerative system either in a testbed or real suspension system.

As noted in the above literature review, the areas in need of further research can be categorized into two main groups: improvements either to the actuators or the power electronics interface. Assuming that there is no unsolvable problem related to the regenerative actuators, this research focused on implementing the regenerative system computer model into a testbed.

1.4 Objectives

The objectives for this dissertation were as follows:

- Modeling of a suspension system. The quarter-car testbed used in this research consisted of a mass-spring damper system, linear EM generator, and power electronics converter. These components were all modeled and analyzed. The numerical results were then compared with the experimental results.

- Since the quarter-car suspension system is commonly used in experiments, the results from active, passive, and regenerative systems had to be used to compare the rider comfort indices of those modes. The harvestable energy and the damping capability of regenerative suspensions were then estimated and analyzed.
- Design and implementation of a regenerative power electronic interface. A simple and efficient converter was designed and implemented in the testbed to develop a regenerative controller. This controller was expected to handle the suspension and harvesting objectives.

Designs for the powered electronics and controller structure is a focus. A regenerative controller needed to be developed to replace the active controller. This replacement, though, came at the cost of reducing controller forces. However, a regenerative controller was used to increase the damping efficiency and harvested power.

1.5 Significance of the Contributions

This work dealt primarily with regenerative suspension modeling and control. The 2-DOF quarter-car suspension commonly used for active and semi-active suspension design and analysis was also used in this numerical and experimental investigation. Other recent studies of this topic used 1-DOF quarter-car suspensions, simplifying the dynamic. The 2-DOF suspension, though, afforded more realistic comparisons among automobile suspensions.

In this study, a linear motor was employed that could lead to further development of regenerative suspension modeling and control. In contrast, most of other studies of this

subject have dealt with rotary actuators. A rotary motor increases the time constant of the system, thereby reducing the bandwidth. However, this research lays out some of the most important aspects of a regenerative suspension, which will be useful when designing more efficient suspension systems. Increasing a suspension's working space could increase the linear motor efficiency in damping and energy regeneration. Such an increase would also improve the relative displacement range, which in turn should lead to an increase in energy regeneration and be used to design larger linear dampers.

The regenerative system was simulated numerically and physically in the quarter-car testbed experiment. The energy consumption and regeneration estimations will be useful in designing real suspension systems. These data could also be useful when designing more efficient four-quadrant rectifiers for hybrid suspension and hybrid controller design. In this work, two controllers were implemented. The first was at a high frequency for the converter. The second manipulated the desired value for the converter control. The latter was at a higher frequency than the disturbance frequency, but was much slower than the converter's switching frequency.

1.6 Dissertation Outline

In Chapter 1, a brief background of types of vehicle-suspension systems are introduced. A literature review of related research results on vehicle suspension systems is also discussed. Specifically, in this chapter various types of regenerative suspensions are considered and compared.

In Chapter 2, the car suspension system represented by the quarter-car testbed is modeled and the test rig construction used in the experiment is presented. An active controller is also designed and implemented in the testbed, and the capabilities of the regenerative suspension system are investigated. Finally, an initial study of a process for converting the system to a regeneration suspension is presented.

In Chapter 3, the regenerative interface requirements are investigated. Then, a short survey of the types of regenerative interfaces in existence are presented. Next, the operation and modeling of a boost converter are discussed. An SBBC is then further investigated and adopted in this work. Then, a controller is designed to manipulate the EM damper current. Finally, the experimental results are presented and compared with the simulation results.

In Chapter 4, regenerative suspension model is once again discussed in order to consider the regenerative interface analyzed in the previous chapter. A literature survey for the regenerative suspension controller is then presented. Next, a control law for the regenerative suspension is offered. The application of this controller in the test-bed is then considered and compared with the simulation results. Finally, the apparatus used in the experiment is shown.

In Chapter 5, the results of the various types of suspensions (active, passive, and regenerative) are summarized. The conclusions of this research are stated, and future work is discussed.

CHAPTER II

ANALYSIS OF THE QUARTER-CAR SUSPENSION SYSTEM*

2.1 Introduction

This chapter provides an analysis of a 2-DOF suspension system. The main goal was to estimate the harvestable energy and damping capability of the 2-DOF suspension system model. For both of these objectives, the numerical estimates experimental results were compared.

Active suspension has been the topic of many studies since the late 1970s. The main issues addressed have primarily advanced the controller or reduced energy consumption. Active suspension is briefly considered in the sections that follow. The same linear actuator was used to passively damp the vibrations. The consumed regenerated energy was then estimated. The data will be discussed in later chapters in relation to the design and control of regenerative suspension.

2.2 Quarter-Car Suspension Modeling

A car suspension system was modeled as a 2-DOF mass-spring damper system. Road roughness was the disturbance input into the system x_r. The stator of the motor was fixed

---

* Reprinted with permission from "Energy Harvesting and Damping Capability of Quarter-Car Test Bed," by Abdullah Algethami and Won-jong Kim, ASME 2016 Dynamic Systems and Control Conference, ISBN 978-0-7918-5069-5. Copyright 2016 by ASME

to the sprung mass. The system variables are summarized in Table 1. The experimental setup is shown in Figure 18 and modeled as in Figure 19. The system motion is described by Eqs. (2) and (3), and $\dot{z}$ is the relative velocity. This linear model is capturing to the quarter-car suspension dynamics [55, 56]. The system has the natural frequency around 3.5 Hz which should be attenuated to improve the rider comfort. The quarter-car suspension captures the main aspect of the real suspension. The damping force F_d is the force provided by the motor in active controller or by the generator in the passive and regenerative controllers.

$$M_s\ddot{x}_s + c\dot{z} + k(x_s - x_{us}) - F_d = 0 \tag{2}$$

$$M_{us}\ddot{x}_{us} - c\dot{z} - k(x_s - x_{us}) + F_d + c_w\dot{x}_{us} + k_w x_{us} = c_w\dot{x}_r + k_w x_r \tag{3}$$

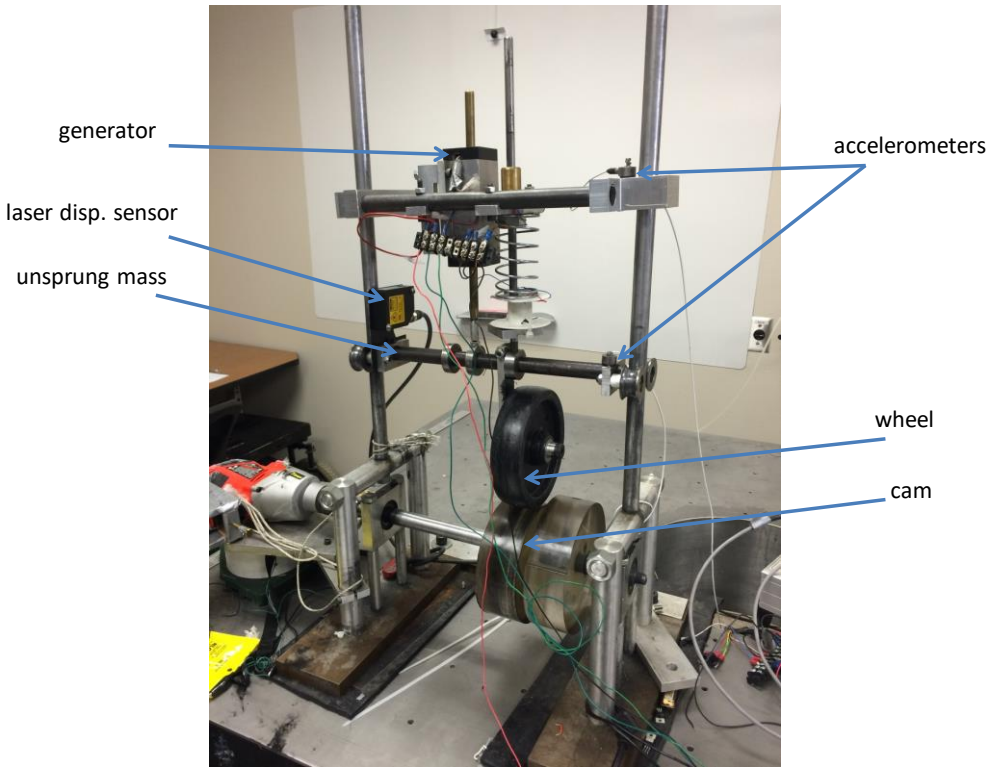

Figure 18. Quarter-car testbed.

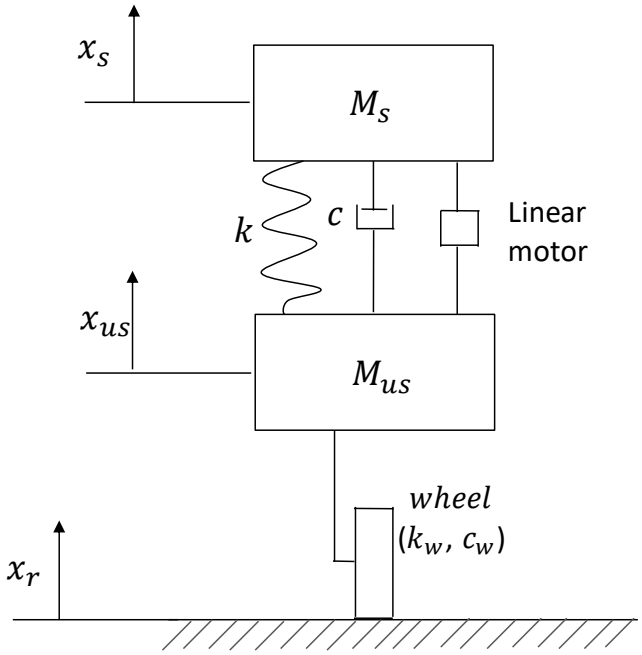

Figure 19. Quarter-car active suspension model.

Table 1. System Parameters [56]

Parameter	Value
M_s	2.34 kg
M_{us}	2.27 kg
c	50 N-s/m
c_w	50 N-s/m
k	1310 N/m
k_w	10000 N/m

The system could be represented by the following:

$$\begin{bmatrix} \ddot{x}_s \\ \ddot{x}_{us} \\ \dot{x}_s - \dot{x}_{us} \\ \dot{x}_{us} - \dot{x}_r \end{bmatrix} = \begin{bmatrix} 0 & 0 & \frac{-k}{M_s} & 0 \\ 0 & \frac{-c_w}{M_{us}} & \frac{k}{M_{us}} & \frac{-k_w}{M_{us}} \\ 1 & -1 & 0 & 0 \\ 0 & 1 & 0 & 0 \end{bmatrix} \begin{bmatrix} \dot{x}_s \\ \dot{x}_{us} \\ x_s - x_{us} \\ x_{us} - x_r \end{bmatrix} + \begin{bmatrix} \frac{1}{M_s} & 0 \\ \frac{-1}{M_{us}} & 0 \\ 0 & 0 \\ 0 & -1 \end{bmatrix} \begin{bmatrix} F_d \\ \dot{x}_r \end{bmatrix} \quad (4)$$

2.3 Application of Active Suspension Controllers in the Testbed

The main function of an automobile suspension system is to attenuate vibrations. There are many control configurations that help to make a ride more comfortable. Active control has provided promising results although it tends to be expensive and increase a vehicle's energy consumption. Figure 18 depicts the experimental setup constructed by Allen [56], including labels of the main components.

2.3.1 Active Suspension Apparatuses

The linear motor was first designed and built by Bryan Murphy [57]. It is comprised of a linear brushless permanent-magnet motor (LBPMM) with a tubular linear actuator. In this research, when given a maximum current of 3 A across each of the three sets of coils, the LBPMM could produce 26 N force. Three Model 12A8K PWM amplifiers made by Advanced Motion Controls managed the current passing through the coils. Each amplifier was capable of continuously outputting ±6 A. The amplifiers were supplied by a Lambda Electronics Model LZS-250-3 regulated power supply.

Two piezoelectric accelerometers (Piezotronics Model 336B18) were used to measure the sprung and unsprung mass accelerations. The accelerometers had a frequency range of 0.5 to 3,000 Hz, with a gain factor of 10.28 mV/g. The outputs of these accelerometers went to the signal conditioner (PCB Model 482A22), which provided power to the accelerometers and produced output voltage in the range of ±10 V, depending on the input.

The Linear Variable Differential Transformer (LVDT) was a Schaevitz Part #02560995-000, Model 4000 DC-SE, with a travel range of 10 cm. The analog output

swing was 0 to 5 VDC. A conditioning circuit was used to shift the output range of the LVDT (0–5 VDC) to match the input range of the A/D channels of the dSPACE DS1104 (± 10 V).

The DS1104 was specially designed for the development of high-speed multivariable digital controllers and has real-time applications in various fields. In this research, it was a standard board that could be plugged in to the PCI slot of a PC.

2.3.2 Active Suspension Controller

The suspension system was modeled as two masses and one wheel (Eqs. (2) and (3)). The plant transfer function $\dot{x}_s$ to F_{act} could be obtain from Eq. (5). Refer to Eq. (6) for the disturbance to $\dot{x}_s$ transfer function:

$$G = \frac{\dot{x}_s(s)}{F_d(s)} = \frac{5.078\,s^2 + 15\,s + 3500}{6.378\,s^4 + 128.3\,s^3 + 14320\,s^2 + 72100\,s + 2940000} \quad (5)$$

$$G_w = \frac{\dot{x}_s(s)}{\dot{x}_r(s)} = \frac{2466000}{6.378\,s^4 + 128.3\,s^3 + 14320\,s^2 + 72100\,s + 2940000} \quad (6)$$

The objective of the active controller was to attenuate the disturbance in a frequency ranging between 10 and 100 rad/s, and to keep the unsprung-mass bounded. A block diagram for the active suspension controller is shown in Figure 20. The following compensator was used to achieve the desired performance:

$$C = \frac{400(s+100)(s+60)(s+3)}{(s+80)(s+90)(s+0.5)} \tag{7}$$

The lag compensator ($(s+3)/(s+0.5)$) needed to improve the system disturbance attenuation at low frequency. The second compensator, lead compensator ($(s+60)/(s+90)$) will keep the required actuator force within the limit. Finally, lag compensator ($(s+100)/(s+80)$) need to attenuate any high frequency disturbance.

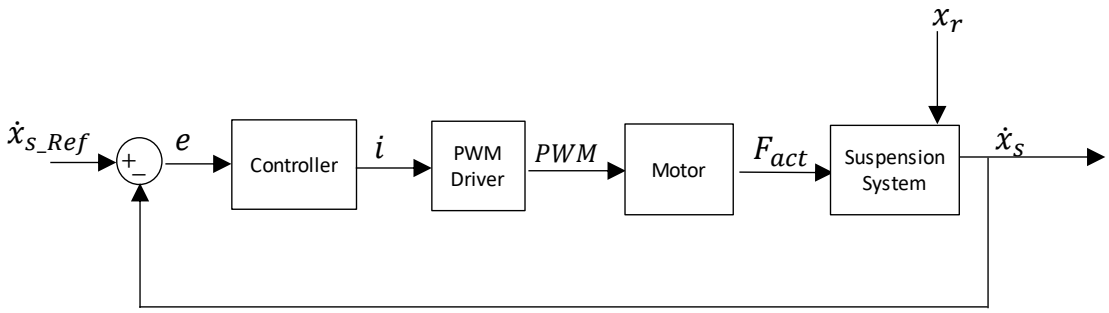

Figure 20. Block diagram of the active suspension control.

A Bode plot of the compensated (CG) and transfer function is shown in Figure 21. The relative velocities with and without the controller are shown in Figure 22. The current used to drive the linear motor is shown in Figure 23.

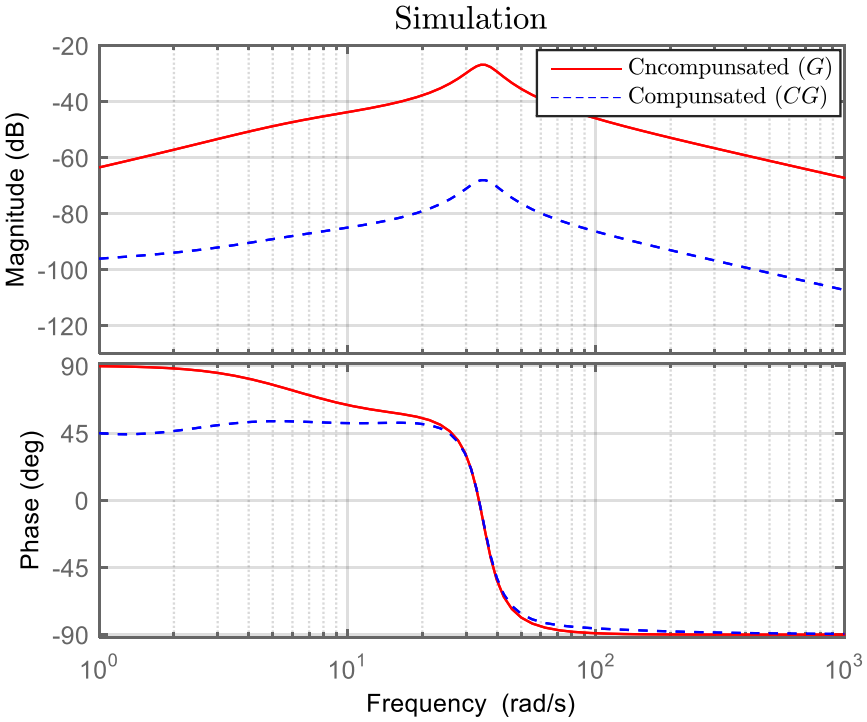

Figure 21. Bode plot of the plant and compensated transfer function.

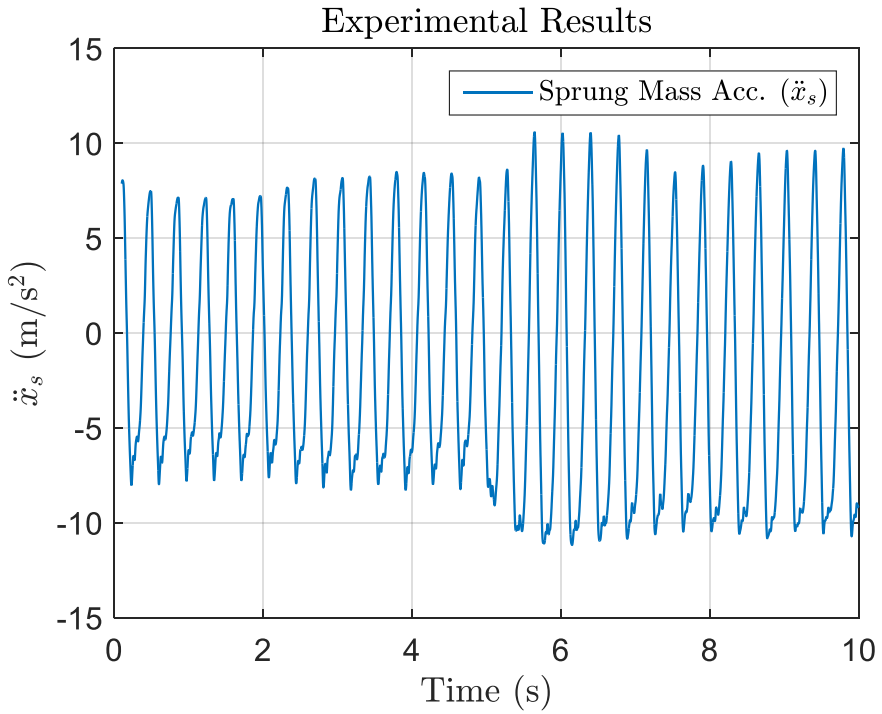

Figure 22. Spring mass acceleration without and with the controller.

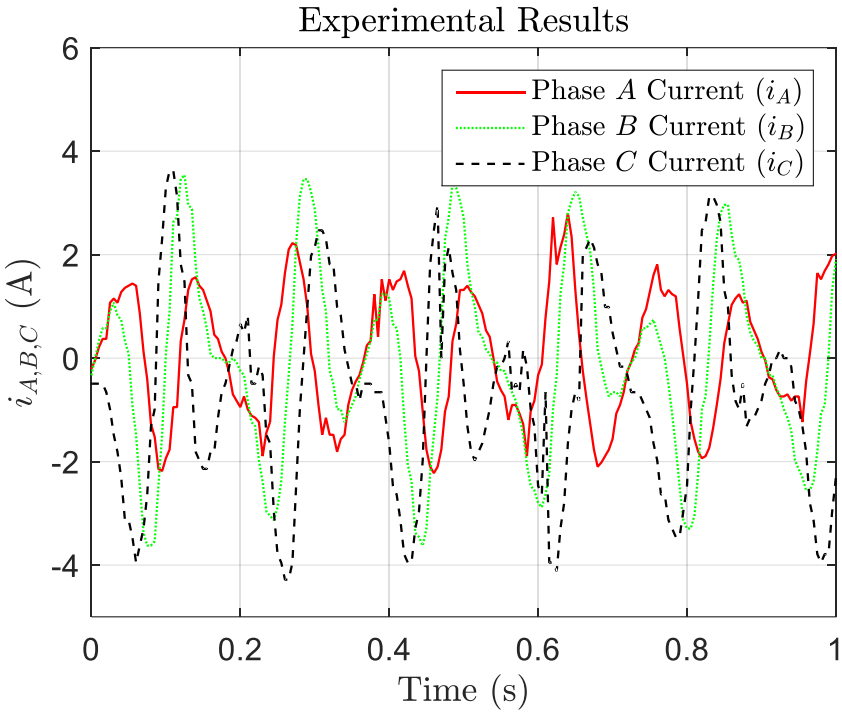

Figure 23. Three-phase current consumed by the controller.

2.3.3 Active Suspension Vibration Suppression and Power Consumption

Active suspension tends to achieve better performance than other methods but consume more energy. In order to compare their performance with that of the regenerative method, the powewas estimated from previous work by using the testbed shown in Table 2. In this research, a different controller was used to suppress vibrations. The motor was supplied by external power to produce the thrust force. The active suspension system suppressed vibrations by 58% to 69% in the performance index whereas the regenerative system suppressed vibrations by only 22%. However, the regenerative method consumed no power. Because the internal resistances of the generator's three phases were equal, the levels of consumed power were identical. The total power consumption for the entire three

phases (*A*, *B*, and *C*) reached around 8.4 to 9 W. The generator's power was calculated by the internal resistance and current flown. While the active suspension system performed three times better than the regenerative one, the active suspension consumed 8 W in order to isolate the rider; the input power was estimated 5 W.

Table 2. Active Control Results and Power Consumption per Phase [55]

Controller	Performance index	Current (A) per phase	Power (W) per phase
Modified lag-lead-lag	67%	1.26	2.8
LQ servo	58%	1.33	3
Fuzzy	69%	1.24	2.8

2.4 Motor/Generator Analysis

The three-phase linear direct-drive tubular linear brushless permanent-magnet motor (LBPMM) has a 10 cm travel range and a 26 N maximum force [57]. Previously, it has been used in an active suspension control that achieved a 69% reduction in sprung mass vibration [55]. However, in this experiment it was used as a generator. The motor construction is shown in Figure 24. The generator constants were evaluated experimentally in a steady-state condition. We assume that the force and voltage constants (K_a, K_b and K_c) are equal in each phase.

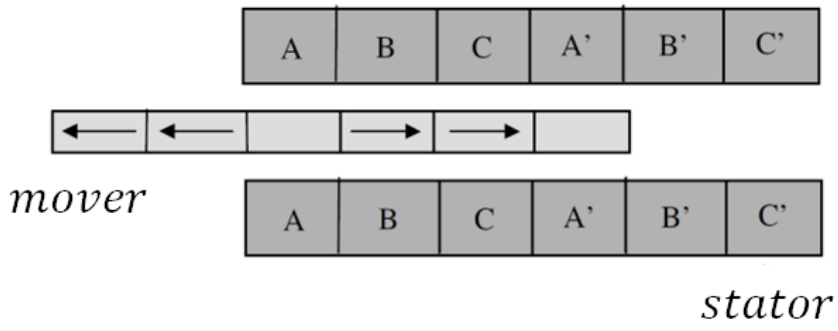

Figure 24. Motor construction.

The three induced phase voltages are:

$$V_a = K_a \sin\left(\frac{2\pi z}{l}\right)\dot{z}$$

$$V_b = K_b \sin\left(\frac{2\pi z}{l} - \frac{2\pi}{3}\right)\dot{z} \tag{8}$$

$$V_c = K_c \sin\left(\frac{2\pi z}{l} + \frac{2\pi}{3}\right)\dot{z}$$

The electromagnetic damping forces generated are:

$$F_a = K_a \sin\left(\frac{2\pi z}{l}\right) i_a$$

$$F_b = K_b \sin\left(\frac{2\pi z}{l} - \frac{2\pi}{3}\right) i_b \tag{9}$$

$$F_c = K_c \sin\left(\frac{2\pi z}{l} + \frac{2\pi}{3}\right) i_c$$

If R_o is the load resistance, R_i is the internal resistance, and V_p is the voltage across one phase, the phase current is:

$$i_p = \frac{V_p}{R_i + R_o} \tag{10}$$

To estimate the generator constants (K_a, K_b and K_c) experimentally, Eq. (8) was used by inputting sinusoidal relative displacement z and measuring the output phase voltages (as shown in Figure 25). The results are shown in Table 3. A Y-configuration was used to

connect the generator's three phases. The pitch of the motor was (l) and the frequency was $\omega = \frac{2\pi \dot{z}}{l}$.

By substituting Eqs. (8) and (10) into Eq. (9), the EM damping coefficient (c_e) could be obtained by Eq. (11). This equation was confirmed by the step response described in the following section.

$$c_e = \frac{{k_a}^2}{R_i + R_o} \tag{11}$$

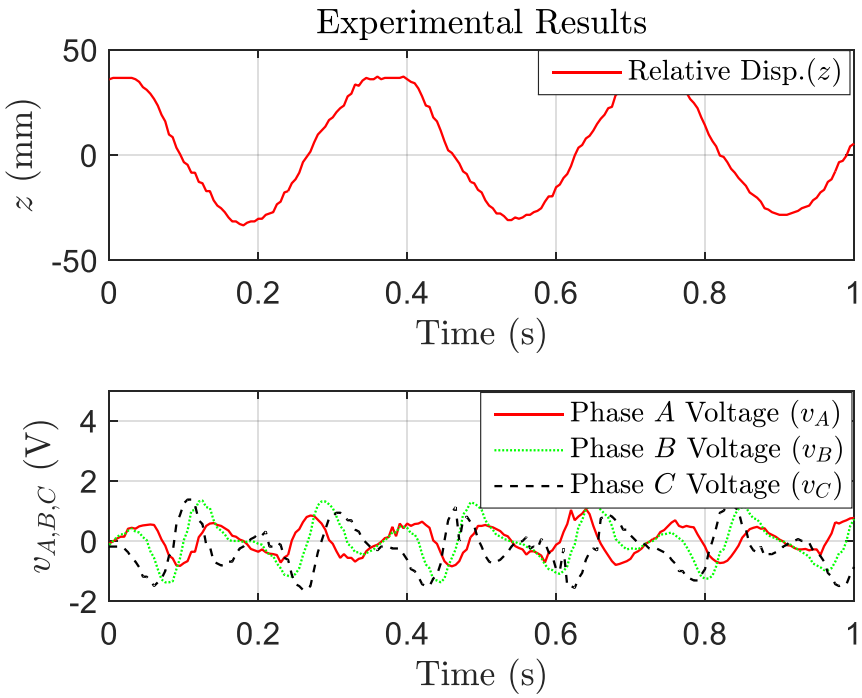

Figure 25. Displacement and output voltages used to estimate the motor constants.

The induced voltage was estimated by using the previous model to measure the relative velocity. In Figure 26, the induced voltage from the model is compared with the induced

voltage from the experiment. The model was able to produce a voltage close to that of the experiment. Both results were obtained by moving the mover at the same speed.

Table 3. Motor Parameters

Parameter	Value
K_a	1.42 N/A
K_b	2.05 N/A
K_c	2.01 N/A
l	63.3 mm
R_i	1.565 Ω

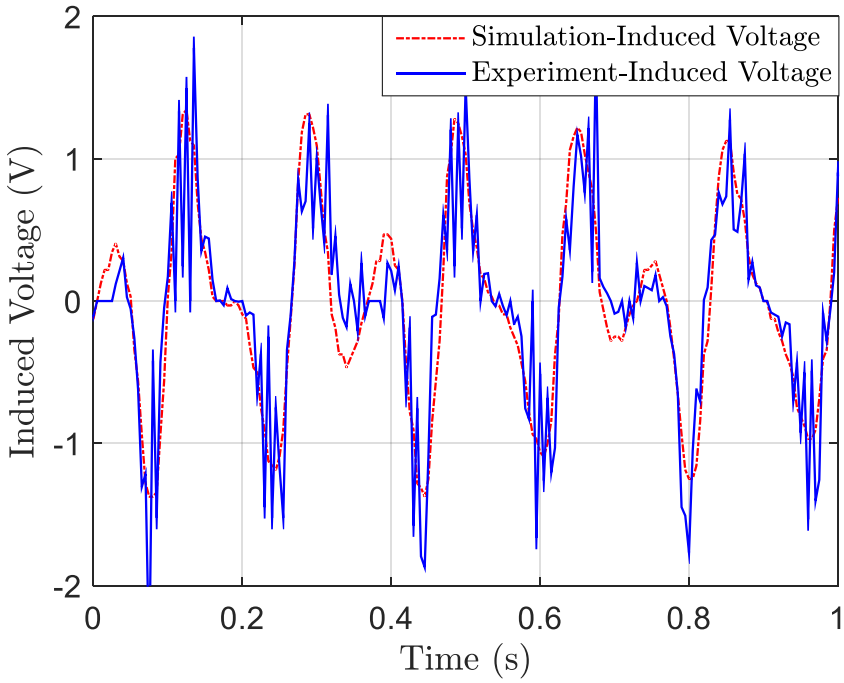

Figure 26. Comparison of the induced voltage from the model with that of the experiment.

This motor was used as a damper to regenerate energy and damp vibrations. Thus, the current needed to be checked. First, the ideal conditions for regenerating the maximum amount of energy were equal for the internal and external resistances of the motor. Figure

28 shows the resulting currents at optimal regeneration. The three induced phase currents were used to charge the load capacitor or fed to another load.

In the second case, the damper was fully utilized to damp the sprung-mass acceleration. Here, the external load was kept at zero to fully utilize the generator's damping capability. Figure 28 shows the increase in the generator's three phase currents, which increased the damping forces.

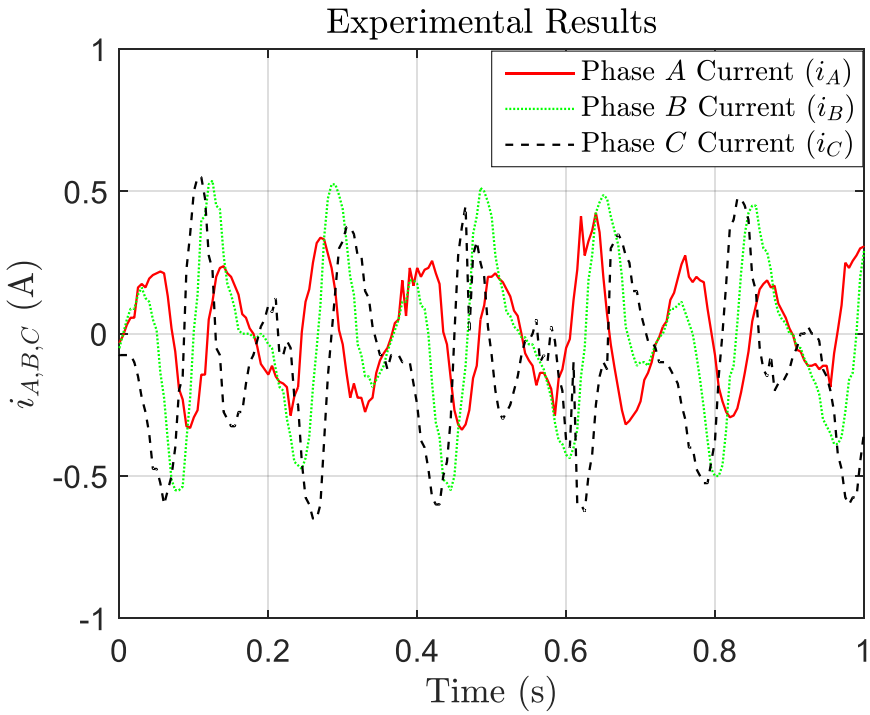

Figure 27. Generated currents at matching external loads.

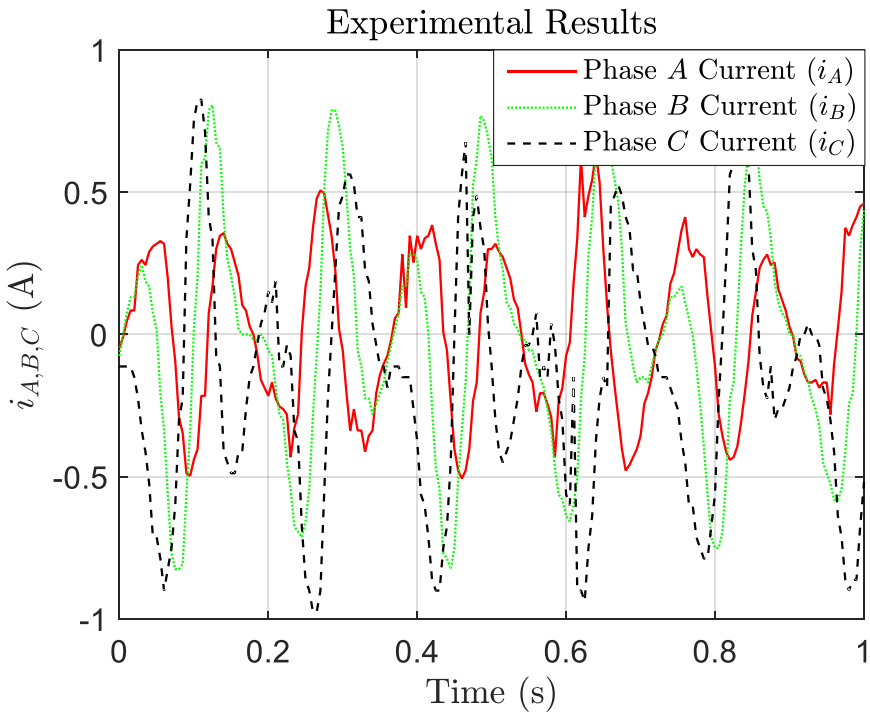

Figure 28. Generated currents at zero external load.

2.5 Passive Suspension Experimental Results and Discussion

A generator produced the power and damping force opposing any relative movement between the mover and the stator. Hence, the generator was modeled as the source of the EM force (F_d). where $F_d = c_e \dot{z}$, $\dot{z} = \dot{x}_s - \dot{x}_{us}$, c_e is the EM damping coefficient. The mechanical damping coefficient, c, is considered high due to the sliding friction of the guidance. It is estimated experimentally. Both damping forces act in parallel.

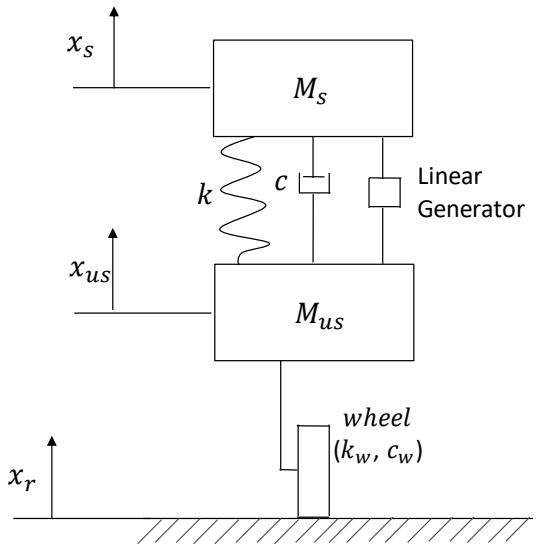

Figure 29. Quarter-car passive suspension system.

2.5.1 Input Power

The suspension system needed to be designed for random road input disturbances. However, due to the experiment's limitations, only specific sinusoidal signals were used to simulate the input disturbance (x_r). The input disturbance was realized by a cam mechanism, as seen in Eq. (12). The excitation frequency of 3.5 Hz was chosen to excite the system at its resonance for a larger vibration amplitude.

$$x_r = 0.015\sin(2\pi \cdot 3.5t) \tag{12}$$

A numerical model was built using Eq. (2) to estimate the amount of power delivered to the suspension system through the disturbance. Eq. (3) represents the disturbance force. The power delivered to the system was estimated to be 5 W, as described by Eq. (13).

$$F_r = c_w\dot{x}_r + k_w x_r \tag{13}$$

$$P_{in} = F_r \dot{x}_r = c_w \dot{x}_r{}^2 + k_w x_r \dot{x}_r \quad (14)$$

2.5.2 Damping Forces

As discussed in Section 2, there were two dampers connected in parallel. The mechanical damper represented the friction, whereas the EM damper represented the generator. The mechanical and EM damping forces were proportional to the relative velocity ($\dot{z}$). The total damping coefficient was the sum of both coefficients, as shown in Eq. (15).

$$F_d = (c + c_e)\dot{z} \quad (15)$$

Both damping coefficients, c and c_e, were found experimentally by imposing a step input, as shown in Figure 30. When the generator circuit was open (i.e., an infinite load), there was zero EM damping ($c_e = 0$) and the magnitude of the displacement response was larger than that of the closed circuit. When the generator was short-circuited (i.e., a zero load), the EM damping was added to the mechanical damping. The responses for the open and closed circuits are shown in Figure 31.

The mechanical damping coefficient, c, was found from the open circuit, whereas the EM damping coefficient could be estimated by comparing the open and closed-circuit responses. The results are shown in Table 4, where c_c is the critical damping coefficient. Another way to find (c_e) was by substituting $K_a = 2.05$ N/m, $R_i = 1.565\ \Omega$, and $R_o =$

0 Ω into Eq. (11). This led to $c_e = 4.01$ N·s/m, which was close to the value found with the step response.

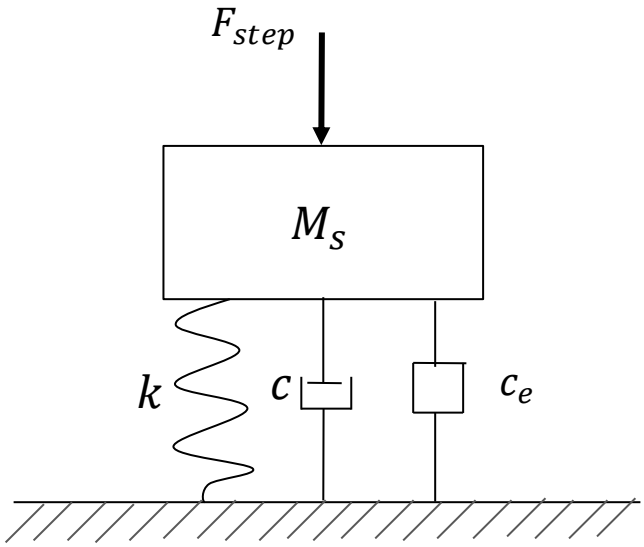

Figure 30. Step input given to the sprung mass.

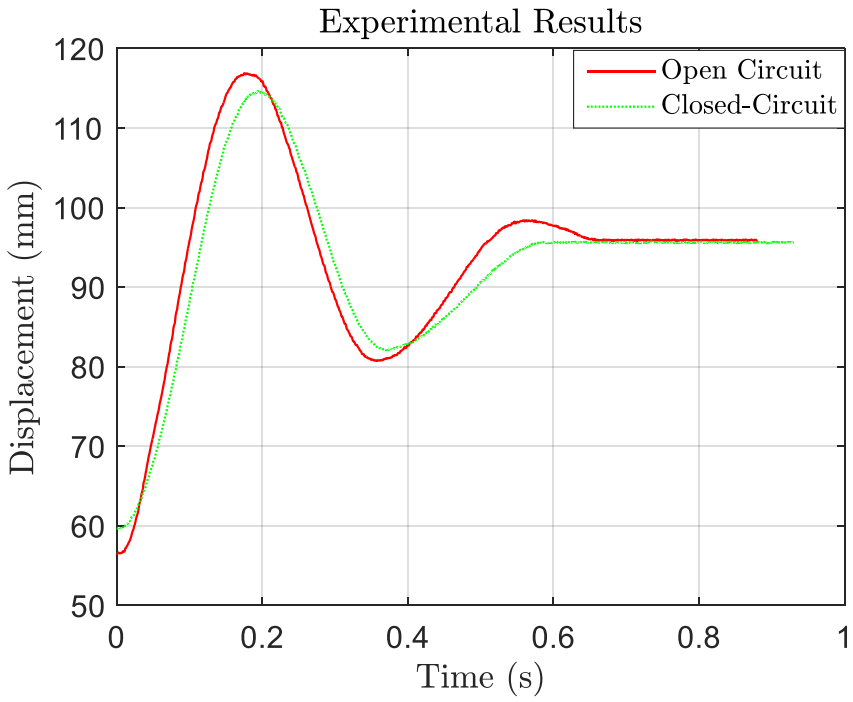

Figure 31. Step responses for open and closed generator circuits to estimate the damping coefficients.

Table 4. Parameters Estimated by Step Response

Parameter	Open circuit	Closed circuit
c_c	122.9	123.4 N·s/m
c	49.62	53.9 N·s/m
ζ	0.404	0.404
K	1310	1309 N/m
c_e	-	4.26 N·s/m

Finally, the effect of the generator damping on the suspension system was investigated to estimate its effect on vibration suppression. This test was accomplished using the quarter-car testbed. Eq. (12) represents the input disturbance. The sprung mass acceleration amplitude is shown in Figure 32. During the period from 0 to 5 s, the generator's circuit was closed, i.e., both dampers were operational. In the second period (from 5 to 10 s), the generator's circuit was open, i.e., only the mechanical damper was operational.

The generator was able to reduce the sprung-mass acceleration amplitude by 22%. Eq. (16) shows the performance index used to find the percentage reduction of the sprung-mass acceleration. This performance index was used as a measure of rider comfort. Vibration reduction was obtained by using a resistive load instead of a short circuit. Thus, the damping force could be controlled with various load resistances.

$$Per.Ind = \left(1 - \frac{RMS_{closed}}{RMS_{open}}\right) \cdot 100 \tag{16}$$

RMS_{closed} was the RMS value of the sprung mass acceleration at the closed circuit and RMS_{open} was the RMS value of the sprung mass acceleration at the open circuit.

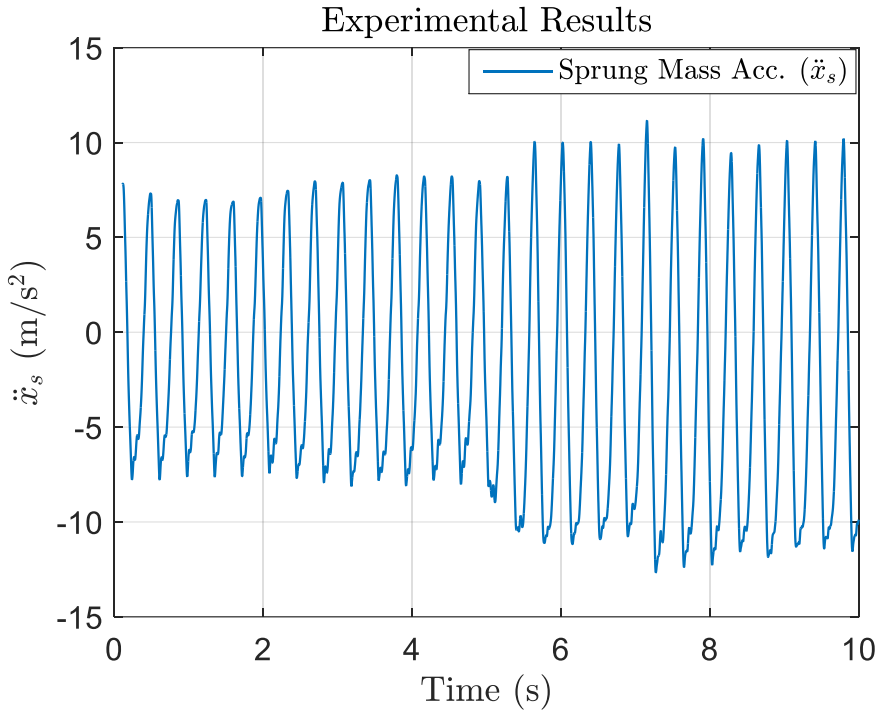

Figure 32. Sprung-mass acceleration with and without EM damper.

2.5.3 Harvested Power

To harvest the maximum amount of power, the external resistive load needed to match the internal impedance. The amount of harvestable power is represented in Eq. (17). The voltage and power obtained from a single phase is shown in Figure 33. The average harvested power was 35 mW. Since all three phases were identical, the total average power could be calculated by multiplying the phase power by three. Hence, the total harvested power was 105 mW. However, some of the harvestable power (P_h) in Eq. (17) was lost in the generator. Damping was decreased by increasing R_o from zero to 1.565 Ω, as can be noted in Eq. (6). Using the principle of impedance matching, the optimal value for the EM damping coefficient ($c_{e,opt}$) was 50% of the value of c_e. Therefore, $c_{e,opt}$ was equal to 2

N·s/m. In this experimental setup, the mechanical friction factor was dominant over the EM damping. The values of c and c_e needed to be close in order to extract more energy from the system.

$$P_h = c_{e,opt}\,\dot{z}^2 \tag{17}$$

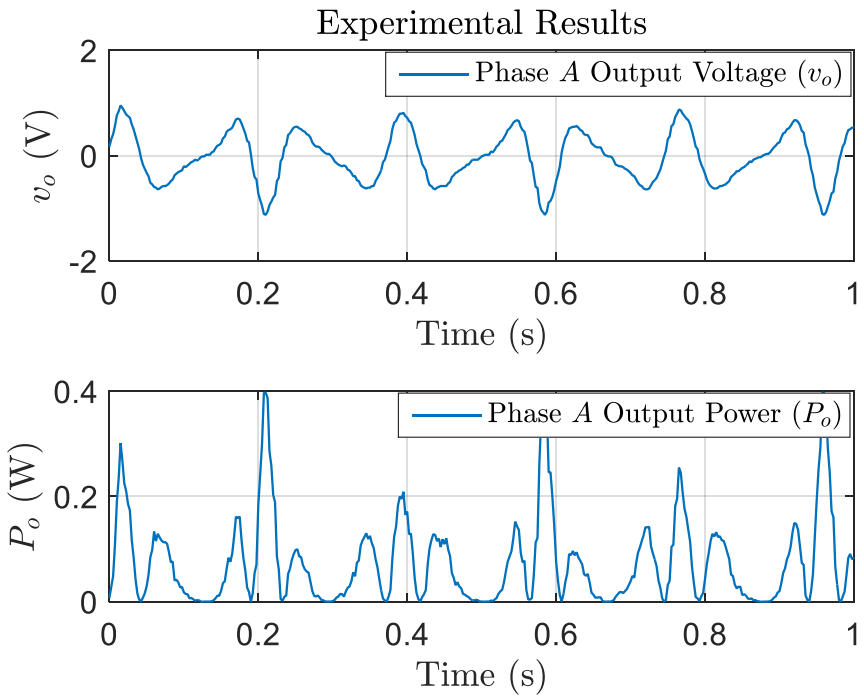

Figure 33. Output voltage and harvested power from Phase *A*.

2.6 Summary

An active car suspension system was experimentally implemented as a 2-DOF mass-spring-damper system using a linear motor. The active suspension was able to suppress up to 69% of the sprung-mass acceleration [55]. It used 8 to 9 W of power.

Experimental investigations were carried out to find the generator's parameters and damping coefficients. The generator damping effect and power generation in the quarter-car testbed were also investigated. The experiments showed that the linear regenerative damper could suppress up to 22% of the vibration and harvest 0.11 W of power at the matching impedance. The suspension measurements used to check the performance of the passive and active suspensions conserved here included rider comfort and energy consumption/recovery. Finally, since both harvesting and damping capabilities were noticeable in the testbed, this process could further be used to design and implement a regenerative suspension system.

CHAPTER III

REGENERATIVE POWER-ELECTRONIC INTERFACE

3.1 Introduction

The previous chapter examined active suspension systems. In addition, the general capabilities of suspension systems were addressed. However, one important component is missing in that the damping and energy regeneration requirements for regenerative suspensions are to be fully realized. A power-electronic interface is investigated and implemented in this chapter.

3.1.1 Interface Requirements

The main requirements for a power electronic interface include:

- Matching the external and internal impedances of the EM transducer;
- Boosting the output voltages to the level of the car battery, which is currently 14 V (see Figure 34); and
- Enabling a change in the EM damping force for use as a control force, and replacing the motor's active force.

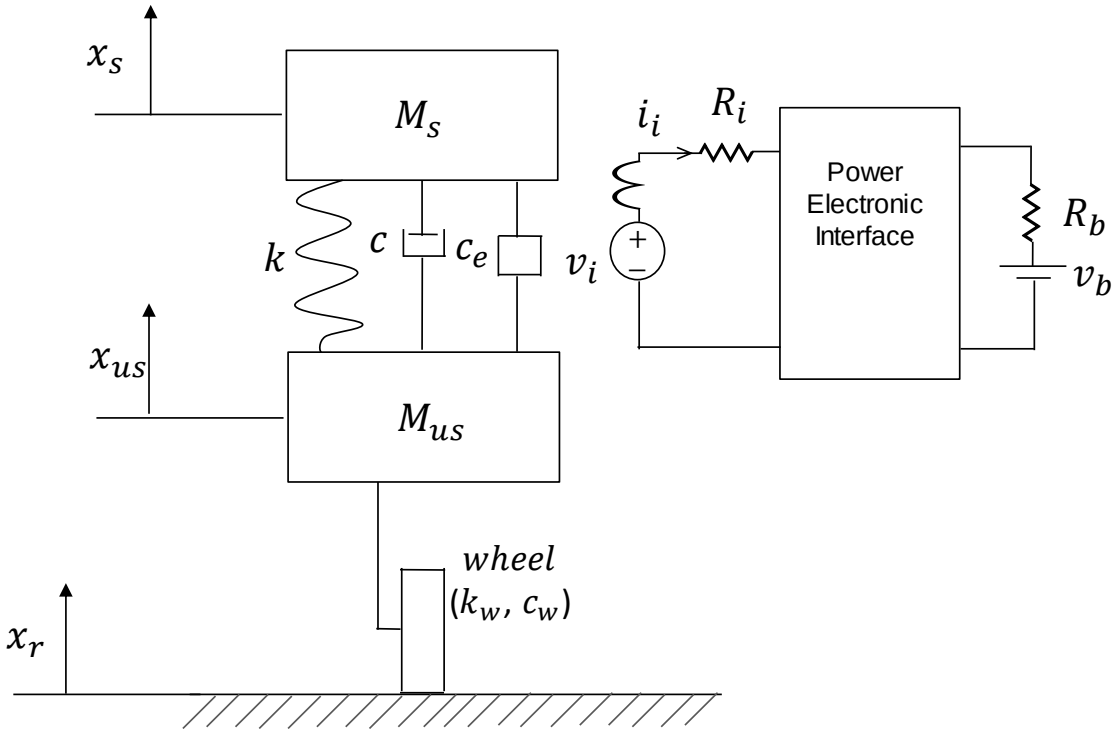

Figure 34. Suspension with a regenerative interface.

3.2 Symmetrical Bridgeless Boost Converter (SBBC)

Boost converters are often used in power electronics to boost voltages. They are more suited to low-power applications, such as suspension systems. They can be used to realize the load of the generator as resistive. Moreover, they have a simple structure, and the MOSEFT of their high side needs no control signals, as is the case with the SBBC.

An SBBC can rectify and boost an AC signal. If the input voltage frequency is very small compared to the switching frequency, the SBBC can be simplified as a single boost converter. In a suspension application, the input frequency depends upon the road disturbances, which usually are modeled as the low frequency, and a 3.5-Hz amplitude is

used in the quarter-car experiment. The carrier frequency used to generate the PWM signals for the MOSFET is 1 kHz.

Figures 35 and 36 illustrate the boost and rectification actions that take place in an SBBC. During the positive input voltage, the switches q_2 and D_1 are on. Switch q_1 switches at high frequency to boost the input signal to the level of the battery potential (Refer to Figure 35). During the negative input voltage switch q_1 and D_2 are on, and q_2 switches at a higher frequency to boost the voltage (Refer to Figure 36). The PWM drive for the SBBC needs to sense the input voltage to generate the required duty ratio during the positive and negative values of the detected voltage.

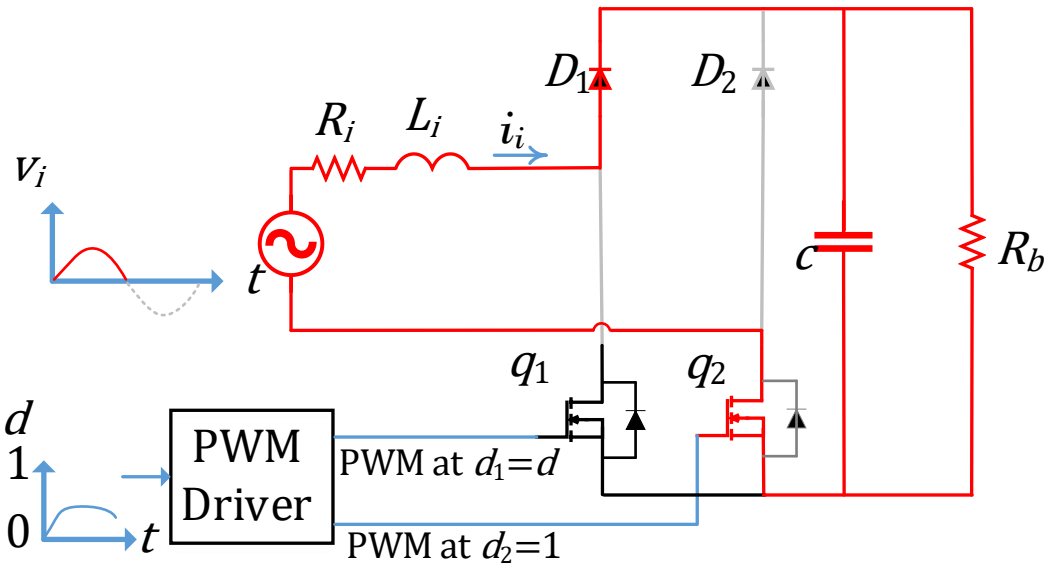

Figure 35. SBBC to rectify and boost the positive AC input.

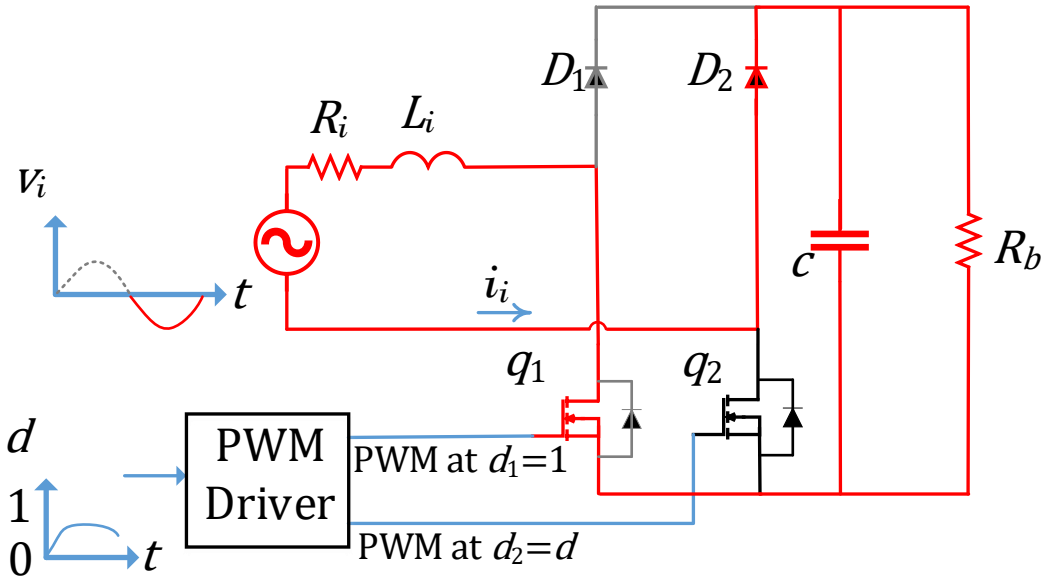

Figure 36. SBBC to rectify and boost the negative AC input.

3.3 Discontinuous-Mode Boost Converter

An SBBC can be represented as a single boost converter, according to the assumptions previously discussed. Depending on the current flowing into the inductor, there are three possible modes of operation: continuous-conduction mode (CCM), discontinuous-mode (DCM), and boundary-condition mode (BCM). CCM is widely used because it is optimal for medium-to-high power applications. However, it requires current and voltage control. The current should be in phase with the voltage, and the output voltage should be regulated [19].

Discontinuous mode (DCM) has the following advantages [58].

- useful for small power applications;
- in steady-state conditions, the average input current automatically follows the input voltage, which leads to a unity power factor without a current control loop;

- simpler control compared to the CCM;
- soft turn-on for main switches;
- reduced diode reversed-recovery losses; and
- decoupled input impedance from the output voltages.

3.3.1 Design and Modeling

The operation of the DCM boost converter is to be analyzed to determine the transfer function for the input current, as well as the output voltage (Refer to Figure 37.). There were three segments of inductor current, as shown in Figure 38. Each segment of current had a different operation mode (Refer to Figure 38.).

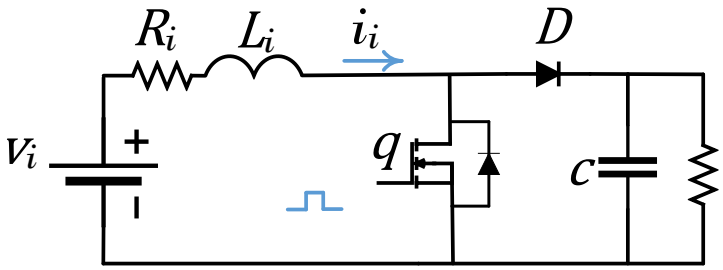

Figure 37. Boost converter.

Below is an analysis of the DC-CD boost converter in the DCM described in [58]. Table 6 shows the values used for this analysis. K and K_{crit} were found from Eqs. (18) and (19), respectively. Then, Eq. (19) was used to find M, which in turn was used to find $i_{i,Avg}$ and v_o. Note that these variables were the average values over the fundamental

switching frequency of the pulse width generation. The variable $i_{i,Avg}$ was distinguished from the instantaneous input current i_i, which will be discussed later in this chapter.

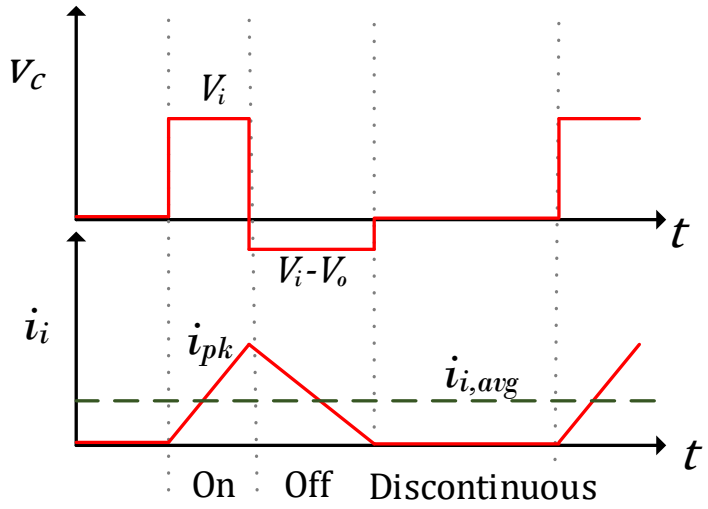

Figure 38. Input current and output voltage of the boost converter.

Table 5. DCM's Three Operation Modes

Mode	Circuit	States space Model
On	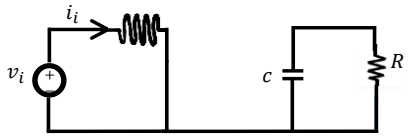	$\begin{bmatrix} \frac{di_L}{dt} \\ \frac{dv_c}{dt} \end{bmatrix} = \begin{bmatrix} 0 & 0 \\ 0 & -\frac{1}{Rc} \end{bmatrix} \begin{bmatrix} i_L \\ v_c \end{bmatrix} + \begin{bmatrix} \frac{1}{L} \\ 0 \end{bmatrix} v_i$
Off	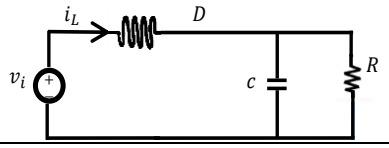	$\begin{bmatrix} \frac{di_L}{dt} \\ \frac{dv_c}{dt} \end{bmatrix} = \begin{bmatrix} 0 & -\frac{1}{L} \\ \frac{1}{c} & -\frac{1}{Rc} \end{bmatrix} \begin{bmatrix} i_L \\ v_c \end{bmatrix} + \begin{bmatrix} \frac{1}{L} \\ 0 \end{bmatrix} v_i$
Discontinuous	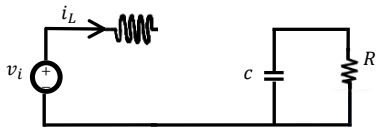	$\begin{bmatrix} \frac{di_L}{dt} \\ \frac{dv_c}{dt} \end{bmatrix} = \begin{bmatrix} 0 & 0 \\ 0 & -\frac{1}{Rc} \end{bmatrix} \begin{bmatrix} i_L \\ v_c \end{bmatrix} + \begin{bmatrix} 0 \\ 0 \end{bmatrix} v_i$

$$K = \frac{2L_i}{R_b T_{pwm}} \tag{18}$$

$$K_{crit} = d(1-d)^2 \tag{19}$$

$$M = \frac{v_o}{v_i} = \frac{1+\sqrt{1+4d^2/K}}{2}\left(1+\frac{R_b}{((1-d)^2 R_b)}\right) \tag{20}$$

Table 6. Boost Converter Values

	Variables	Values
Internal inductor	L_i	1.5 mH
Internal resistance	R_i	1.565 Ω
Input voltage	v_i	1.2 V
Capacitor	c	68 mF
Load resistance	R_b	80 Ω
Fundamental carrier period	T_{pwm}	1 ms

The dimensionless parameter K (see Eq. (18)) is the measure for the operation mode. This converter was placed in the DCM due to the small value of the inductor. To change it to the CCM, we either need to add an external inductor or use a very high switching frequency. Figure 39 shows that the converter was in the DCM for most of the d values, when K was less than K_{crit}.

The boost converter conversion ratio M is shown in Figure 40. The average inductor input current increased as the duty-ratio increased from 0 to 1 (Refer to Figure 41). Because the DCM always kept the input current in phase with the voltage, the equivalent resistance R_e could be estimated as in Figure 42. The output voltage is shown in Figure 43.

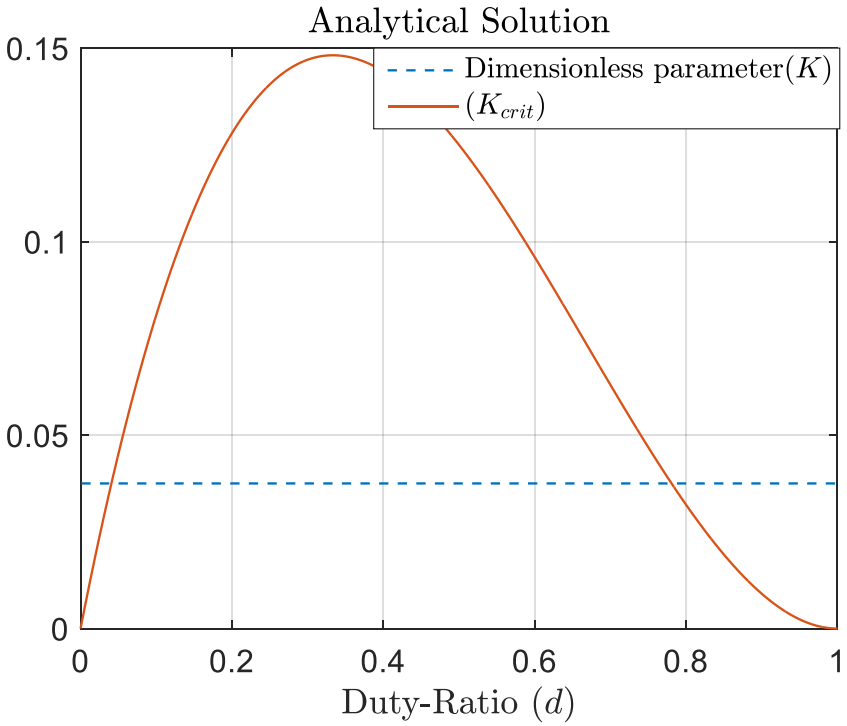

Figure 39. Converter operation modes.

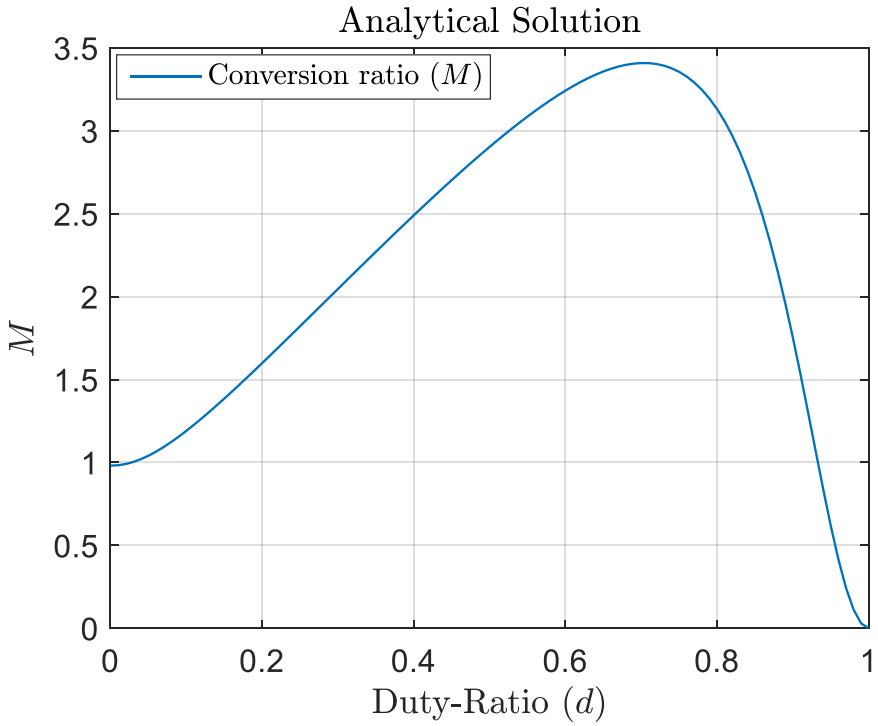

Figure 40. Boost converter conversion ratio.

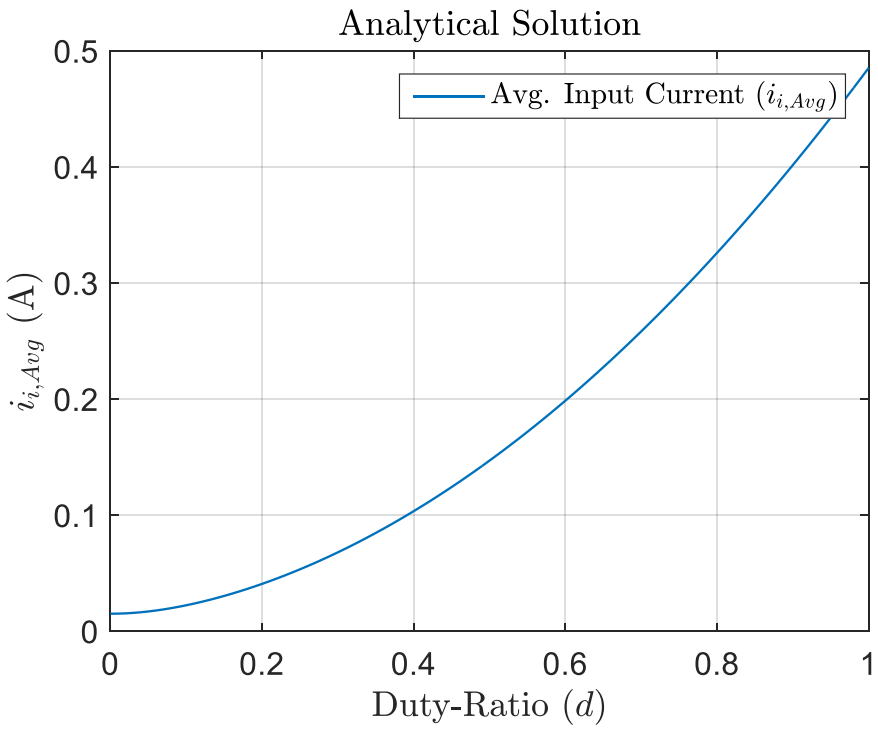

Figure 41. Boost converter input current versus duty-ratio.

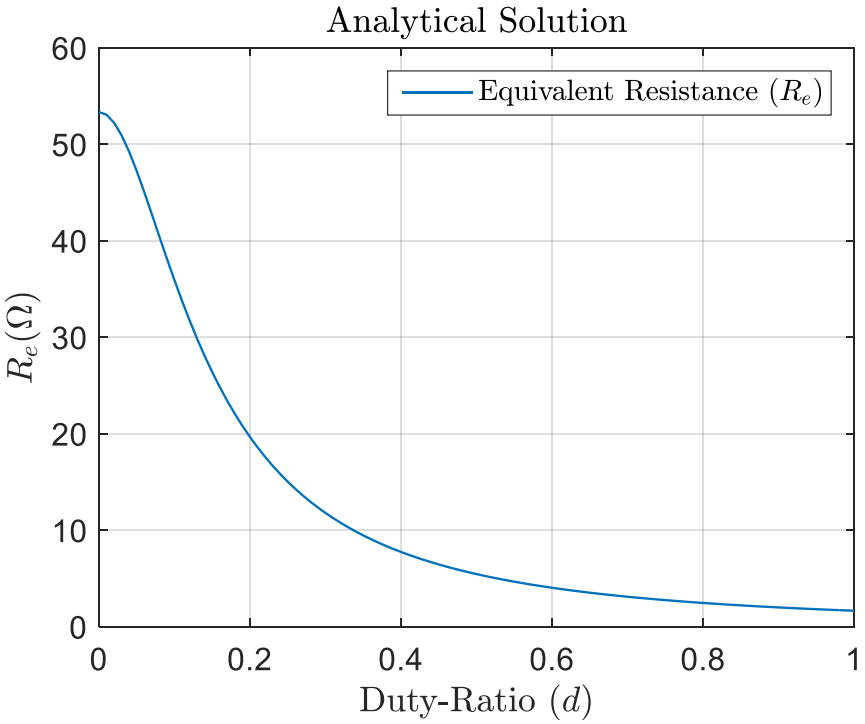

Figure 42. Equivalent resistance versus duty ratio.

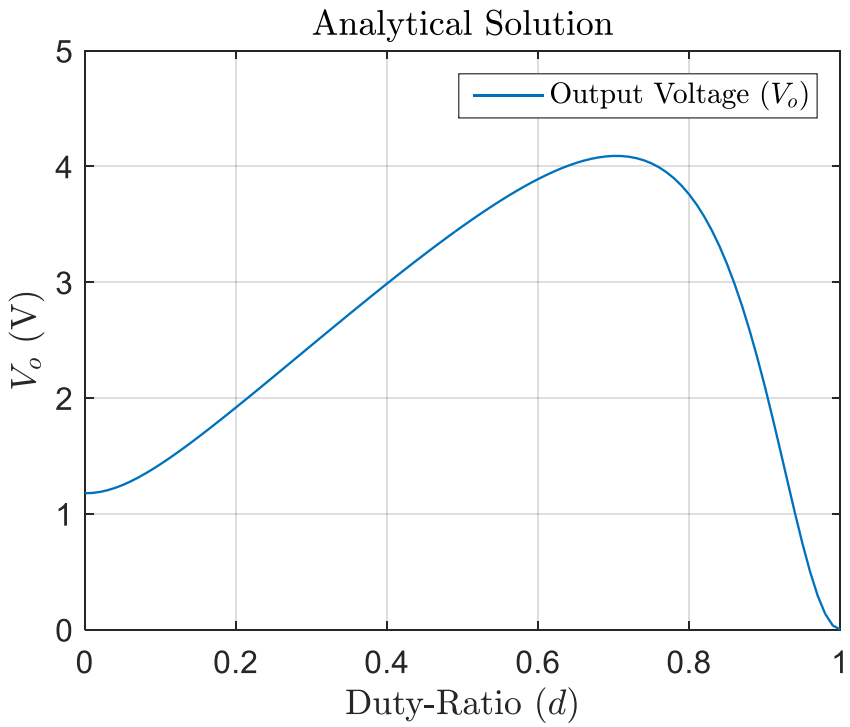

Figure 43. Output voltage as a function of the duty ratio.

3.3.2 Open-Loop Test Results

The objective of an open-loop test is to observe the responses of the open-loop system. Figure 44 shows a boost converter with the values used in this test. The input was the duty-ratio value in dSPACE. According to d, the PWM was generated to switch the MOSFET at 1 kHz. The measured outputs were i_i and v_o. Figure 95 illustrates how the PWM signal was generated using a sawtooth carrier wave with a frequency of 1 kHz. The PWM varied according to the variable d. Figure 45 includes a block diagram of this open-loop test.

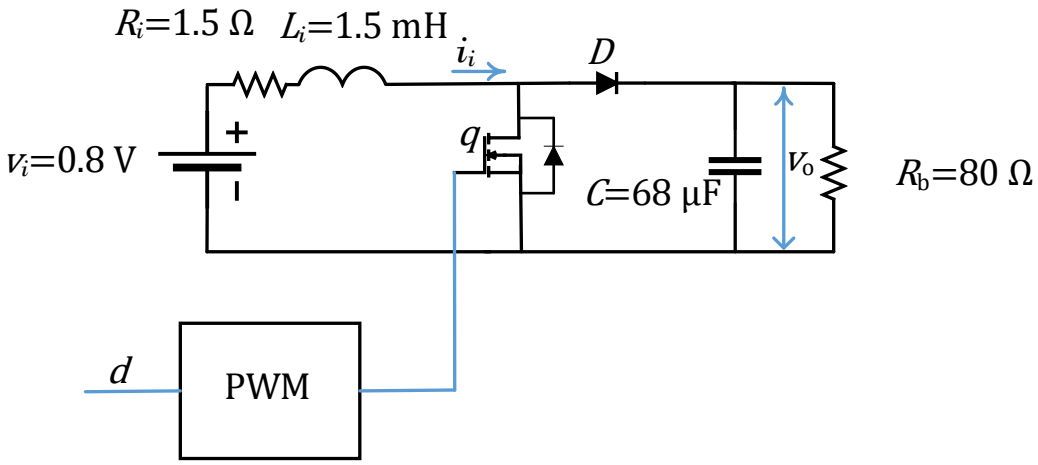

Figure 44. Boost converter open-loop test.

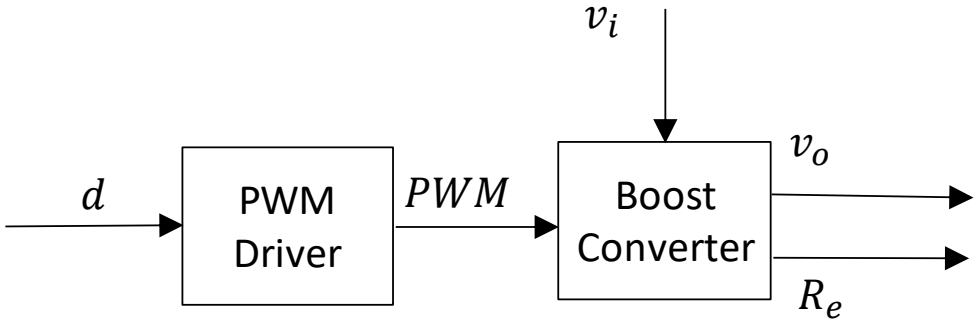

Figure 45. Block diagram of the boost converter open-loop test.

The simulation and experiment results are shown in Figures 46–48. These plots indicate the relationship between the input current, equivalent resistance, and output voltage virus duty ratio. The current increased as the duty-ratio went from zero to unity, where at unity duty ratio the generator is short circuit without any external load as shown in Figure 46. Because boost converter in DCM, equivalent resistance (R_e) could be estimated as a function of the duty ratio. In section 3.3.3, R_e will be manipulated by the controller in the feedback loop. The output voltage (v_o) is shown in Figure 48. Note that v_o was at its maximum when $d = 0.7$. Figure 49 shows how the input current (i_i) varied at $d = 0.4$, as

well as the moving average for the input current. The duty ratio was generated at 1 kHz. The booster current was in the DCM because it reached zero. The average current $i_{i,Avg}$ was used to estimate R_e. Figure 50 shows the booster current at $d = 0.4$ for the experiment.

Appendix A.1 shows the Simulink® model used for the simulations in this test. Figure 93 shows the open-loop test with the desired input, as a constant from 0 to 1 in increments of 0.1. The Simscape model for the boost converter is shown in Figure 94.

For the experiment, the following components were used: a logic level gate field-effect transistor (IRF3708) and Schottky diode with a forward voltage drop of 0.15 V. The boost converter was built on a breadboard. This experiment was executed using the dSPACE.

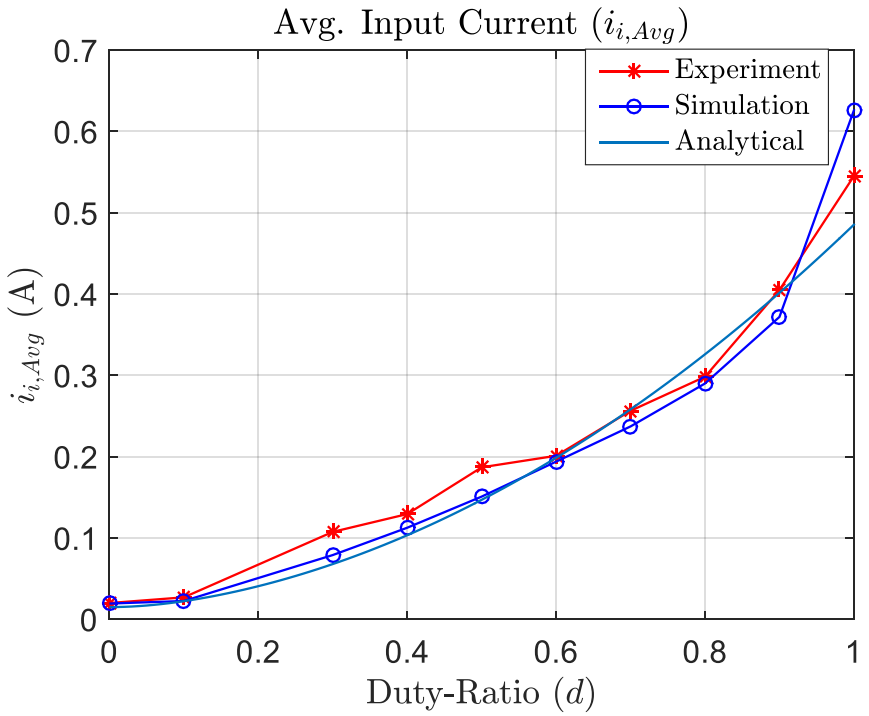

Figure 46. Average input current versus duty ratio in the boost converter.

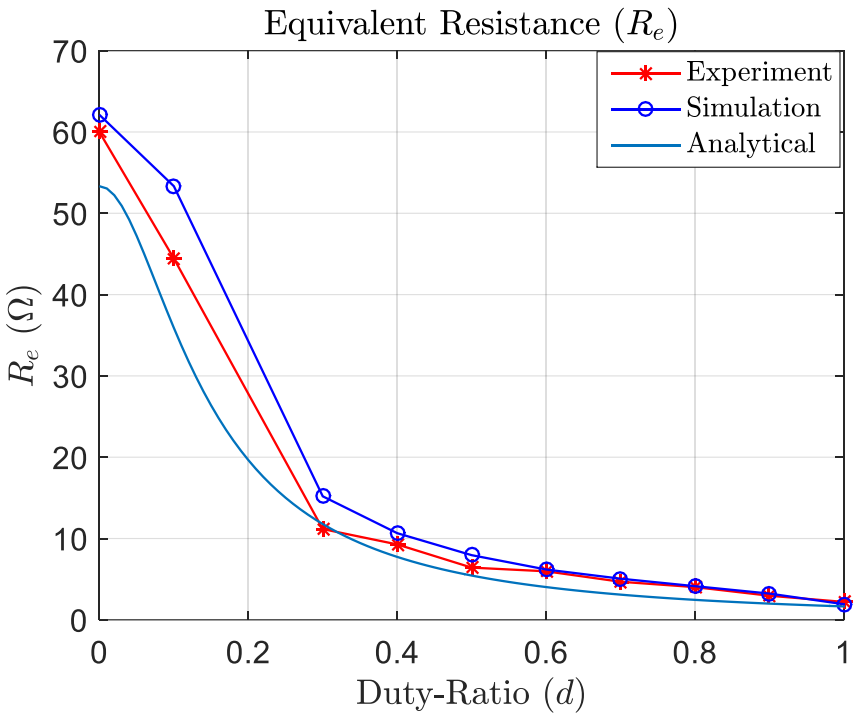

Figure 47. Equivalent resistance versus duty ratio in the boost converter.

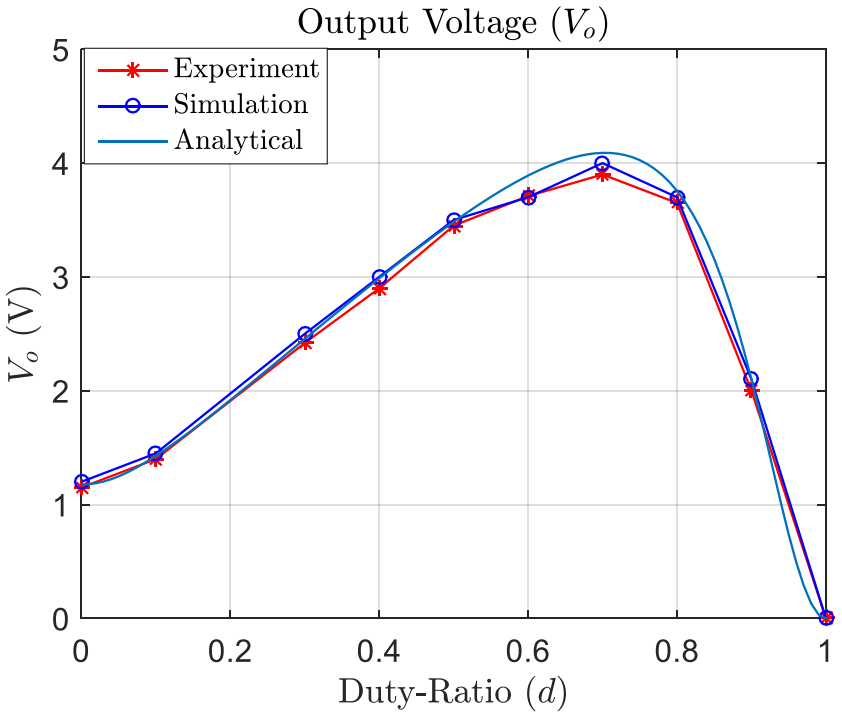

Figure 48. Output voltage versus duty ratio in the boost converter.

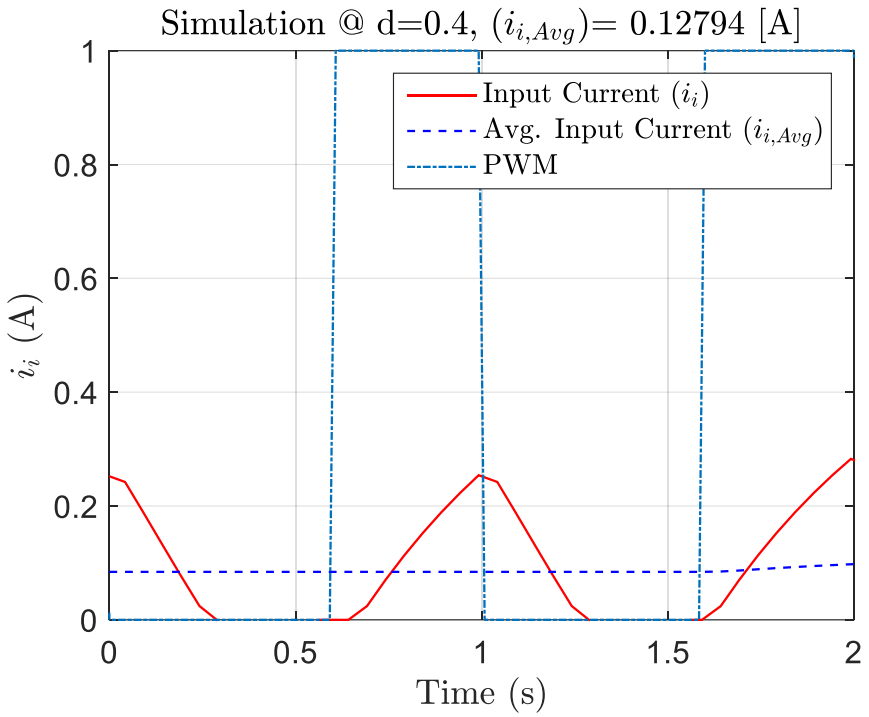

Figure 49. Inductor current at a 40% numerical duty ratio.

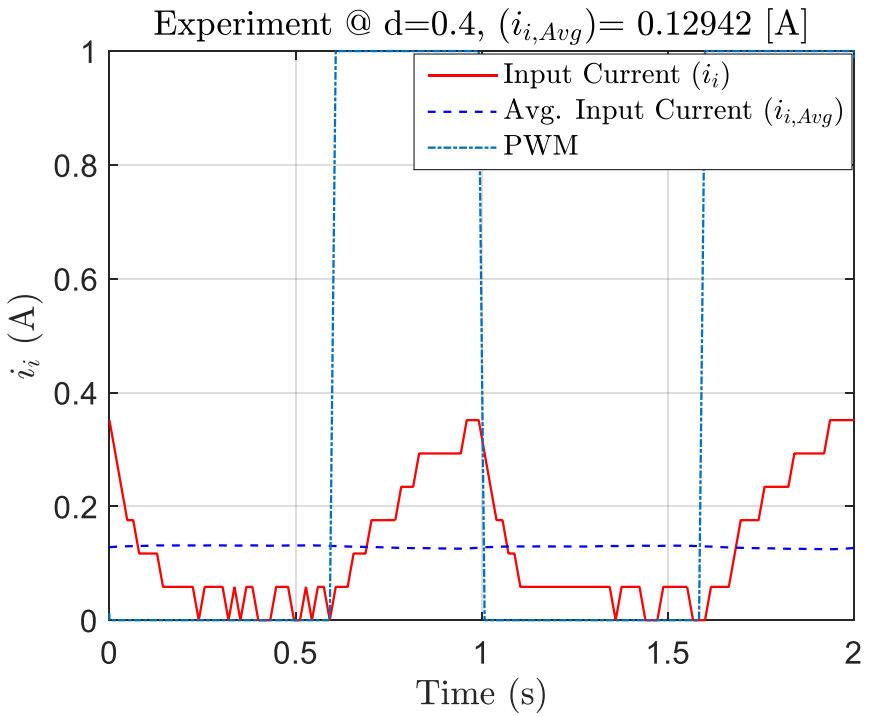

Figure 50. Inductor current at a 40% duty ratio in breadboard.

3.3.3 Closed-Loop to Control Equivalent Resistance

The average current signal was used to obtain the equivalent resistance R_e and then fed back to the PI controller, which controls the duty ratio (d). A block diagram of this control system is shown in Figure 51. Either $i_{i,Avg}$ or R_e could be the controlled variable. However, R_e was chosen because it included the input disturbance v_i.

The PI constants were chosen to keep R_e track $R_{e,des}$. The boost converter can be simplified by DC source, inductor, resistor, and switch in serious. The system pole will be at R_i/L_i. So, the system has fast-tracking. However, there is some damping related to R_i. Small integral gain needed to improve the system response error. A small gain is enough to increase the system response after introducing the integral gain. The PI controller gains were chosen to be k_p =0.000228 s and $k_i = 2.4$ S · s.

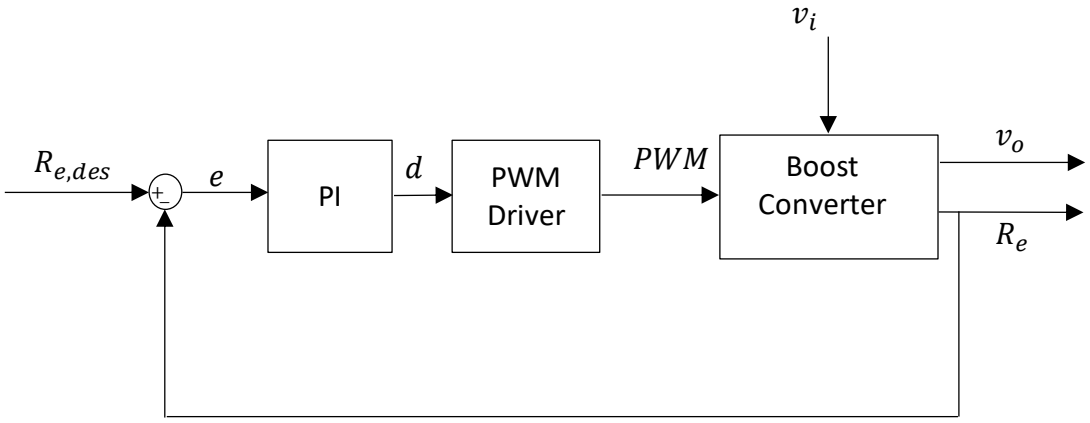

Figure 51. Block diagram to control the equivalent resistance.

3.3.4 Closed-Loop Test Results

By using the PI controller, the system was able to track the desired resistance. To check the performance, the system was tested using square and sinusoidal desired resistances. In Figure 52, the resistance is tracked according to the desired square value. The average input current was varied from 0.05 to 0.13 A. The control effort in this case was d where it changed from 0.3 to 0.55 as shown in Figure 53. The error was less than 8 Ω. The results shown in Figure 54 indicate the resistance and track the desired value. There was some delay, due to unmodeled dynamics. The control effort ranged from 0.2 to 0.35, which was less than the simulation results (Refer to Figure 55.). This means that more control effort could be used to improve the results. Table 6 displays the boost converter variables used in closed-loop simulation and experimental test. The Simulink® model used in the closed-loop simulation is shown in Figure 96 in Appendix A.1.

In Figure 56, the resistance is tracked as the desired sinusoidal value. The input average current varied from 0.05 to 0.13 A. The control effort in this case was d, which changed in sinusoidal form from 0.45 to 0.57, as shown in Figure 57. The error was less than 5 Ω. The results shown in Figure 58 indicate the resistance, which tracks the desired value with some delay due to unmodeled dynamics. In Figure 59, the control effort ranged from 0.2 to 0.35, which was less than that in the simulation results due to the averaging of the current. This means that more control effort could be used to improve the results.

There was a discrepancy between the experiment and the simulation results regarding the resistivity of the internal components and no other simulated dynamics. Generally, the results were acceptable and could be carried on to the design of the SBBC.

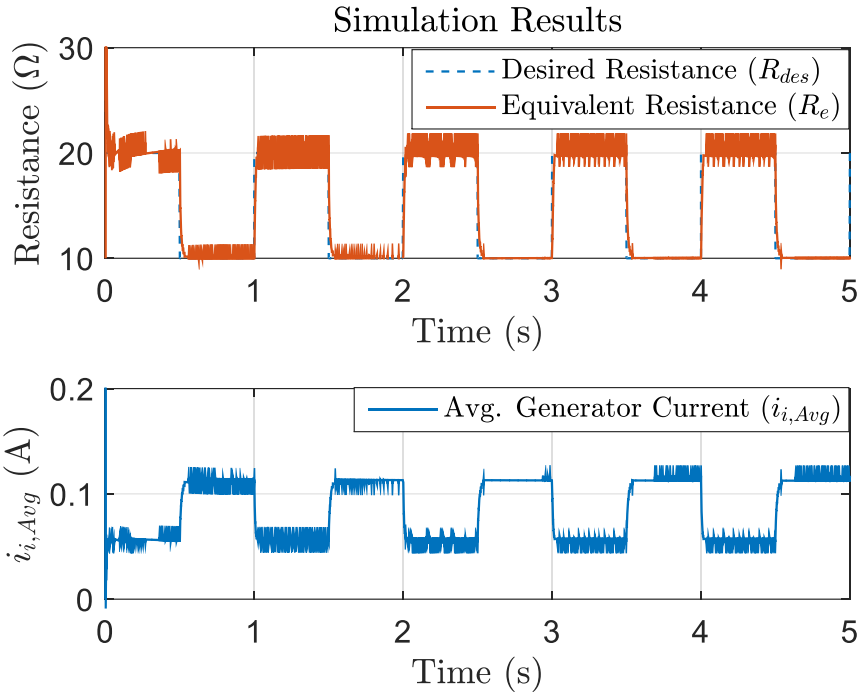

Figure 52. Equivalent resistance and average input current of the closed-loop boost converter by simulation for the desired square-wave reference input.

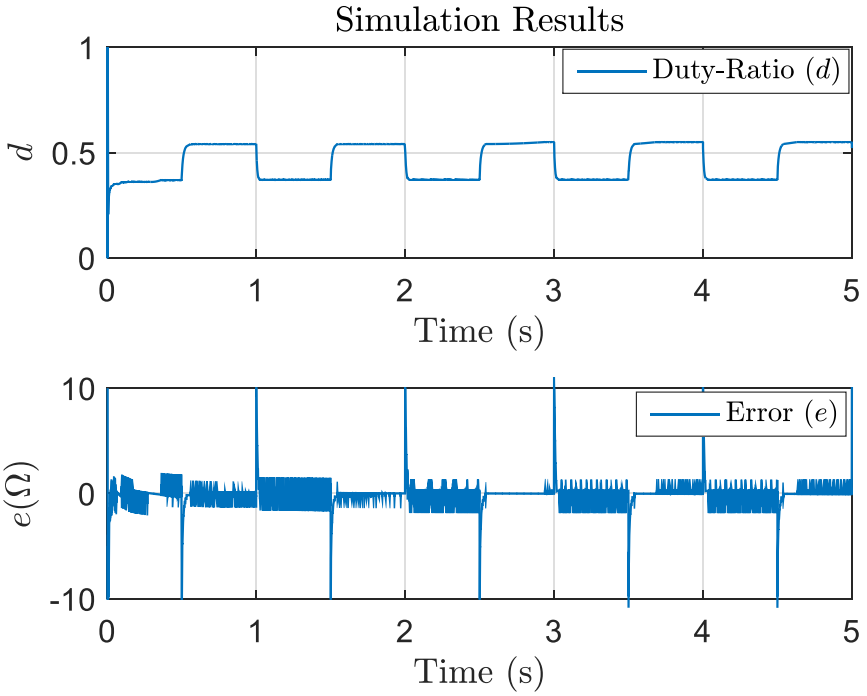

Figure 53. Duty-ratio and error of the closed-loop boost converter by simulation for the desired square-wave reference input.

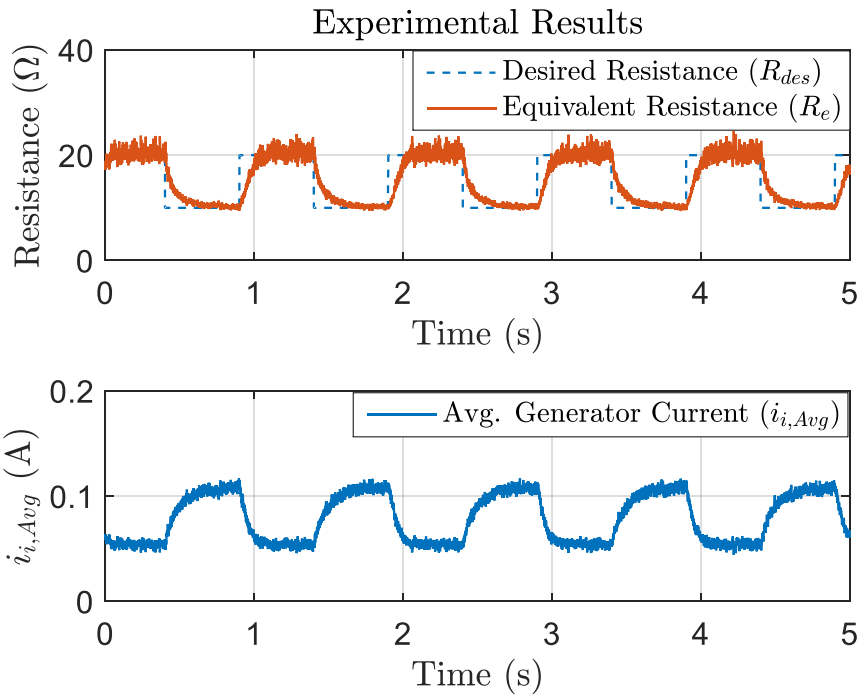

Figure 54. Equivalent resistance and average input current of the closed-loop boost converter by experiment for the desired square-wave reference input.

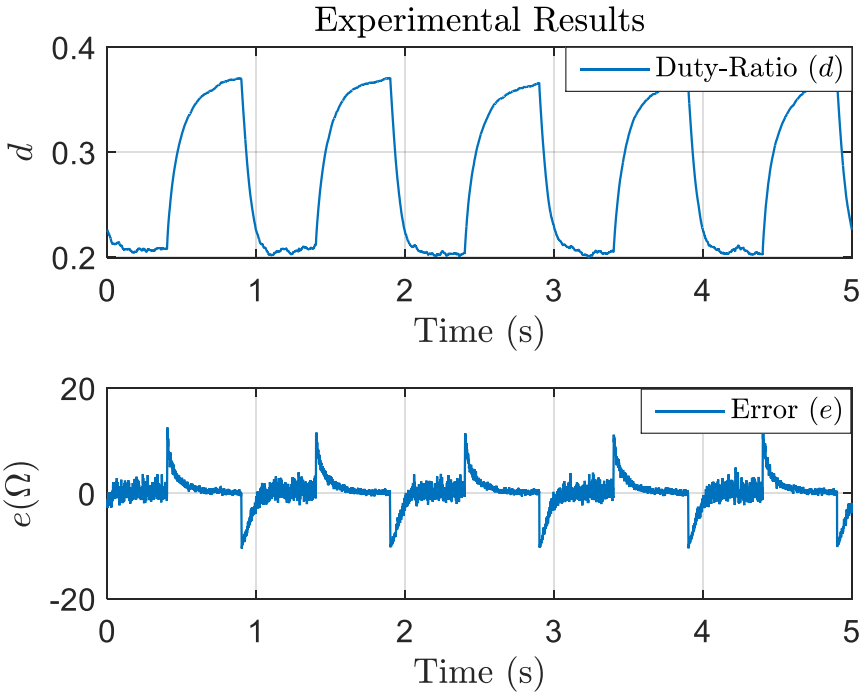

Figure 55. Duty-ratio and error of the closed-loop boost converter by experiment for the desired square-wave reference input.

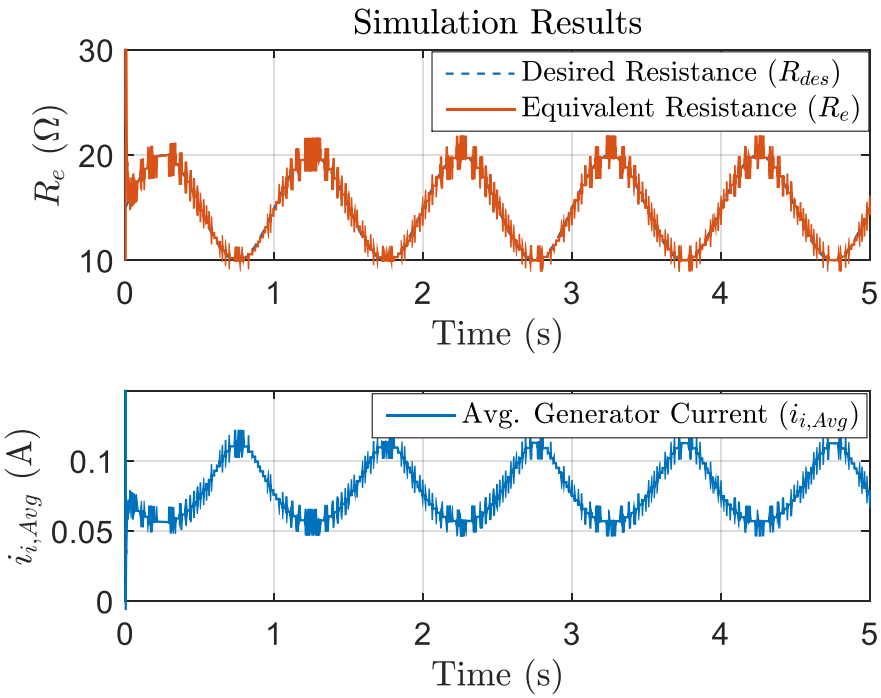

Figure 56. Equivalent resistance and average input current of the closed-loop boost converter by simulation for the desired sine-wave reference input.

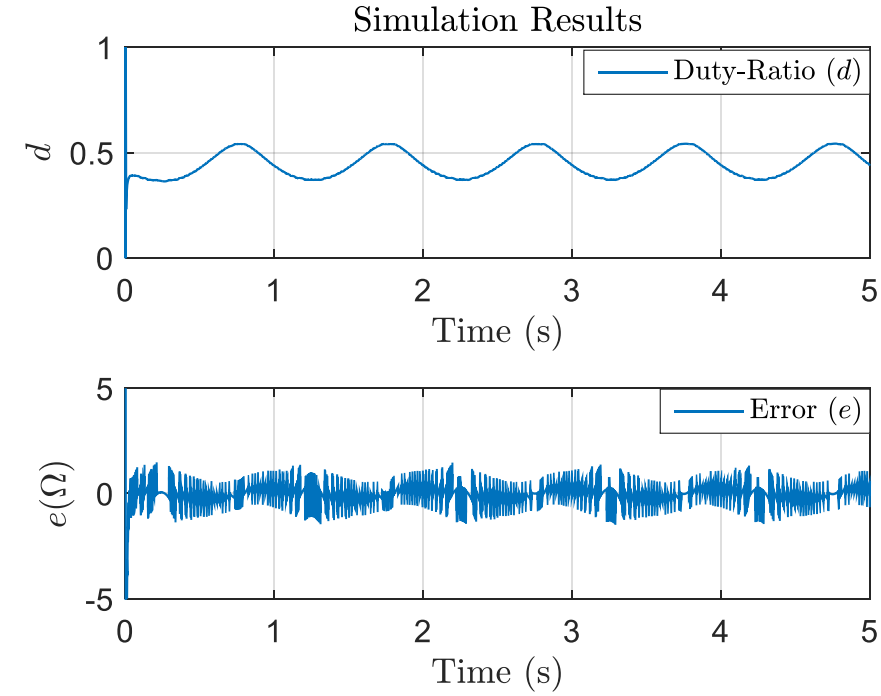

Figure 57. Duty-ratio and error of the closed-loop boost converter by simulation for the desired sine-wave reference input.

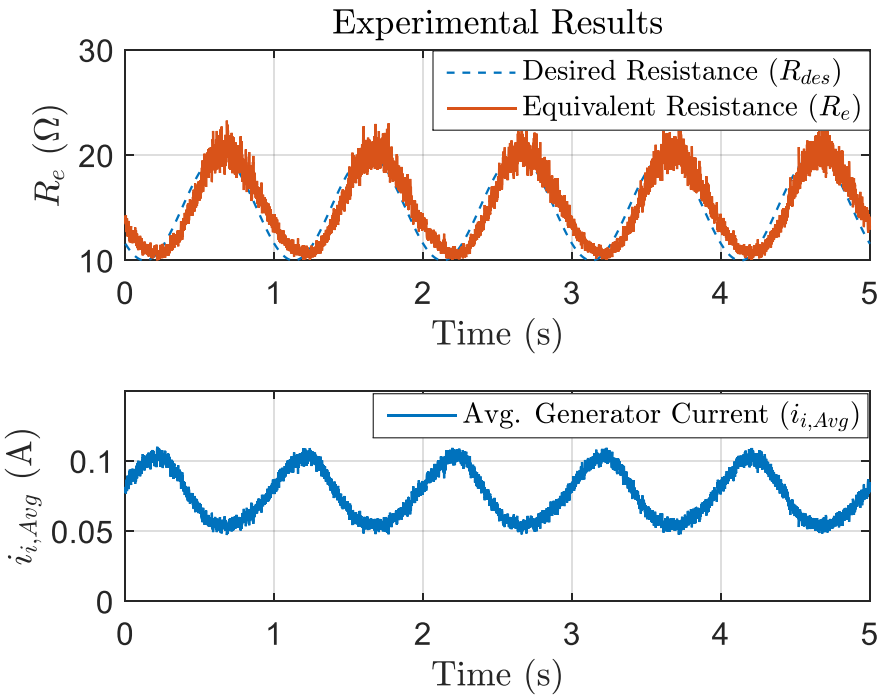

Figure 58. Equivalent resistance and average input current of the closed-loop boost converter by experiment for the desired sine-wave reference input.

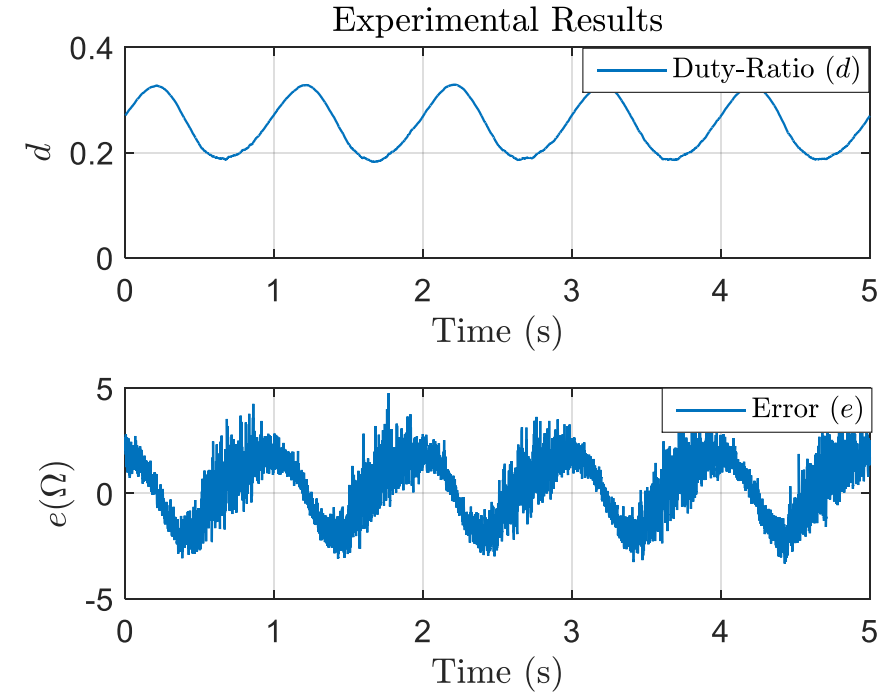

Figure 59. Duty-ratio and error of the closed-loop boost converter by experiment for the desired sine-wave.

3.4 AC-DC SBBC Converters

3.4.1 Open-Loop Test Results

The purpose of the open-loop test is to verify the SBBC's performance. The voltage input to the converter was a sine wave with a frequency of 3.5 Hz and an amplitude 0.8 V, which was close to the induced voltage produced by external disturbances in the experiment setup. However, in the experiment the sprung mass was fixed and a cam mechanism was used to produce the sinusoidal motion. A block diagram for this test can be found in Figure 60, and its circuit appears in Figure 61. The input to the system was the duty-ratio d which was introduced as a step function from 0.4 to 0.6. The PWM driver generated the required modulation for the MOSFET switches q_1 and q_2. Figure 99 in Appendix A.2 illustrates how the PWM signals were generated for the AC signal and how v_i was used to switch between d_1 and d_2. Note that when v_i was DC, d_1 and d_2 were equal to d and the PWM driver was the typical one described in the previous section. More details about the Simulink® model are presented in Appendix A.2.

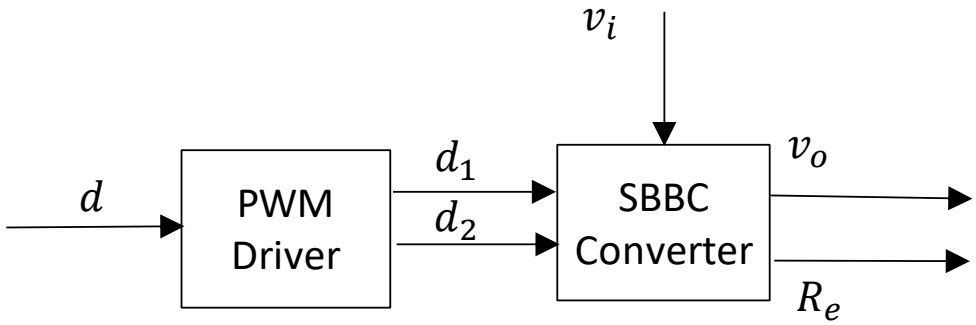

Figure 60. Block diagram of the open-loop test of the electronic interface.

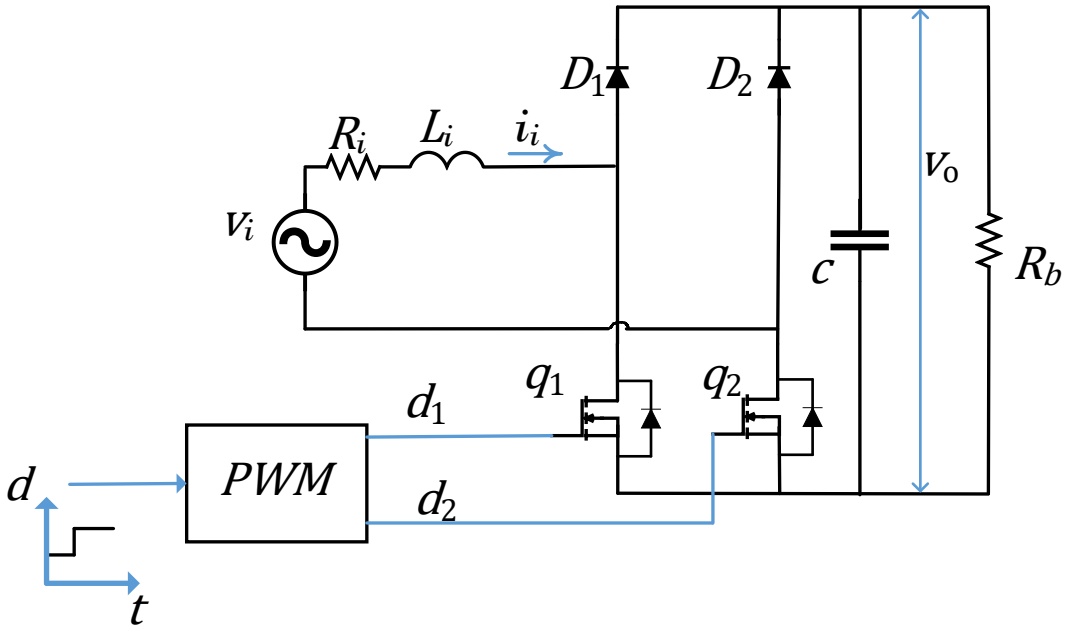

Figure 61. Open-loop test of the electronic interface.

The simulation results are shown in Figures 62 and 63. The average generator current $i_{i,Avg}$ increased as d increased from 0.4 to 0.6. It continued to increase until it reached the maximum induced current at $d = 1$. The equivalent resistance R_e was estimated from the input voltage and current. There was some noise in this signal due to the zero current. This resistance was decreased as the MOSFET switches was fully closed. The output voltage (V_o) was increased as (d) stepped up from 0.4 to 0.6. The output voltage was still not DC, but this could be improved by resizing the capacitor or using the feedback controller. The RMS values for $i_{i,Avg}$, R_e, and V_o can be compared to the boost converter's open-loop test.

The experimental results are shown in Figures 64 and 65. The value of $i_{i,Avg}$ increased as d increased from 0.4 to 0.6. The experiment current was less than that in the simulation

due to the switching and conduction losses that were neglected in the simulation. The value for R_e changed as a function of d. The controller was designed later to change the suspension system's damping force. The value for v_o increased as d was stepped up from 0.4 to 0.6.

Appendix A.2 shows the Simulink® model used for the simulated test. Figure 97 illustrates the open-loop test with the desired input d. The Simscape model of the SBBC is shown in Figure 98. For the experiment, the following components were used: a logic level gate FET (IRF3708) and Schottky diode with a forward voltage drop of 0.15 V. The SBBC was built on a breadboard. This experiment was executed using dSPACE.

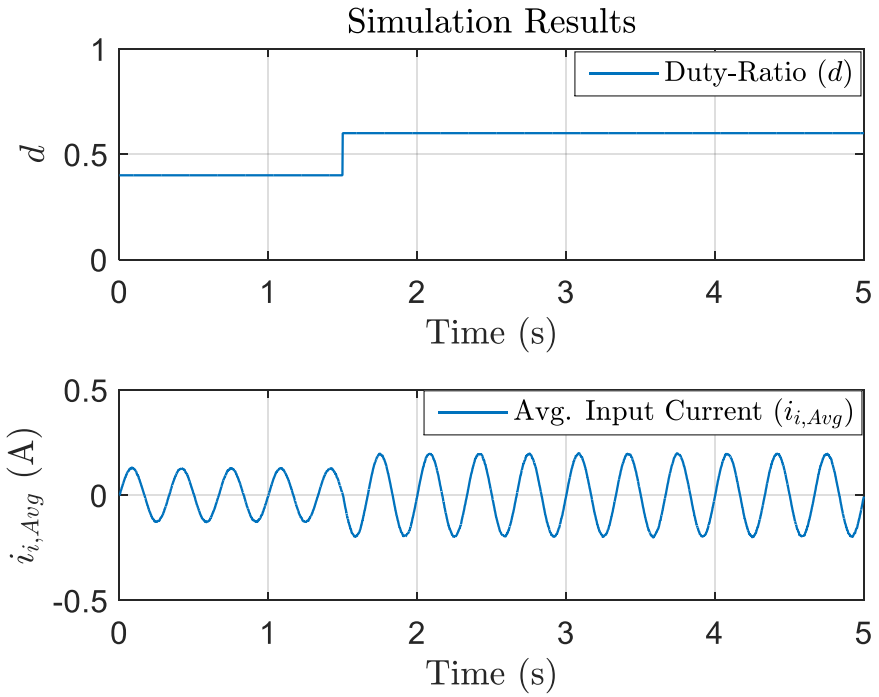

Figure 62. Average input current of the SBBC for the step input duty ratio.

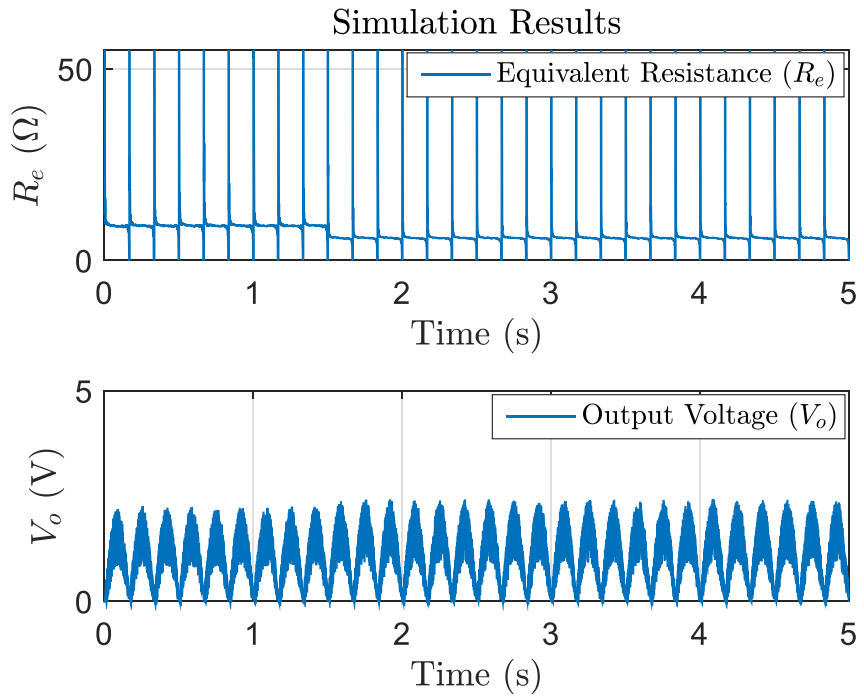

Figure 63. Equivalent resistance and output voltage of the SBBC for the step input duty ratio.

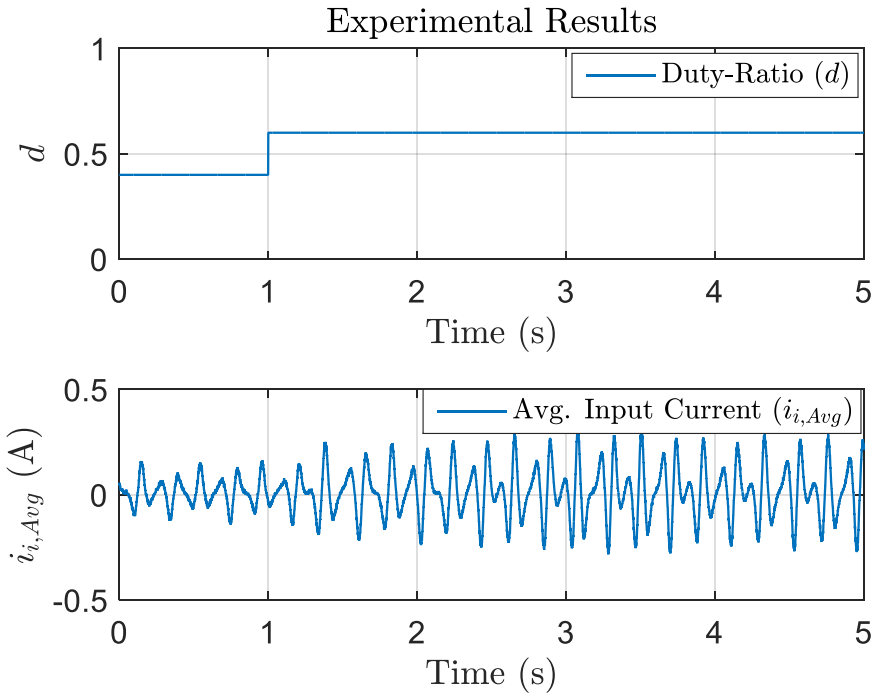

Figure 64. Average input current of the SBBC for the step input duty ratio by experment.

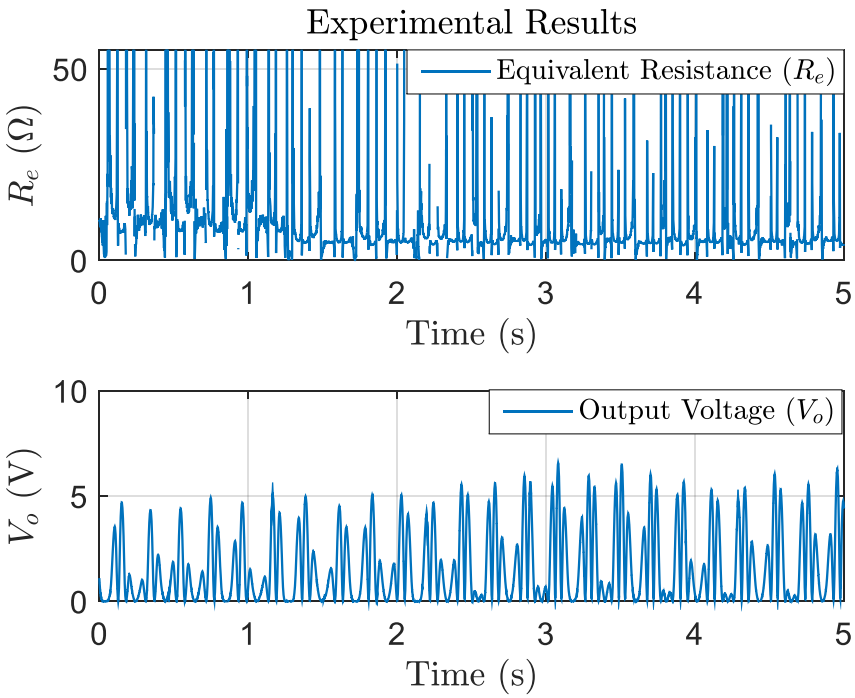

Figure 65. Equivalent resistance and output voltage of the SBBC for the step input duty ratio by experment.

3.4.2 Converter Controller Design

Since the SBBC could be simplified as a single boost converter, the same PI controller was used here were k_p =0.000228 s and $k_i = 2.4\ \mathrm{S \cdot s}$. However, the performances needed to be checked because switching from the positive to negative rectification cycle could have degraded the performance, and this performance verification is presented in section 3.4.3.

3.4.3 Closed-Loop Simulation Results

To validate the performance of the controller, the desired resistance was simulated by a square-wave signal that varied between 5 and 25 Ω. A block diagram of the SBBC controller is shown in Figure 66. This test was illustrated by the block diagram shown in

Figure 67. A Simulink® model was used in the closed-loop simulation shown in Figure 100 in Appendix A.2.

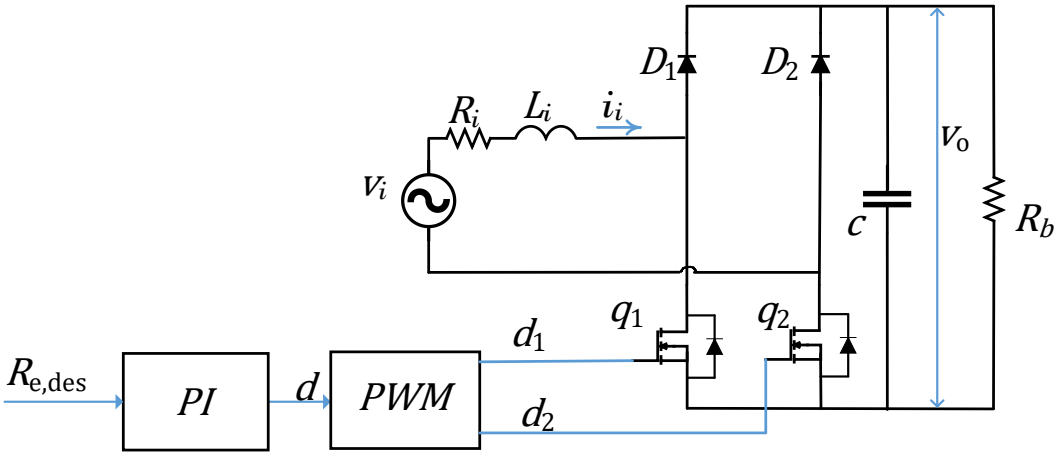

Figure 66. Closed-loop to control the equivalent resistance of the SBBC.

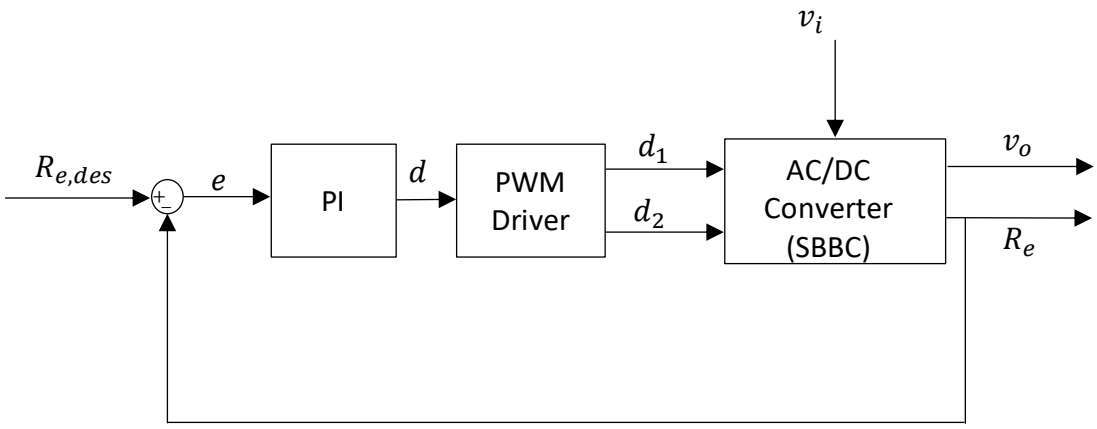

Figure 67. Block diagram for controlling the equivalent resistance of the SBBC.

The simulation results are shown in Figures 68 and 69. The results shown were acceptable for resistance, tracking the desired reference. The error signal was $\pm 8\ \Omega$.

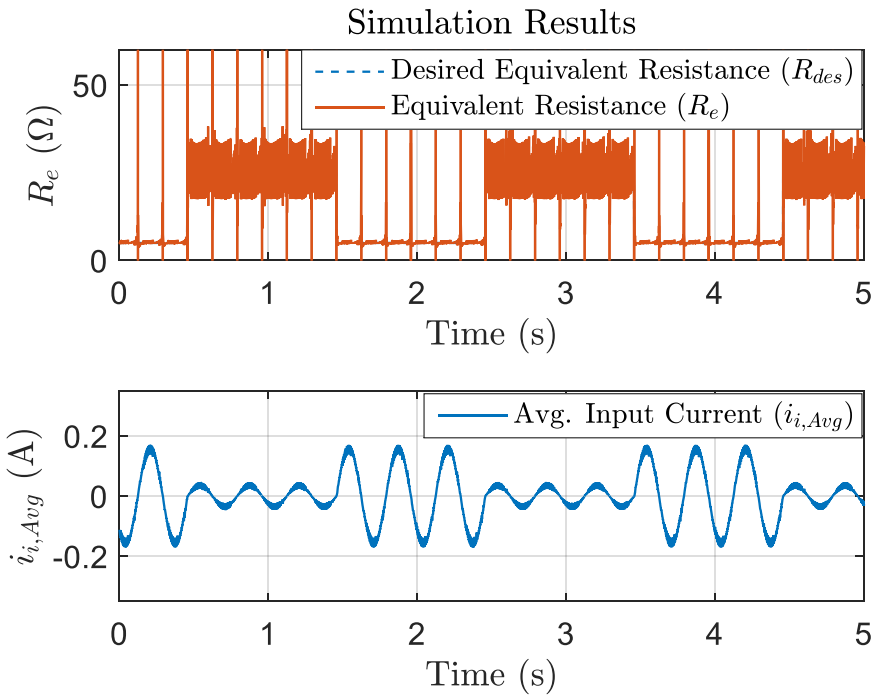

Figure 68. Equivalent resistance and average input current of the closed-loop SBBC by simulation for the desired square-wave reference input.

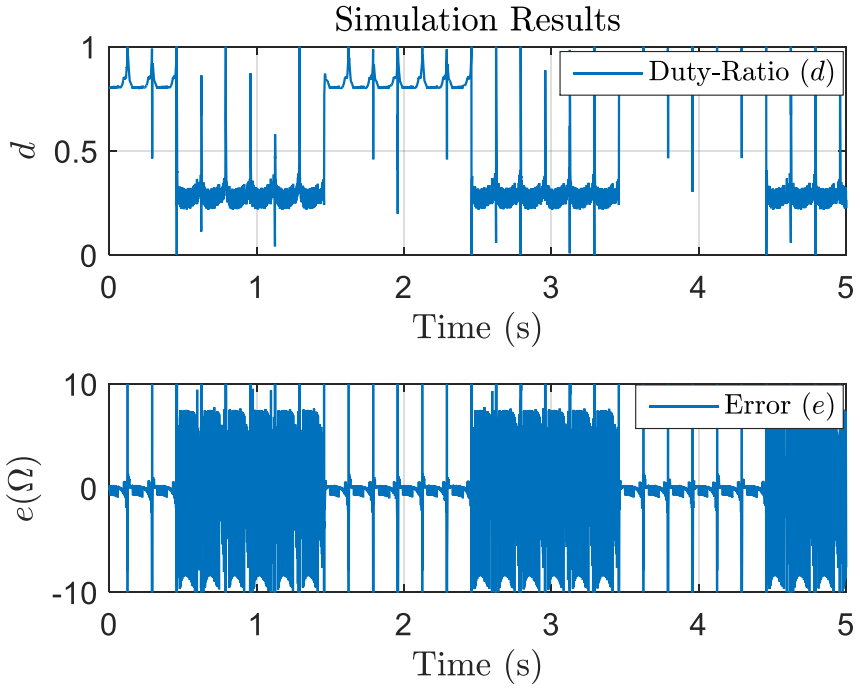

Figure 69. Duty-ratio and error of the closed-loop SBBC by simulation for the desired square-wave reference input.

Figures 70 and 71 show the experiment results. There was a slight variation primarily because the input voltage was not a pure sine wave.

The power electronic converter could now be used to change the EM damper's current, which led to changes in the damping force. The control input to this closed-loop test was the desired resistance. Another controller is needed to be designed to manipulate this value and described in the following chapter.

From these preliminary results, it was determined that the controller could only manipulate the output resistance in a range of 0 to no more than 70 Ω. The EM damper size used in this study was smaller than the damper used in an actual suspension. It was used here as proof of concept.

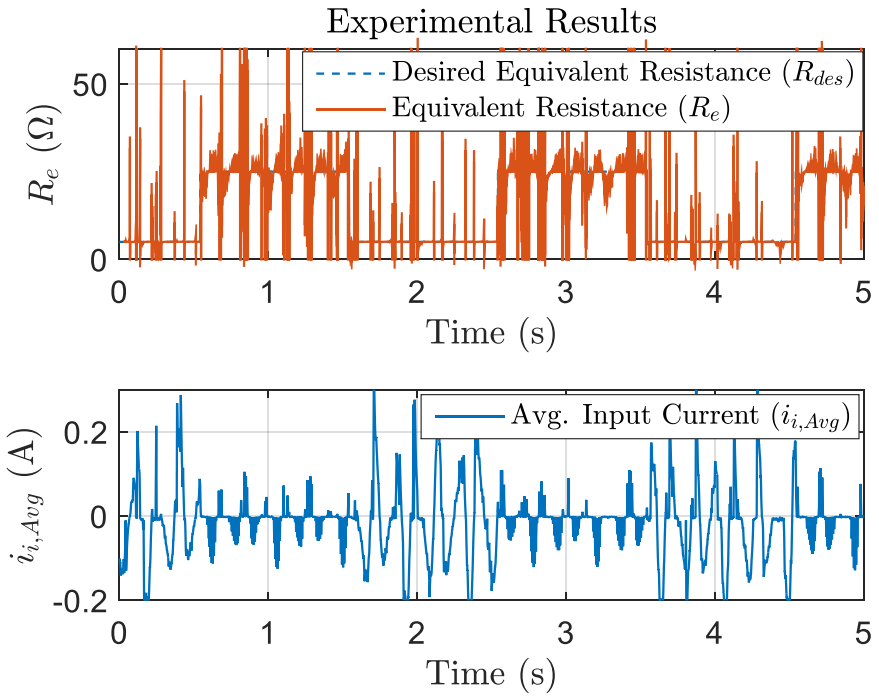

Figure 70. Equivalent resistance and average input current of the closed-loop SBBC by experment for the desired square-wave reference input.

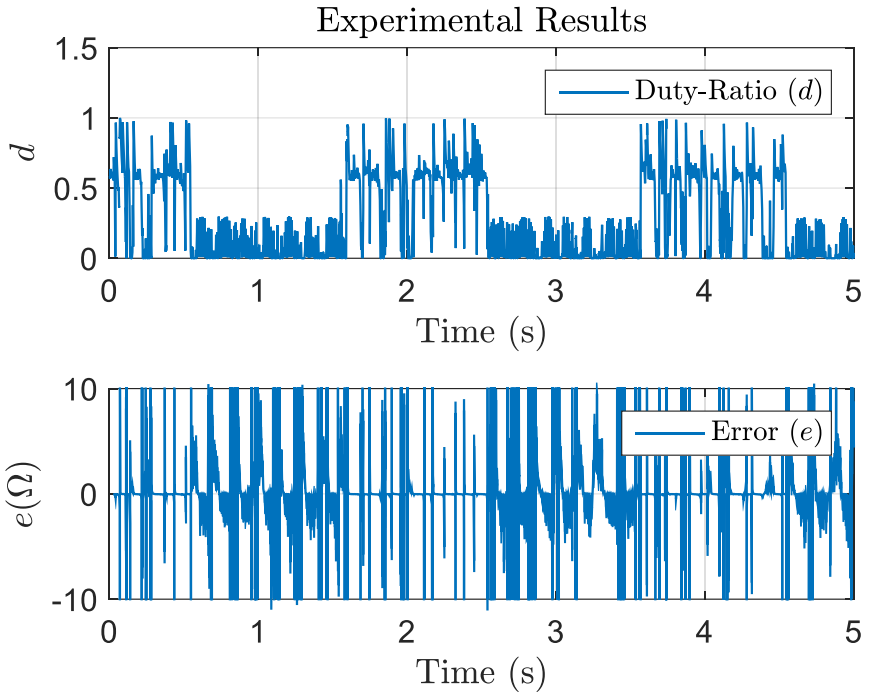

Figure 71. Duty-ratio and error of the closed-loop SBBC by experment for the desired square-wave reference input.

3.5 Summary

This chapter investigated the power electronic interface. An SBBC was determined to be a good candidate for regenerative suspension due to its few components and less control effort. The converter was modeled in a manner that kept the current and voltage in phase, for a maximum power factor. The motor's external load was purely represented as resistance. The generator could be considered a voltage source for energy-regeneration purposes.

CHAPTER IV

REGENERATIVE CONTROLLER DESIGN

4.1 Introduction

In the previous chapter, the modeling of the regenerative power converter was described. The controlled input to this converter was the duty ratio that could be used to control the equivalent resistance of the generator. The generated voltage v_i was the input disturbance to the converter control as shown in Figure 45. The results of this process were a variable damper and rectified output voltage. The regenerative mode was introduced in this research to replace the active mode, which enabled energy regeneration and vibration damping. Regenerative suspensions have frequently been the topic of research in the past two decades. However, yet no regenerative suspensions have been implemented in automobiles.

In this work, the regenerative suspension was measured according to the rider comfort index. The main assumption was that priority must be given to rider comfort, which led to a reduction in sprung-mass acceleration. The generator was not able to completely isolate the sprung-mass acceleration due to the small damping force. This meant that there was little energy left for harvesting. Therefore, a generator is needed to be redesigned to provide the required damping force.

The main objective of this regenerative controller design is to damp the sprung-mass vibrations; harvesting and tire holding were not considered. To achieve this goal, the following steps were followed:

- integration of the variable damper into the suspension,
- comparison of the active, regenerative, and passive forces using the rider comfort index; and
- application of the regenerative suspension controller

This chapter revisits the suspension model, updating it to include the regenerative damper. The results from the simulation and experimental results are also analyzed and discussed.

4.2 Regenerative System Modeling and Analysis

In this section, the quarter-car suspension system that was modeled in Chapter 2 and the converter modeled in Chapter 3 are combined into a single system. The active suspension system was replaced with a regenerative suspension system (Refer to Eq. (1).). The EM damping force (F_d) replaced the motor force F_{act} (Refer to Eq. (21).). The controlled variable for the regenerative control was the equivalent resistance R_e. The controller described in the following section varied the $R_{e,des}$ values according to the force needed to damp the vibration. The PI controller altered the generator current to make R_e equal to $R_{e,des}$ (Refer to Figure 72.).

$$F_d = k_p i_p = \frac{k_p V_p}{R_i + R_o} \text{ where; } R_e = R_i + R_o \tag{21}$$

Here, R_e was the equivalent resistance, which served as the input variable. The objective of the controller was not only to dampen the vibration (as in an active suspension), but also to harvest the vibrational energy. The control effort was the regenerative damping force F_d. The next section addresses the control law for manipulating this variable to achieve a higher level of rider comfort.

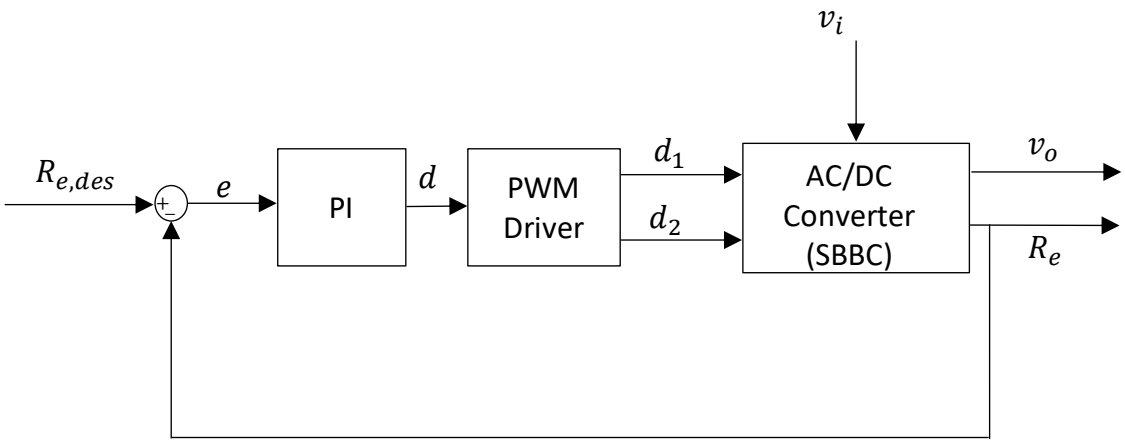

Figure 72. Block diagram for the EM regenerative damper replacing the active suspension.

4.3 Controller Design

This section describes the control law used for 2-DOF regenerative suspension. The EM damper was mounted between the sprung and unsprung masses, which were used to realize the skyhook damper. The skyhook damping-force law was as follows:

$$F_d = \begin{cases} c_{e,max} & \dot{x}_s \dot{z} \leq 0 \\ c_{e,min} & \dot{x}_s \dot{z} > 0 \end{cases} \quad (22)$$

where c_e is the EM damping coefficient. The regenerative damping force was always in the opposite direction of the relative velocity $\dot{z}$. When $\dot{z}$ and $\dot{x}_s$ were in the same direction, F_d could be usful for reducing $\dot{x}_s$. However, when $\dot{z}$ and $\dot{x}_s$ were in the opposite directions, F_d increased $\dot{x}_s$, which meant it increased the sprung-mass vibrations. Thus, the controller is needed to set the force to zero. Otherwise, the forces would increase the sprung mass vibrations. The vibration damping and energy regeneration was made feasible by using this control law. The regenerative controller could set F_d to zero when it worsened the vibration whereas in a passive suspension there is no control mechanism for turning this force off. This is one advantage to using a regenerative suspension over a passive one. This study experimentally tested this law.

Rakheja-Sankar [58] recommended another control law, which depends only on the relative displacement and velocity between the sprung and unsprung masses (z and $\dot{z}$). This could be simplified in an on-off control form, as shown in Eq. (22). The sprung-mass vibrations could be reduced if any force trying to move them was canceled. If the friction force was neglected, the only force trying to increase the sprung mass vibrations was the spring force. To overcome the effect of this spring force, [59] suggested that the damping force should oppose (or at least not increase) a spring force set by F_d to zero. However, F_d was not always equal to the spring force. The skyhook damping-force law could be simplified to the on/off form shown in Eq. (22). As described in the previous chapter, F_d

was at a maximum at $d = 1$, where (R_e) could be set to the smallest possible value of 0 Ω. On the other hand, F_d was at a minimum at $d = 0$, where R_e could be set to the highest possible value, such as infinity. We chose to set $R_e = 70\ \Omega$ because as shown in the converter design, this was the maximum value the controller could obtain, which meant that the generator's circuit was open with no current flowing to the load. With the high load connected to the converter output, the current reached zero.

$$F_d = \begin{cases} -k\ z & z\dot{z} \leq 0 \\ 0 & z\dot{z} > 0 \end{cases} \tag{23}$$

$$F_d = \begin{cases} c_e\ \dot{z} & \dot{x}_s\dot{z} \geq 0 \quad where;\ R_e = 0\ \Omega \\ 0 & \dot{x}_s\dot{z} < 0 \qquad\qquad R_e = 70\ \Omega \end{cases} \tag{24}$$

4.4 Implementation of the Regenerative Controller

4.4.1 Apparatus

This section describes the experimental setup used to implement the regenerative controller in the quarter-car testbed. The same apparatus that was previously used in the active suspension controller was also used here, in addition to the current sensor. The regenerative controller needed only the current sensor to measure the generator current required for the converter control.

Three PWM amplifiers made by Advanced Motion Controls managed the current passing through the coils of the active motor that was removed and replaced by the converter described in Chapter III. The converter took its input from Phase *C*. Each of phases *A* and *B* provided two MOSFET switches to block the current in a bidirectional fashion. The bidirectional current blocking was realized by two MOSFET switches that

connected the drain to the source. The same gate signal drove both on and off so that the body diodes blocked the current in the opposite direction. Phases *B* and *C* were employed here to utilize the full generator damping capability (Refer to Figure 73 and 74.). However, only Phase *C* was the measure of the regenerated energy. Figure 78 shows the experimental implementation layout used.

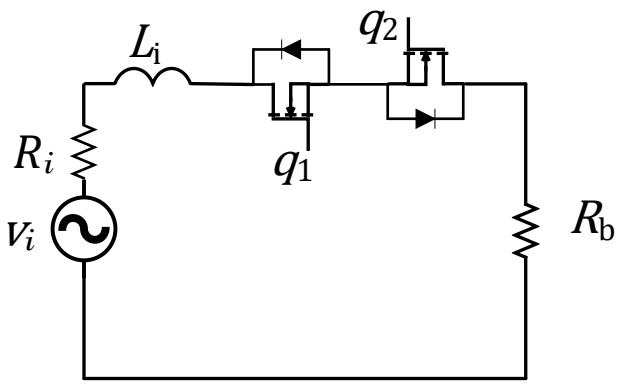

Figure 73. Phase *A* and *B* connections.

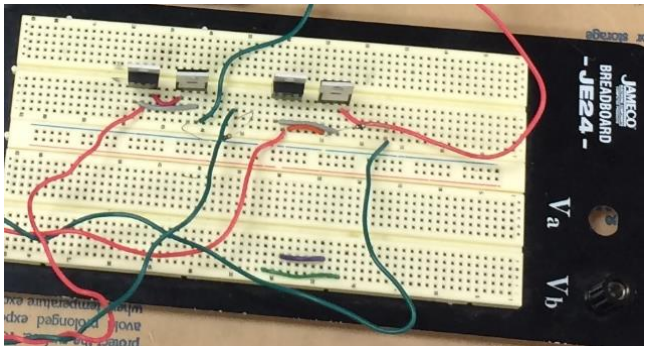

Figure 74. Phase *A* and *B* MOSFETs to block bidirectional currents flow.

Current Sensor is an Agilent 1146A Hall-effect probe that provided accurate measurements of currents from 100 mA to 100 A RMS, DC to 100 kHz, without breaking

the circuit. The Agilent 1146A used Hall-effect technology to measure AC and DC signals.

The motor shaft position was monitored with a laser distance sensor (Model OADM 20I6460/S14F by Baumer Electric), which had a resolution of 5 μm and measuring distance range from 30 mm to 130 mm (Refer to Figure 75.). The voltage supply was 12 V and the output voltage varied between 0 and 10 VDC. The output voltage was sent to the A/D channel of the DSP board and displayed in the user interface control panel. A laser sensor connection diagram is shown in Figure 76. The laser sensor took the place of the LVDT because it added no friction to the system.

Another way to estimate the relative velocity $\dot{z}$ was by measuring the damper-induced voltages using the motor model. However, this work used a laser sensor because the harvested energy was proportional to $\dot{z}$.

Figure 75. Laser distance sensor.

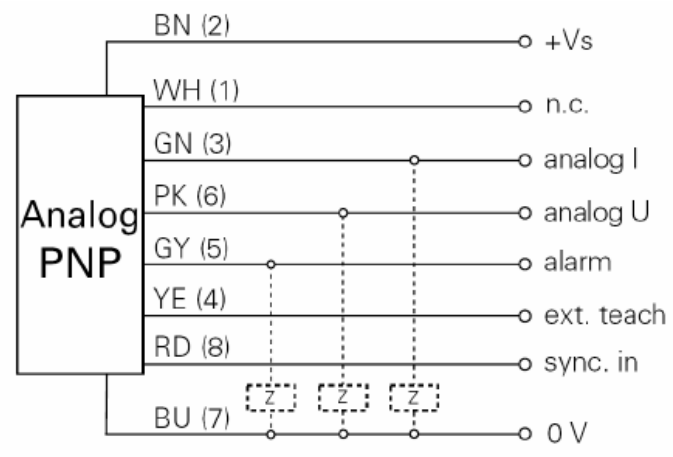

Figure 76. Laser sensor connection diagram

Figure 77 shows the regenerative suspension system experiment. The dSPACE PNC connector (CLP1104) used for all input and output signals. The regenerative controller designed in Simulink. Then, it executed in executed on real-time by the ControlDesk software. Refer to the experiment layout in Figure 79.

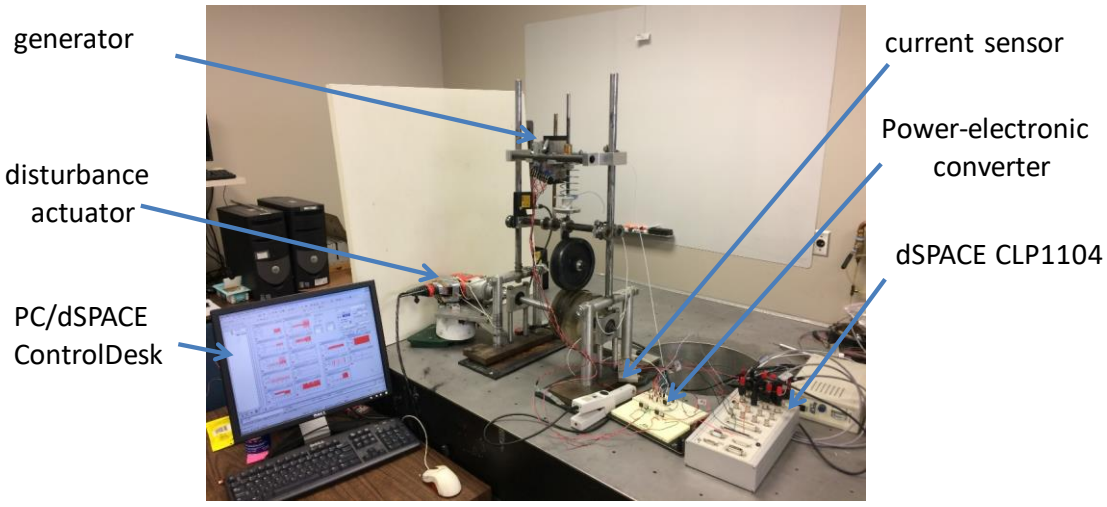

Figure 77. Laboratory experiments setup.

Figure 79 shows the experimental layout of the closed -loop. The three measurements from the quarter-car suspension were $\ddot{x}_s$, $\ddot{x}_{us}$, and z. The unsprung-mass acceleration was not necessary for the implementation of the regenerative controller. It was used in this research to show the effect, if any, of regeneration in the unsprang mass. The two acceleration measurements were performed by using the accelerometer from the active controller. Another three measurements from the electronic-interface appear in Figure 79 as v_i, i_i, and v_o. As discussed above, the SBBC was used only in Phase *C*. The generator phases connected separately and we assumed that all phases were balanced. The harvested power could be estimated with known v_o and R_b. However, the generator damping force was recognized by its effect on the sprung mass acceleration, which was compared when the system lost control. A Simulink®/dSPACE controller was used for the implementation. See Appendix B for more detailed information about this experiment.

At least four measurements $\ddot{x}_{us}$,v_i, v_c and v_g could be neglected. Measuring $\ddot{x}_{us}$ was not necessary for implementation of the regenerative controller, since $\ddot{x}_s$ and z were measured. The value for v_i could be estimated by knowing z and the motor model. However, $\ddot{x}_{us}$ was the measure for tire skipping, which could be used to monitor any violation of rider safety. Both v_c and v_g could be neglected by proper grounding in common between the load and the EM damper.

The components used to build the electronic interface were the same ones described in Chapter III. The generator was represented in this layout as a three-voltage source and only one EM damper (c_e). Therefore, using the SBBC and simply switching the generator produced the one EM damping force acting in the suspension. Only one voltage source was used to estimate the power regeneration.

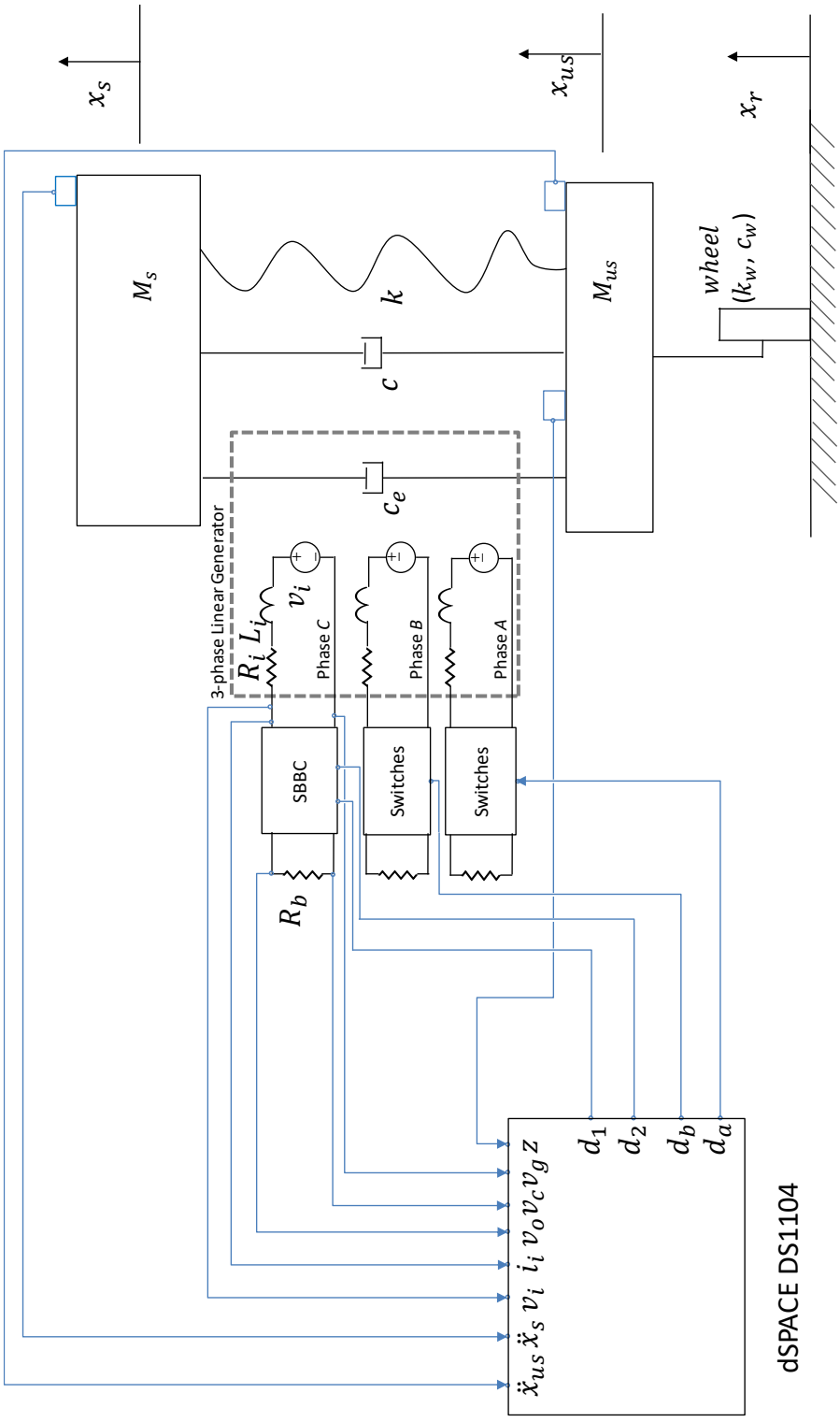

Figure 78. Layout of the closed-loop test.

4.4.2 Closed-Loop Controller Implementation Results

This section describes the experimental implementation of the skyhook control law discussed in the previous section. In Chapter II, the generator was used passively. Here, the objective of the generative controller was to enhance the EM damper effect, instead of just using it passively.

The block diagram for the closed-loop control is shown in Figure 79. The control law used here is represented by Eq. (24). The controlled variables are $R_{e,des}$ and d_{abc}. The previous chapter described the PI controller and where it varied the duty ratio d_c to track $R_{e,des}$ and the regenerative controller varied d_{abc}. For Phases *A* and *B*, a simple switch was introduced to change the internal currents so that each phase could produce the same damping force for the system. In this experiment, some assumptions were made. The phase differences between Phases *A* and *B* were neglected, and all three phases were balanced and could produce the same output power, as well as damping forces.

To study the effects of the controller, a switch was introduced to turn it on and off. The "off" status represented an open-loop for the EM damper, so no forces could have an effect.

The results shown include the first 5 seconds with the open-loop, which means that the resistor was much higher than the internal resistance. Here, R_{e} = 70 Ω was chosen because i_i reached zero, as shown in Figure 47. In the open-loop case, $d_{abc} = 0$. In the later 5 seconds, the regenerative controller worked to reduce vibration and increase energy regeneration.

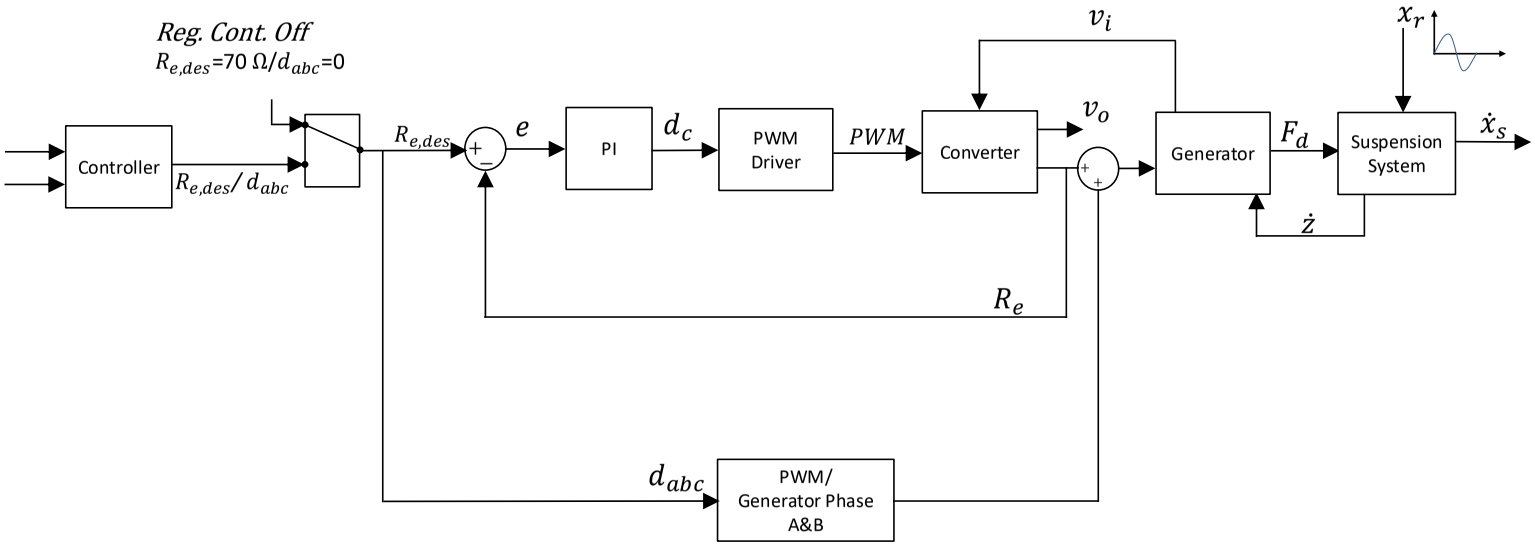

Figure 79. Regenerative control.

Figure 80 shows the duty-ratio d_{abc} and the generator current $i_{i,Avg}$. The d_{abc} variable switched on and off during the period when the controller was switched on. The average was $d_{abc,mean} = 0.6768$ whereas, the mean value of equivalent resistance $R_{\mathrm{e}} = 15\ \Omega$, which is close to the internal resistance $R_{\mathrm{i}} = 1.565\ \Omega$. This value for the duty-ratio was the best for regeneration and damping. An increase in d_{abc} could have worsened both damping and regeneration.

Figure 81 illustrates the generator variables v_i and v_{o}. The input voltage (v_i) was constant during all of the testing periods because the voltage across the generator terminal was considered as a voltage source. The output voltage was the voltage across the capacitor. The capacitor charged more during the uncontrolled periods whereas during the closed -loop the controller tried to use most of the available energy as a control input into the suspension system to reduce vibrations.

Figure 82 indicates the sprung-mass displacement x_s and velocity $\dot{x}_s$. The small damping force had a negligible effect on the sprung mass displacement because the controller was designed to reduce the acceleration (and not the displacement). The sprung mass velocity $\dot{x}_s$ also showed no change. The relative displacement z and velocity $\dot{z}$ showed no effect on the regenerative controller, as indicated in Figure 83. This was promising, because it underscored that energy regeneration would not be significantly reduced by the controller.

In Figure 84, the main measure of rider comfort $\ddot{x}_s$ is shown. The RMS value during the uncontrolled period was $\ddot{x}_{s,RMS} = 8.3\ \mathrm{m/s^2}$. However, during the control period it was $\ddot{x}_{s,RMS} = 7\ \mathrm{m/s^2}$, which means that the regenerative controller was successfully able to

recycle the power and reduce vibrations. Due to significant friction in the mechanical system, the regenerative damper only reduced vibrations by 23.52%. This amount of reduction was slightly more than what was estimated by the passive damper introduced in Chapter II. Conversely, the regenerative damper was unable to achieve the amount of reduction that the active damper could. The simulation results shown in Figure 84 indicate a small change in the unsprung mass acceleration amplitude. However, the tire skipping should be checked to avoid any violation of rider safety. Figure 85 shows the final results of this simulation study, the error and equivalent resistance of inner control loops of the SBBC control. The variable e was 5 Ω, which was acceptable and within the working range of 0–70 Ω. Moreover, R_e fluctuated during the last 5 seconds between high and low, which indicated some current flowing to the load.

The Simulink® model built to simulate the regenerative suspension is presented in Appendix B.1. Figure 101 illustrates all of the components of the closed-loop test. One SBBC was built to represent the dynamics of the converter under to the assumption that the three phases behaved in a similar manner. Combining the damping forces generated by the three-phase EM damper as one in the quarter-car model. The Figure also shows all 15 signals combined and send to MATLAB workspace for further analysis. Appendix B.1 also includes the MATLAB codes used to plot and analyze these signals. The quarter-car model for the regenerative suspension was identical to that which was used in Chapter II for the active suspension simulation. The only difference is that the actuator force F_{act} was replaced by the regenerative damping force F_d, as shown in Figure 102.

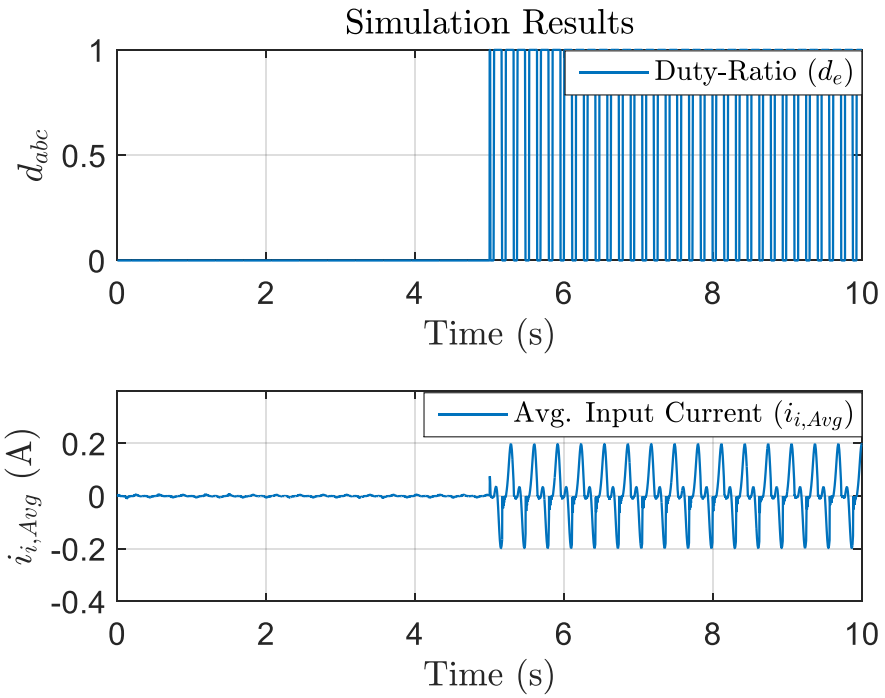

Figure 80. Regenerative control output variable and current by simulation.

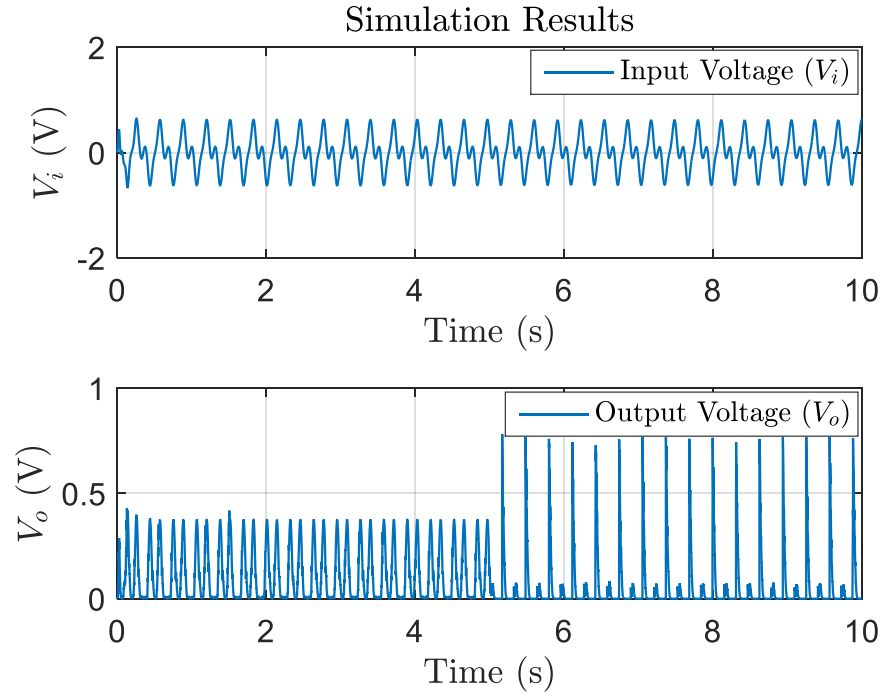

Figure 81. Input and output voltages by simulation.

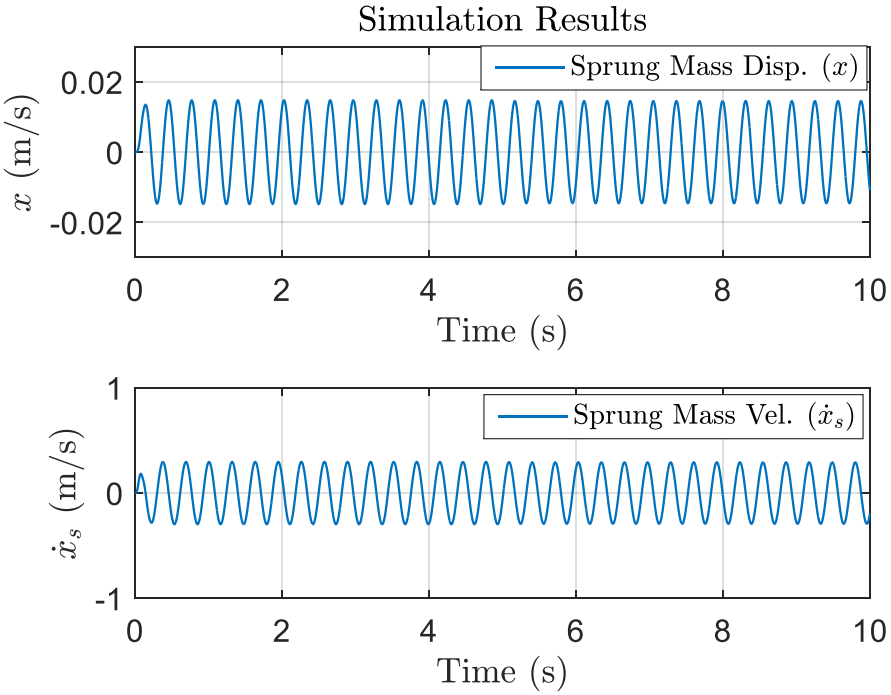

Figure 82. Sprung-mass displacement and velocity by simulation.

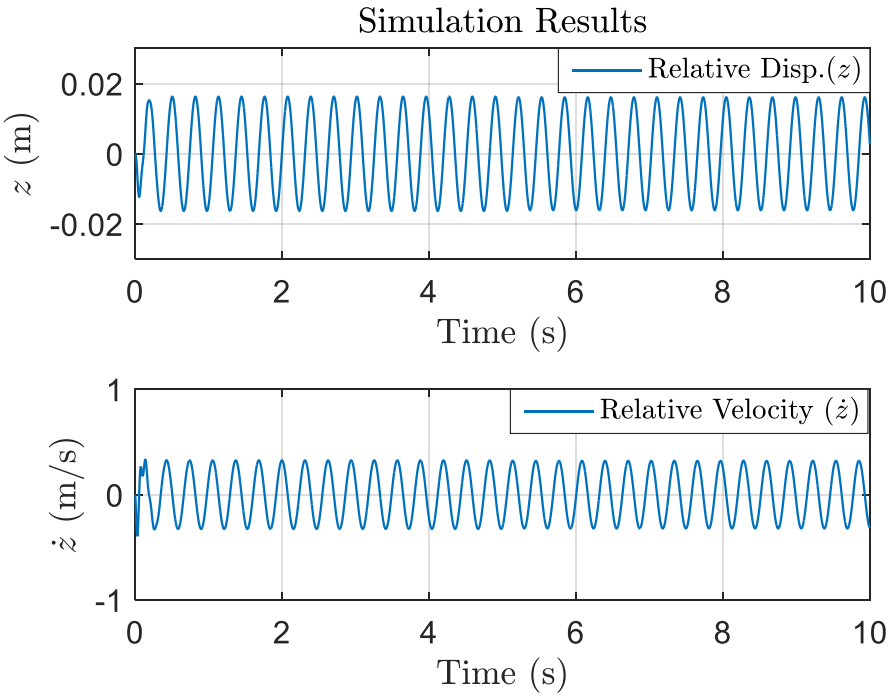

Figure 83. Relative displacement and velocity by simulation.

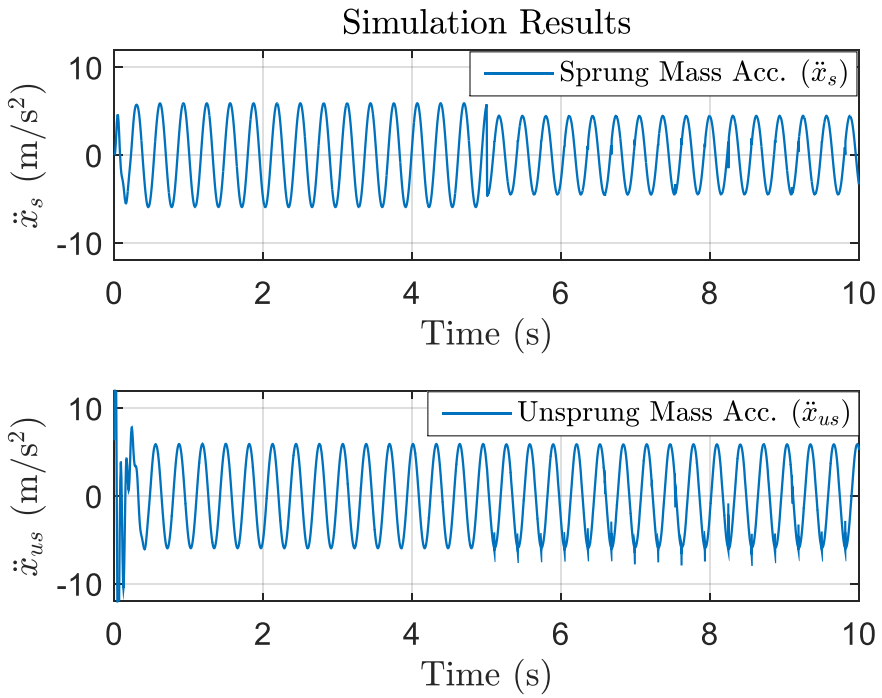

Figure 84. Sprung and unsprung-masses accelerations by simulation.

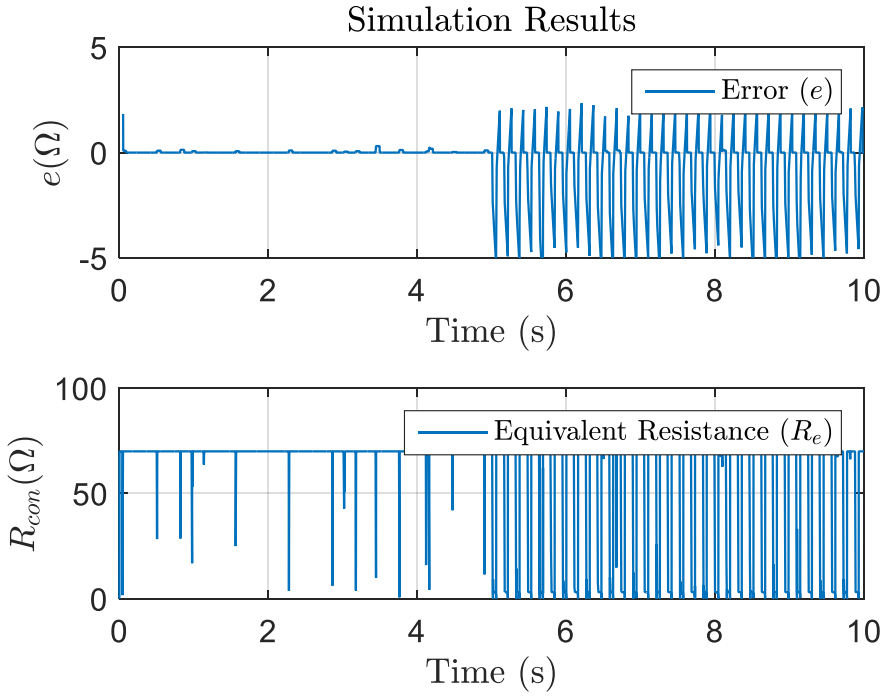

Figure 85. Converter control results—error and equivalent resistance.

Additional experiments were performed to verify the regenerative controller, which was designed to enhance rider comfort. Figure 86 shows the duty-ratio d_{abc} and the generator current $i_{i,Avg}$. The d_{abc} variable was switched on and off during the period when the controller was switched on. The average was $d_{abc} = 0.55$. This value for the duty-ratio was less than the value from the simulation. However, it was of a higher frequency, due to noise in the $\ddot{x}_s$ and $\dot{z}$ signals. The current flowing during the controller's "off" period was almost zero. When the controller was on, the current increased. The $i_{i,Avg}$ was close to the previously presented signal resulting from the simulation.

Figure 87 shows the generator variables v_i and v_o. The input voltage v_i was constant throughout the testing period. However, when the controller was on, the signals experienced more noise from the switching actions of the MOSFET. The output voltage v_o experience some noise. However, the RMS value was 0.62 V, which was close to the passive damper case. The output filter could be redesigned to reduce this noise.

Figure 88 shows the sprung-mass displacement x_s and velocity $\dot{x}_s$. The small damping force had a negligible effect on the sprung mass displacement and velocity. The relative displacement z and velocity $\dot{z}$ were shown to have no effect on the regenerative controller, as can be seen in Figure 89. The relative velocity RMS value was (0.2 m/s) for both periods. This was a promising indicator that the energy regeneration would not be reduced significantly with this controller.

Figure 90 indicates the main measure of rider comfort $\ddot{x}_s$. The RMS value during the uncontrolled period was $\ddot{x}_{s,RMS} = 8.35\ \mathrm{m/s^2}$. However, in the controlled period, it was $\ddot{x}_{s,RMS} = 7.05\ \mathrm{m/s^2}$. Both values were close to those in the simulation. The simulation

results showed that $\ddot{x}_{us}$ revealed no changes in the unsprung-mass acceleration amplitude. This signal showed that no sudden changes caused tire skipping, which meant that there was no violation of rider safety. Figure 91 illustrates the final results shown in this experiment, the error 3 Ω. Both were concerned with the inner control loop of the SBBC control. The R_e value during the last 5 seconds fluctuated between high and low, which indicated that there was some current flowing to the load.

The Simulink® model was built to run the regenerative suspension in a dSPACE environment; it is presented in Appendix B.2. Figure 103 shows all the components of the closed-loop. The first subsystem captured in Figure 104 shows the input signals coming from the ADC, containing $\ddot{x}_s$, $\ddot{x}_{us}$, v_o, v_g, v_i, z, and i_i. The filtered and offsetting signals were introduced as needed for the hardware, before they were used in the closed -loop. The regenerative control law discussed above was embedded as a MATLAB function. The outputs from the controller were $R_{e,des}$ and d_{abc} and could be estimated from one another, as shown in Eq. (24), which meant that only one controlled input was used here for the implementation of the regenerative suspension. The $R_{e,des}$ value was needed for use as a tracking reference for the converter's controller, as discussed in Chapter III. The d_{abc} variable was used as input for generator's phases A and B to vary the resistive load, as needed, and damp the sprung mass acceleration. Phases *A* and *B* used without the SBBC converter could encounter a reactive load, but for the sake of simplicity and because the internal inductor was small, the reactive load was assumed to be negligible.

For Phase C where the SBBC was used, the PI controller sent the duty ratio d_c to meet the desired reference tracking. This duty-ratio showed good values through the PWM

generation, as shown in Figure 105, before sending the PWM to the output. This process was necessary because v_i was not a DC signal. The PWM generation had a fundamental frequency of 1 kHz, which made it possible for the low frequency of v_i to be assumed a DC-DC converter. The v_i value's frequency depended on the tiered disturbance, which in practice was around 50 Hz.

The output PWM signals needed to be sent to the power MOSFETs, as shown in Figure 106. They were as follows:

- d_1 was needed for the positive signal of v_i for phase C.
- d_2 was needed for the negative signal of v_i for phase C.
- d_{abc} was needed to for the positive/negative signals of v_i for phases A and B.

Finally, the simulation and experimental signals for the sprung mass acceleration are presented in Figure 92. The sprung-mass acceleration was reduced by using the regenerative controller. The RMS value of the acceleration during the uncontrolled period was equal to 8.35 $\mathrm{m/s^2}$. When the controller was in place, the acceleration was reduced to 7.05 $\mathrm{m/s^2}$. This reduction represented approximately a 23.52% reduction when using the rider performance index. There was a slight improvement from using the EM damper as an active component. In the open-loop test discussed in the previous section, the reduction in sprung-mass acceleration was 21.46% whereas when using the regenerative, the damper made a slight improvement.

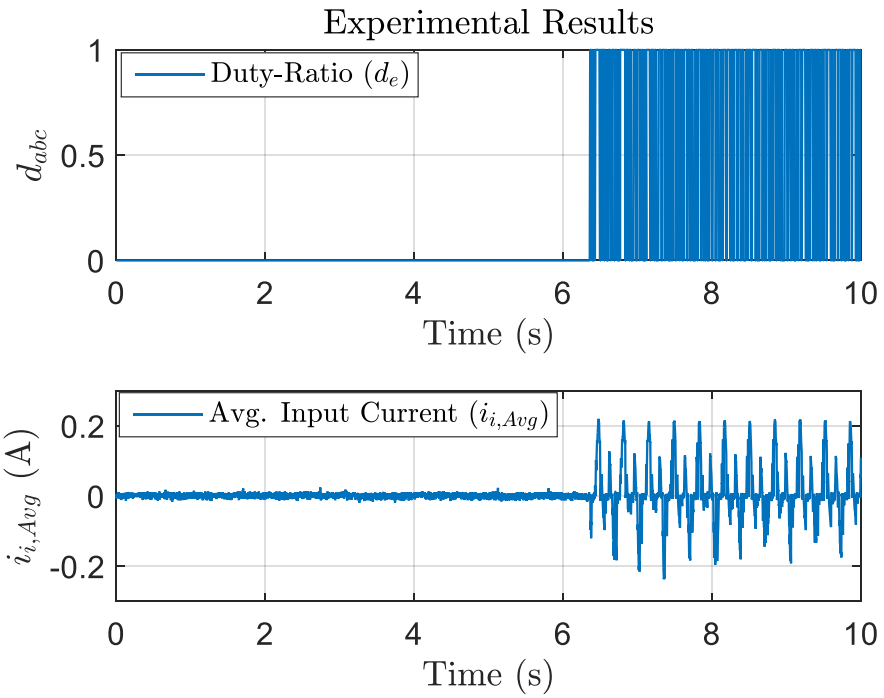

Figure 86. Resistance manipulated by the regenerative controller in the experiment and the input current.

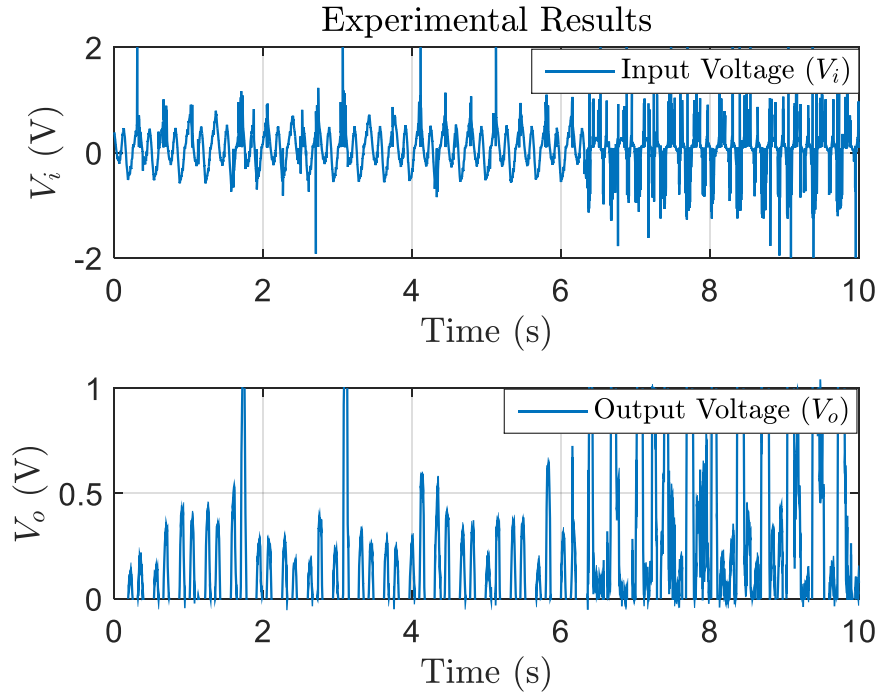

Figure 87. Input and output voltages in the experiment.

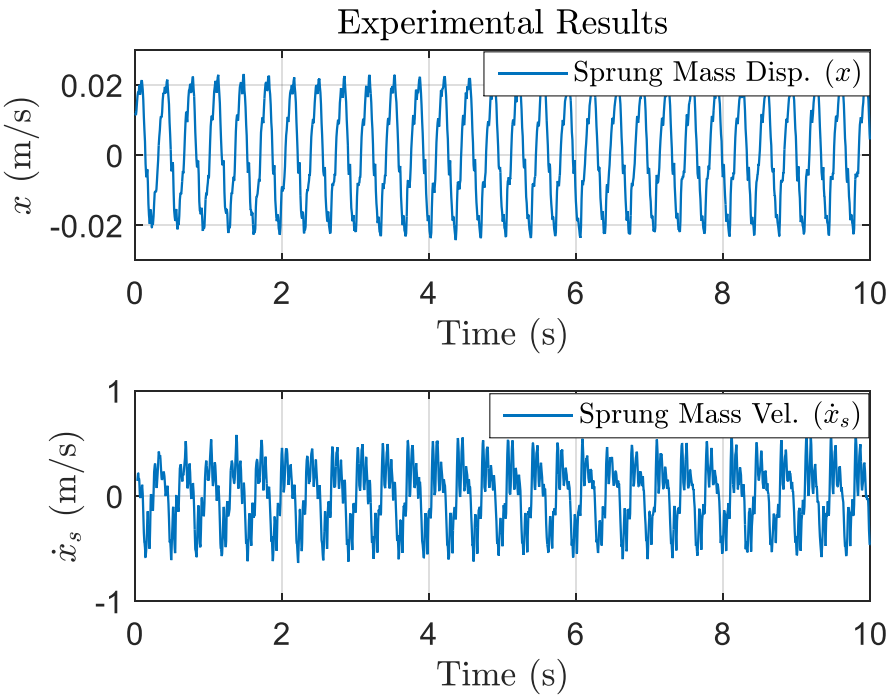

Figure 88. Sprung-mass displacement and velocity in the experiment.

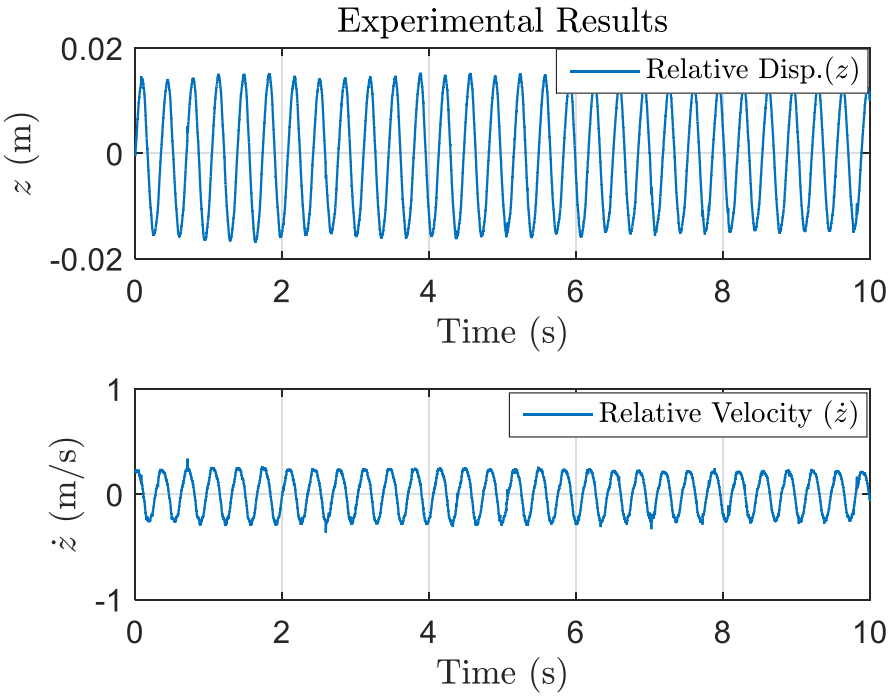

Figure 89. Relative displacement and velocity in the experiment.

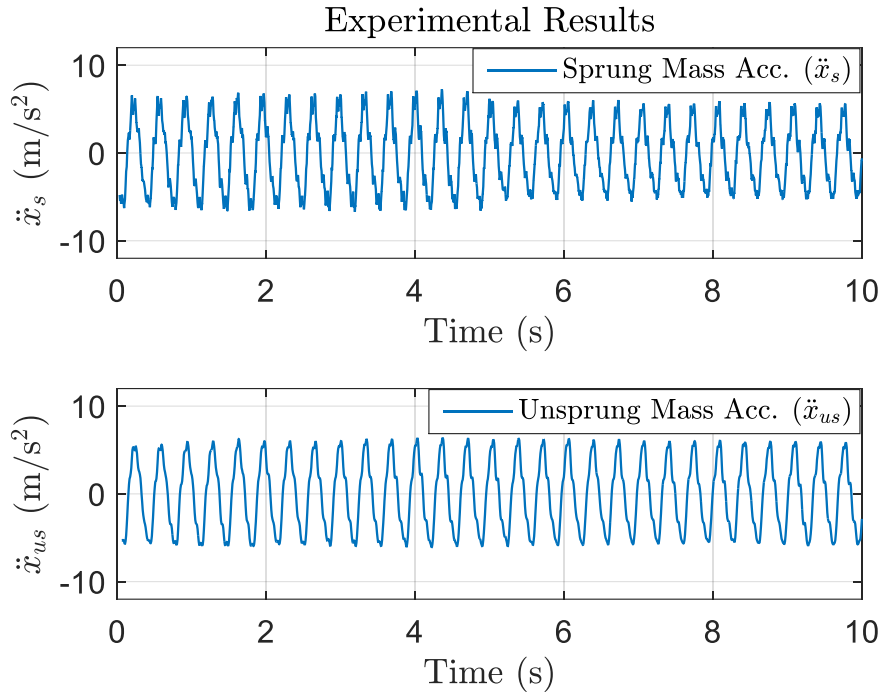

Figure 90. Sprung and unsprung-masses accelerations in the experiment.

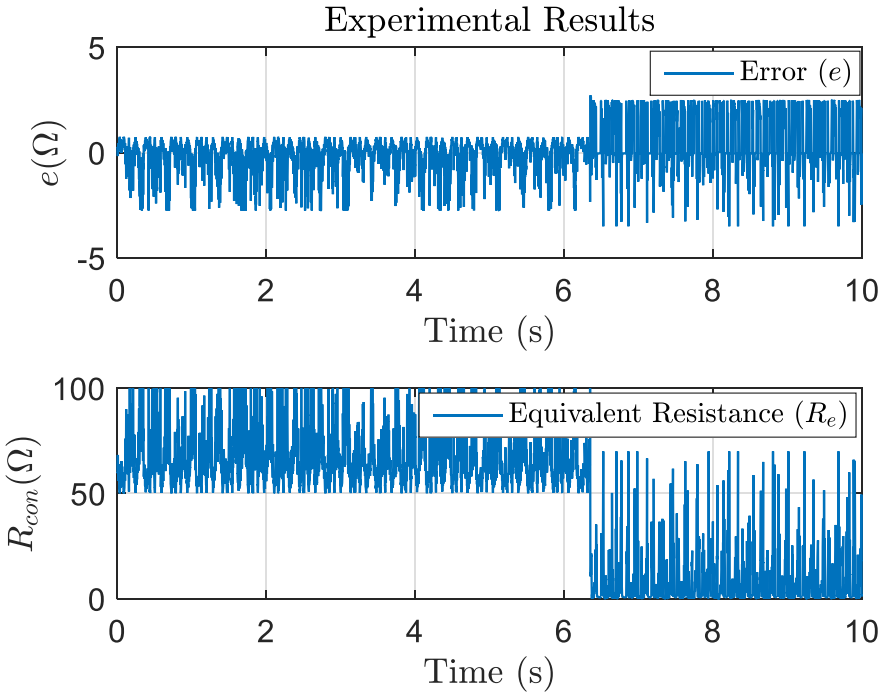

Figure 91. Error and equevelent resistance of the SBBC in the experiment.

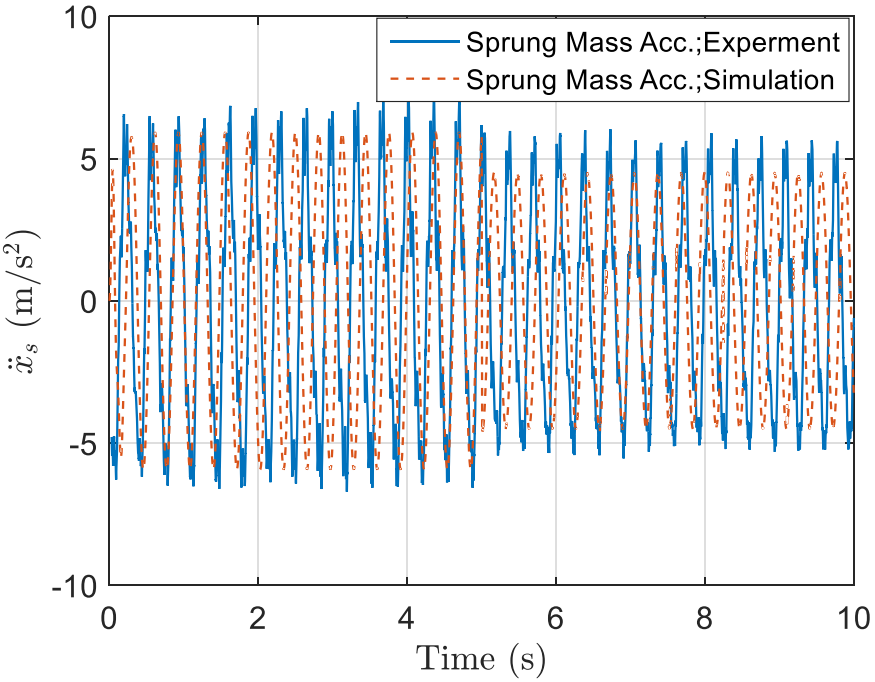

Figure 92. Sprung-mass acceleration for the simulation and experiment with a regenerative control.

4.5 Summary

- Regenerative suspension offers better results than passive suspension. This is because not all passive forces are useful in suppressing sprung-mass vibration. This improvement was small but could be better with a more efficient controller.
- The harvested energy was very small in this experiment. This is due to the inefficient damper that was used. However, in practice, the damper could be more efficient.
- The regenerative damper saved more energy than the passive damper in the same duration of time and could suppress more vibration.

- The active suspension offered the best performance. On the other hand, the regenerative suspension exhibited a moderate level of performance improvement and could also regenerate energy. A hybrid suspension system would combine the benefits of the active and regenerative designs.
- The regenerative suspension controller exhibited no rider safety violations, as measured by the sprung mass acceleration. However, further study should be done to introduce any necessary constraints to the regenerative controller.

CHAPTER V

CONCLUSIONS AND FUTURE WORK

5.1 Conclusions

All the energy indicators show that there is an increasing deficit in world resources. The demand for portable energy sources is also on the rise, inspiring the invention of energy harvesters and regenerative systems. This work dealt primarily with the modeling and control of regenerative suspension.

In this research, an active controller was designed for a quarter-car suspension testbed using a linear motor. During the experiment, a 69% improvement was achieved in rider comfort, which was measured by the reduction of sprung mass acceleration. The linear motor used 8 to 9 W of power during the experiment. The active suspension system was expensive to implement and required a power source. The regenerative suspension system saved energy that was otherwise spent in active suspension, approximately several kilowatts for a real car. Furthermore, the regenerative suspension could also regenerate energy.

A quarter-car testbed is widely used to experimentally develop various types of suspensions prior to conducting real-life experiments, because it captures the main dynamic characteristics of automobile suspensions. Experimental investigations were conducted in this research to determine the generator constants and damping coefficients. The generator damping effects and power regeneration were also investigated in the quarter-car test bed. The experiments showed that the linear regenerative damper could

suppress up to 22% of the vibrations and harvest 0.11 W of power at the matching impedance. From the initial study described in Chapter II regarding active and passive EM dampers, and since both harvesting and damping capabilities were noticeable in this testbed, further study is warranted on regenerative suspensions. A regenerative controller should be also developed to provide further rider comfort.

Before a regenerative controller can be implemented, however, an electronic interface must be designed to facilitate control of the regenerative force and storage of energy after the rectification process. Therefore, a power electronic interface must also be investigated. The SBBC was considered a good candidate for the regenerative suspension, due to its few components and even less control efforts. A power converter was then modeled in a manner that kept the current and voltage in phase for the maximum power factor. In the current research, the motor's external load was represented purely as resistance. The generator could be considered a voltage source for energy regeneration purposes.

The converter control was designed to vary the equivalent resistance and damping coefficient of to the suspension. This controller worked at a PWM carrier frequency of 1 kHz, which was much higher than road disturbance frequency (3.5 Hz). The objective of the regenerative controller was to manipulate the desired regenerative damping force. The combination of converter and regenerative controller was able to replace the active controller. This combination may look complicated but could be accomplished with only the addition of a current sensor.

The structure of the regenerative suspension controller was similar to one that is semi-active. Therefore, the literature on semi-active controllers was useful for designing the

regenerative controller. The regenerative controller was designed to improve vibration suppression and enhance energy-harvesting capabilities. The regenerative suspension system showed better results than the passive suspension system. This is because not all passive forces are useful in suppressing sprung-mass vibrations. The improvements were minimal; however, there was the potential for greater improvement with the addition of a more efficient EM damper. The harvested energy was so small in this experiment because the damper was inefficient. In practice, the damper's efficiency could be improved. Another limiting factor in increasing energy regeneration was the high mechanical friction inherent in by the suspension. The regenerative damper could save more energy than the passive damper, and at the same time suppress more vibrations. The regenerative controller was only able to recycle energy when it was needed for damping, and otherwise let the energy flow to the load.

The active suspension showed a superior performance. The regenerative suspension, on the other hand, had a modest performance but could regenerate energy. A hybrid suspension could combine the benefits of the active and regenerative systems.

5.2 Comparison of the Passive, Active, and Regenerative Controller Results

In Chapter 2, the same EM damper was originally designed as a motor for actively controlling the suspension. The results were high, as represented in the index performance. Table 7 shows the results of the same motor when it was used as active, regeneration, and

passive dampers. The active suspension achieved the highest performance in terms of rider comfort. However, it consumed more power than the energy produced from the input disturbance, which was 5 W. Regeneration achieved a much lower level of rider comfort than did the active suspension. On the other hand, regeneration introduced a slight improvement in the performance as compared to passive suspension. Also, the regenerated energy was low. However, this energy could be stored and reused for other applications, or for further improvement in this suspension system.

Table 7. Rider Performance Index and Powers of Different Controllers

Controller	Performance Index	Power (W) per Phase
Active	70%	-8
Regenerative	23.8%	0.11
Passive	21.46%	-

5.3 Future Work

In conducting the experiments for this dissertation, the system was found to be difficult to work with. The quarter-car suspension system was built mainly for use with active controllers, and it was difficult to convert the system to be compatible with a regenerative controller. An optimal suspension system should be designed to obtain all of the benefits of energy conversion, as well as the damping requirements. To achieve these results, the following should be pursued:

- The mechanical damping, which represents the friction and sliding forces, should be as small as possible. The EM damper will add some more damping, which should be taken into consideration.

- The EM damping at maximum harvestable power should be comparable to the mechanical damping.
- The EM damper should be able to increase the total damping in a controllable manner.

Recommendations for further study:

- Energy harvesting was briefly discussed here. It is recommended that it be studied in greater detail, especially in terms of energy storage. The switching of the converter occurs at high frequencies. There is a choice in capacitors and batteries parameters. They should be chosen to optimize the energy harvesting and damping.
- In this study, the motor was designed as an active actuator for suspension system. However, other pathways are worthy of investigation. If the actuator were designed as a regenerative damper, a complex design would have been required to increase the damping force with minimum friction. It would be helpful to develop a linear damper with greater force than the prototype damper. The linear actuator would have the advantage of producing the EM force without increasing the mechanical friction, as is the case with the rotary actuator.
- The electronic power converter was challenging to work with because of the suspension system low-power regeneration. The regenerative interface requires additional detailed investigation, especially in terms of applying the

four-quadrant converter such that the power can flow in a bidirectional way. This type of converter is required for a self-powered suspension system.

REFERENCES

[1] Outlook, A. E., 2016, "International Energy Outlook 2016," U.S. Department of Energy, Washington, DC.

[2] Ozkop, E. and Altas, I. H., 2017, "Control, Power and Electrical Components in Wave Energy Conversion Systems: A Review of the Technologies," Renewable and Sustainable Energy Reviews, **67**, pp. 106–115.

[3] Hedrick, M. D. J., "Implementation of an Active Suspension, Preview Controller for Improved Ride Comfort." *Nonlinear and Hybrid Systems in Automotive Control.* R. Johansson, Rantzer, Anders ed. 2001

[4] Zuo, L. and Tang, X., 2013, "Large-Scale Vibration Energy Harvesting," Journal of Intelligent Material Systems and Structures, **24**(11), pp. 1405–1430.

[5] Zhu, S., Shen, W.-A. and Xu, Y.-L., 2012, "Linear Electromagnetic Devices for Vibration Damping and Energy Harvesting: Modeling and Testing," Engineering Structures, **34**, pp. 198–212.

[6] Zeng, P. and Khaligh, A., 2013, "A Permanent-Magnet Linear Motion Driven Kinetic Energy Harvester," IEEE Transactions on Industrial Electronics, **60**(12), pp. 5737–5746.

[7] Segel, L. and Lu, X., 1982, "Vehicular Resistance to Motion as Influenced by Road Roughness and Highway Alignment," Australian Road Research, **12**(4), pp. 211–222.

[8] Browne, A. and Hamburg, J., "On Road Measurement of the Energy Dissipated in Automotive Shock Absorbers," Symposium on Simulation and Control of Ground Vehicles and Transportation Systems, Anaheim CA, USA, pp. 167–186.

[9] Montazeri-Gh, M. and Soleymani, M., 2010, "Investigation of the Energy Regeneration of Active Suspension System in Hybrid Electric Vehicles," IEEE Transactions on Industrial Electronics, **57**(3), pp. 918–925.

[10] Zuo, L. and Zhang, P.-S., 2013, "Energy Harvesting, Ride Comfort, and Road Handling of Regenerative Vehicle Suspensions," Journal of Vibration and Acoustics, **135**(1), pp. 011002–011010.

[11] Niu, P., Chapman, P., DiBerardino, L. and Hsiao-Wecksler, E., "Design and Optimization of a Biomechanical Energy Harvesting Device," Power Electronics Specialists Conference, 2008. PESC 2008, IEEE, pp. 4062–4069.

[12] Zeng, P., 2011, "Design and Analysis of an Unconventional Permanent Magnet Linear Machine for Energy Harvesting," Ph.D. thesis, Illinois Institute of Technology.

[13] Rajasekaran, A., Hande, A. and Bhatia, D., 2008, "Buck-Boost Converter Based Power Conditioning Circuit for Low Excitation Vibrational Energy Harvesting," Third Annual Austin Conference on Integrated Circuits and Systems, Austin, TX.

[14] Ottman, G. K., Hofmann, H. F., Bhatt, A. C. and Lesieutre, G. A., 2002, "Adaptive Piezoelectric Energy Harvesting Circuit for Wireless Remote Power Supply," IEEE Transactions on Power Electronics, **17**(5), pp. 669–676.

[15] Luan, H., Onar, O. C. and Khaligh, A., "Dynamic Modeling and Optimum Load Control of a Pm Linear Generator for Ocean Wave Energy Harvesting Application," Applied Power Electronics Conference and Exposition, 2009. APEC 2009. Twenty-Fourth Annual IEEE, IEEE, pp. 739–743.

[16] Graves, K. E., 2000, "Electromagnetic Energy Regenerative Vibration Damping," Ph.D. thesis, Swinburne University of Technology.

[17] Suntio, T., *Dynamic Profile of Switched-Mode Converter: Modeling, Analysis and Control*. John Wiley & Sons, 2009

[18] Asai, T., Araki, Y. and Ikago, K., 2017, "Energy Harvesting Potential of Tuned Inertial Mass Electromagnetic Transducers," Mechanical Systems and Signal Processing, **84**, pp. 659–672.

[19] Sabzehgar, R. and Moallem, M., 2013, "A Boost-Type Power Converter for Energy-Regenerative Damping," IEEE/ASME Transactions on Mechatronics, **18**(2), pp. 725–732.

[20] Figueiredo, J. P. M., Tofoli, F. L. and Silva, B. L. A., "A Review of Single-Phase Pfc Topologies Based on the Boost Converter," Industry Applications (INDUSCON), 2010 9th IEEE/IAS International Conference on, IEEE, pp. 1–6.

[21] Savaresi, S. M., Poussot-Vassal, C., Spelta, C., Sename, O. and Dugard, L., *Semi-Active Suspension Control Design for Vehicles*. Elsevier, 2010

[22] Bullock, K. J., 1989, "The Technological Constraints of Mass, Volume, Dynamic Power Range and Energy Capacity on the Viability of Hybrid and Electric Vehicles," No. 0148-7191, SAE Technical Paper.

[23] Karnopp, D., 1989, "Permanent Magnet Linear Motors Used as Variable Mechanical Dampers for Vehicle Suspensions," Vehicle System Dynamics, **18**(4), pp. 187–200.

[24] Ryba, D., 1993, "Semi-Active Damping with an Electromagnetic Force Generator," Vehicle System Dynamics, **22**(2), pp. 79–95.

[25] Suda, Y. and Shiiba, T., 1996, "A New Hybrid Suspension System with Active Control and Energy Regeneration," Vehicle System Dynamics, **25**(S1), pp. 641–654.

[26] Okada, Y. and Harada, H., 1995, "Active and Regenerative Control of Electrodynamic Vibration Damper," Proceedings of the 1995 Design Engineering Technical Conferences, pp. 84–83.

[27] Okada, Y. and Harada, H., 1996, "Regenerative Control of Active Vibration Damper and Suspension Systems," Proceedings of the 35th IEEE Conference on Decision and Control, IEEE, pp. 4715–4720.

[28] Okada, Y., Harada, H. and Suzuki, K., 1996, "Active and Regenerative Control of Linear Dc Motor Type Damper," Proceedings of the Third International Conference on Motion and Vibration Control, pp. 1–6.

[29] Okada, Y., Harada, H. and Suzuki, K., 1997, "Active and Regenerative Control of an Electrodynamic-Type Suspension," JSME International Journal Series C Mechanical Systems, Machine Elements and Manufacturing, **40**(2), pp. 272–278.

[30] Suda, Y., Nakadai, S. and Nakano, K., 1998, "Study on the Self-Powered Active Vibration Control," ratio, **10**, p. 9.

[31] Martins, I., Esteves, M., Da Silva, F. P. and Verdelho, P., "Electromagnetic Hybrid Active-Passive Vehicle Suspension System," Vehicular Technology Conference, 1999 IEEE 49th, IEEE, pp. 2273–2277.

[32] Martins, I., Esteves, J., Marques, G. D. and Da Silva, F. P., 2006, "Permanent-Magnets Linear Actuators Applicability in Automobile Active Suspensions," IEEE Transactions on Vehicular Technology, **55**(1), pp. 86–94.

[33] Nakano, K., Suda, Y. and Nakadai, S., 2003, "Self-Powered Active Vibration Control Using a Single Electric Actuator," Journal of Sound and Vibration, **260**(2), pp. 213–235.

[34] Gupta, A., Mulcahy, T. and Hull, J., 2003, "Electromagnetic Shock Absorbers," Proceedings of 21th International Modal Analysis Conference Kissimmee, FL, USA.

[35] Gupta, A., Jendrzejczyk, J., Mulcahy, T. and Hull, J., 2006, "Design of Electromagnetic Shock Absorbers," International Journal of Mechanics and Materials in Design, **3**(3), pp. 285–291.

[36] Suda, Y., Shiiba, T., Hio, K., Kawamoto, Y., Kondo, T. and Yamagata, H., 2004, "Study on Electromagnetic Damper for Automobiles with Nonlinear Damping Force Characteristics:(Road Test and Theoretical Analysis)," Vehicle System Dynamics, **41**, pp. 637–646.

[37] Nakano, K., 2004, "Combined Type Self-Powered Active Vibration Control of Truck Cabins," Vehicle System Dynamics, **41**(6), pp. 449–473.

[38] Jones, W., 2005, "Easy Ride: Bose Corp. Uses Speaker Technology to Give Cars Adaptive Suspension," IEEE Spectrum, **42**(5), pp. 12–14.

[39] Kawamoto, Y., Suda, Y., Inoue, H. and Kondo, T., 2007, "Modeling of Electromagnetic Damper for Automobile Suspension," Journal of System Design and Dynamics, **1**(3), pp. 524–535.

[40] Zhang, Y., Huang, K., Yu, F., Gu, Y. and Li, D., "Experimental Verification of Energy-Regenerative Feasibility for an Automotive Electrical Suspension System," Vehicular Electronics and Safety, 2007. ICVES. IEEE International Conference on, IEEE, pp. 1–5.

[41] Stribrsky, A., Hyniova, K., Honcu, J. and Kruczek, A., "Energy Recuperation in Automotive Active Suspension Systems with Linear Electric Motor," Control & Automation, 2007. MED'07. Mediterranean Conference on, IEEE, pp. 1–5.

[42] Zhang, Y., Yu, F. and Huang, K., 2009, "Permanent-Magnet Dc Motor Actuators Application in Automotive Energy-Regenerative Active Suspensions," No. 0148-7191, SAE Technical Paper.

[43] Wang, Z., Chen, Z. and Spencer, B. F., "Self-Powered and Sensing Control System Based on Mr Damper: Presentation and Application," SPIE Smart Structures and Materials+ Nondestructive Evaluation and Health Monitoring, International Society for Optics and Photonics, pp. 729240–729240–729210.

[44] Choi, Y.-T. and Wereley, N. M., 2009, "Self-Powered Magnetorheological Dampers," Journal of Vibration and Acoustics, **131**(4), p. 044501.

[45] Ebrahimi, B., Bolandhemmat, H., Khamesee, M. B. and Golnaraghi, F., 2011, "A Hybrid Electromagnetic Shock Absorber for Active Vehicle Suspension Systems," Vehicle System Dynamics, **49**(1-2), pp. 311–332.

[46] David, S. B. and Bobrovsky, B. Z., 2011, "Actively Controlled Vehicle Suspension with Energy Regeneration Capabilities," Vehicle System Dynamics, **49**(6), pp. 833–854.

[47] Cassidy, I. L., 2012, "Control of Vibratory Energy Harvesters in the Presence of Nonlinearities and Power-Flow Constraints," Ph.D. thesis, Duke University.

[48] Li, Z., Zuo, L., Luhrs, G., Lin, L. and Qin, Y., 2013, "Electromagnetic Energy-Harvesting Shock Absorbers: Design, Modeling, and Road Tests," IEEE Transactions on Vehicular Technology, **62**(3), pp. 1065–1074.

[49] Singal, K. and Rajamani, R., 2013, "Zero-Energy Active Suspension System for Automobiles with Adaptive Sky-Hook Damping," Journal of Vibration and Acoustics, **135**(1), p. 011011.

[50] Sabzehgar, R., Maravandi, A. and Moallem, M., 2014, "Energy Regenerative Suspension Using an Algebraic Screw Linkage Mechanism," IEEE/ASME Transactions on Mechatronics, **19**(4), pp. 1251–1259.

[51] Roshan, Y. M., Maravandi, A. and Moallem, M., 2015, "Power Electronics Control of an Energy Regenerative Mechatronic Damper," IEEE Transactions on Industrial Electronics, **62**(5), pp. 3052–3060.

[52] Karnopp, D., Crosby, M. J. and Harwood, R., 1974, "Vibration Control Using Semi-Active Force Generators," Journal of Engineering for Industry, **96**(2), pp. 619–626.

[53] Huang, B., 2016, "An Energy-Regenerative Vehicle Suspension System–Development, Optimization, and Improvement," Ph.D. thesis, Simon Fraser University.

[54] Montazeri-Gh, M. and Kavianipour, O., 2014, "Investigation of the Active Electromagnetic Suspension System Considering Hybrid Control Strategy," Proceedings of the Institution of Mechanical Engineers, Part C: Journal of Mechanical Engineering Science, **228**(10), pp. 1658–1669.

[55] Lee, S. and Kim, W.-J., 2010, "Active Suspension Control with Direct-Drive Tubular Linear Brushless Permanent-Magnet Motor," IEEE Transactions on Control Systems Technology **18**(4), pp. 859–870.

[56] Allen, J. A., 2008, "Design of Active Suspension Control Based Upon Use of Tubular Linear Motor and Quarter-Car Model," M.S. thesis, Texas A&M University.

[57] Kim, W.-J. and Murphy, B. C., 2004, "Development of a Novel Direct-Drive Tubular Linear Brushless Permanent-Magnet Motor," International Journal of Control Automation and Systems, **2**, pp. 279–288.

[58] Erickson, R. W. and Maksimovic, D., *Fundamentals of Power Electronics*. Springer Science & Business Media, 2007

[59] Alanoly, J. and Sankar, S., 1987, "A New Concept in Semi-Active Vibration Isolation," Journal of Mechanisms, Transmissions, and Automation in Design, **109**(2), pp. 242–247.

APPENDIX A

CHAPTER III MATLAB/SIMULINK® FILES

A.1 Chapter III Simulations Files (Boost Converter)

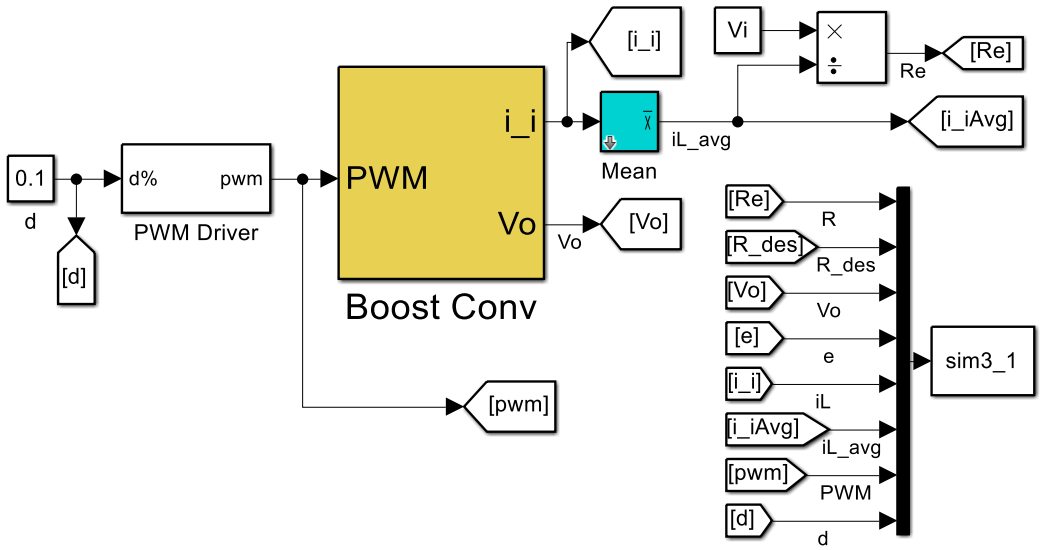

Figure 93. Open-loop boost converter test.

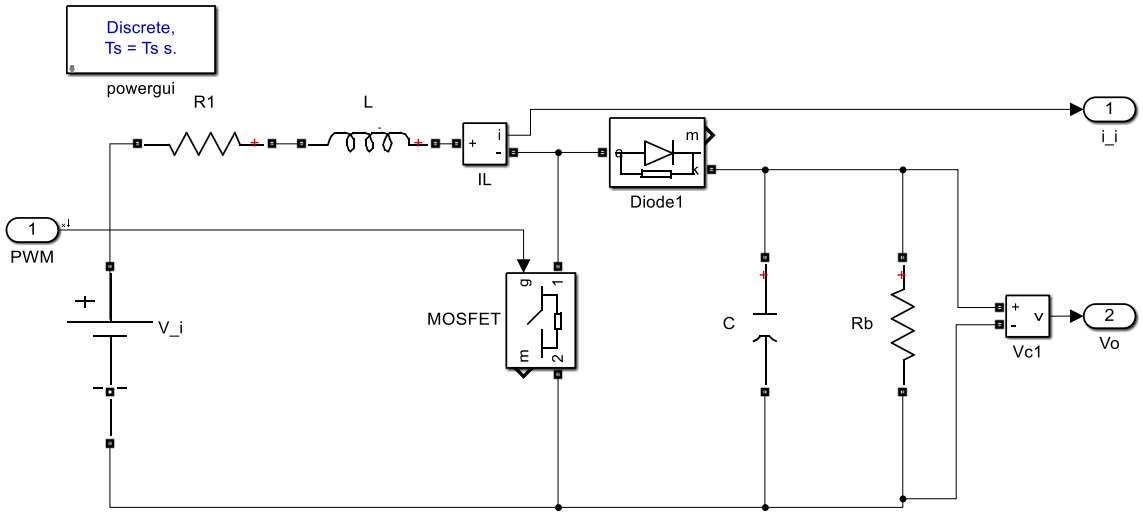

Figure 94. Boost converter model.

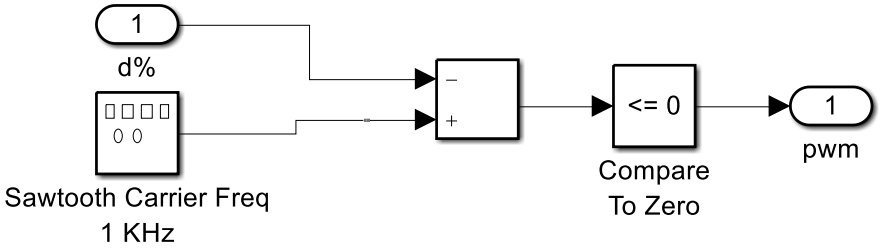

Figure 95. Pulse-width driver.

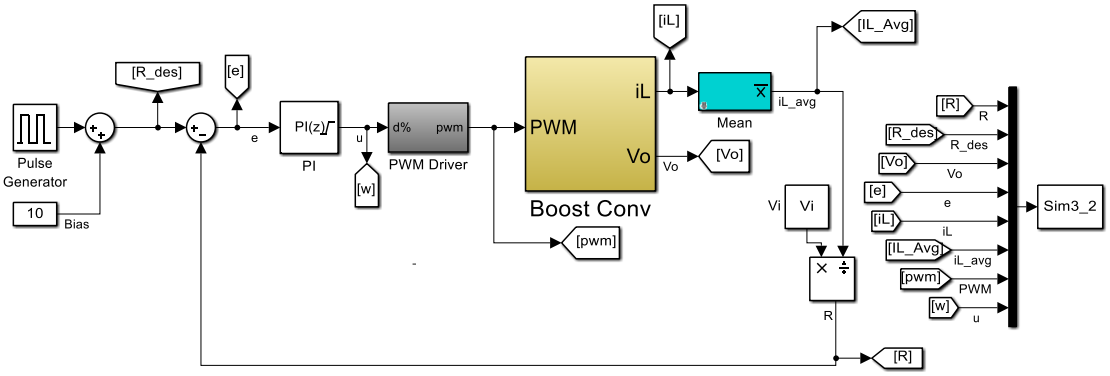

Figure 96. Boost converter equivalent resistance control.

A.2 Chapter III Experiments Files (SBBC)

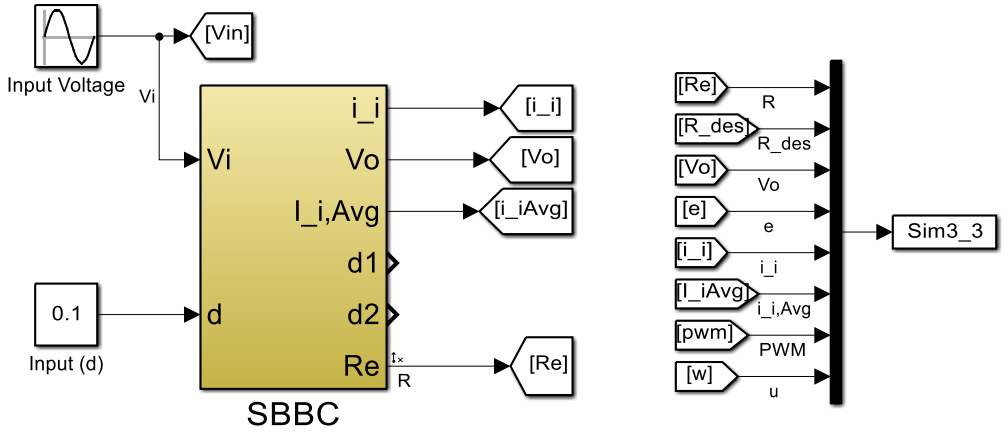

Figure 97. Open-loop SBBC test.

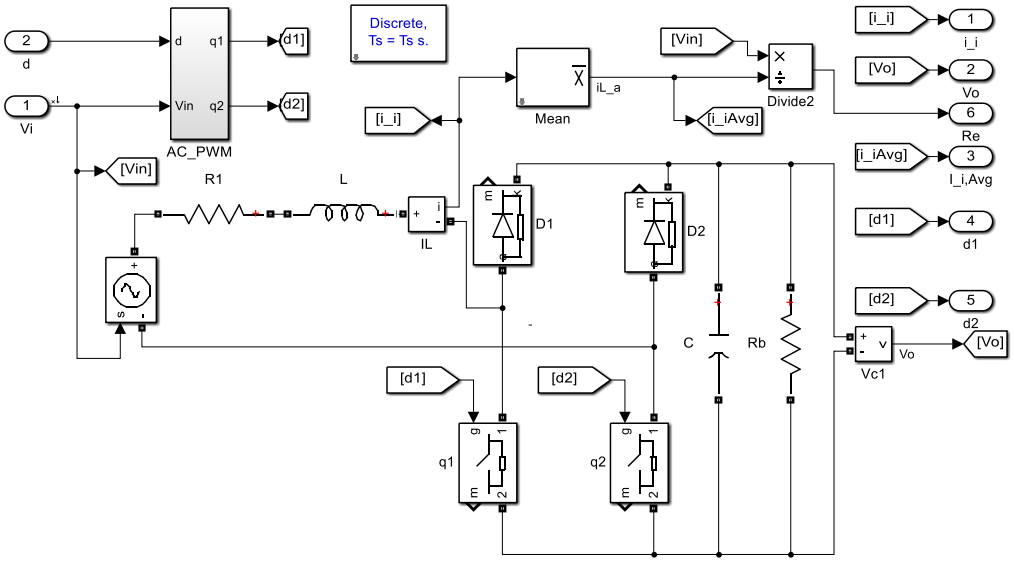

Figure 98. SBBC model.

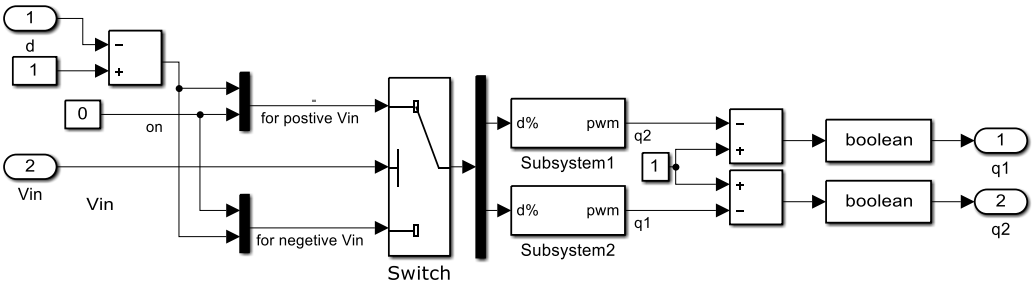

Figure 99. Pulse width generation for AC signal

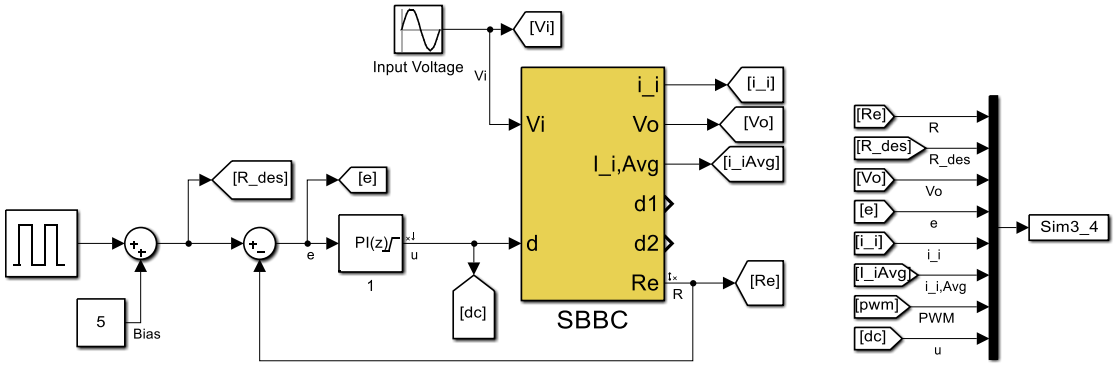

Figure 100. SBBC equivalent resistance control.

APPENDIX B

CHAPTER IV MATLAB/SIMULINK® FILES

B.1 Chapter IV Simulation Files

This section is dedicated to show the details for the regenerative controller simulation. The quarter-car subsystem is shown in Figure 102. The SBBC PowerSim model is the same used in chapter III, see Figure 98

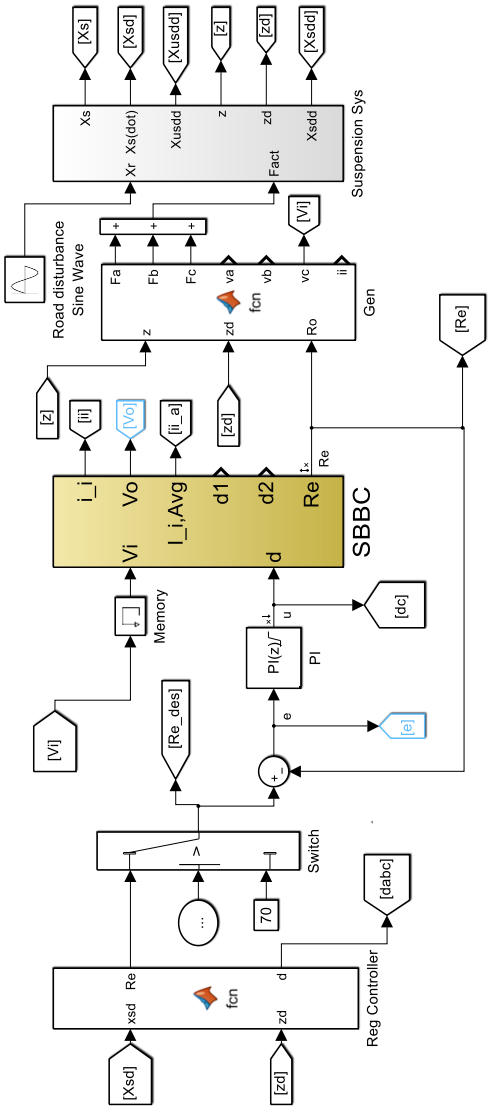

Figure 101. Simulation Regenerative suspension system control.

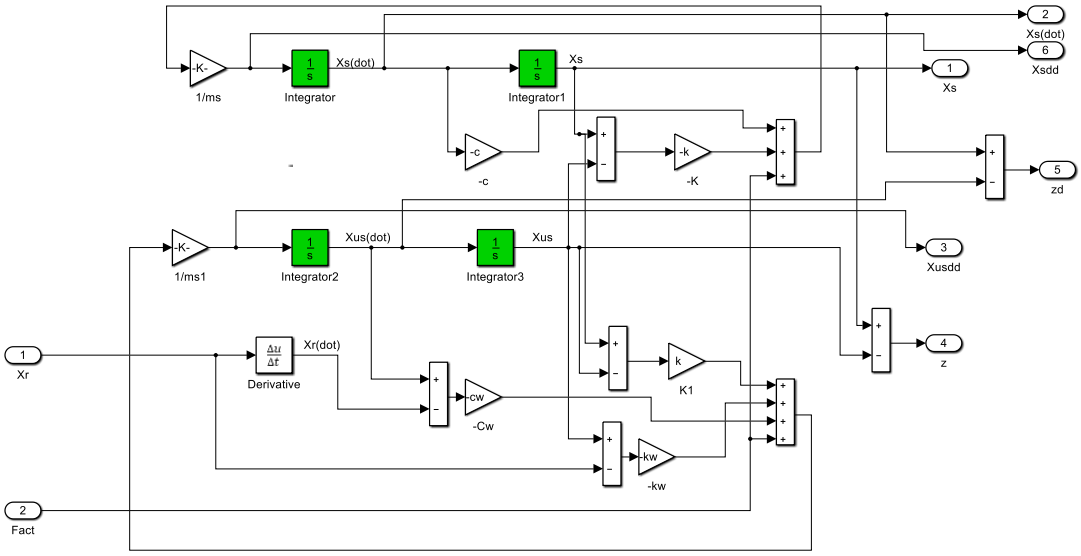

Figure 102. Quarter-car suspension system.

MATLAB code used to simulate the generator

```
function [Fa,Fb,Fc,va,vb,vc,Poa] = fcn(z,zd,Ro)
l=63.3/1000;  % pitch of the motor(m)
gama1=2*pi/l;  % mag of spatial wave # of 1st harmonic
 % back-emf constants
Ria=1.565;Rib=1.565;Ric=1.565; % internal resistance
ka=2;kb=2;kc=2;
% Induced Voltages
va=ka*sin(2*pi*z/l+2*pi/3).*zd;
vb=kb*sin(2*pi*z/l).*zd;
vc=kc*sin(2*pi*z/l-2*pi/3).*zd;
% Assume Steady state  No Effect for internal inductors
ia=va/(Ria+Ro);
ib=vb/(Rib+Ro);
ic=vc/(Ric+Ro);
Fa=-ka*sin(2*pi*z/l+2*pi/3).*ia;
Fb=-ka*sin(2*pi*z/l).*ib;
Fc=-ka*sin(2*pi*z/l-2*pi/3).*ic;
% Output Power Ro*i^2
Poa=ia^2*Ro;
```

Skyhook control law written as a MATLAB function (Refer to Figure 101.).

```
function Re    = fcn(xsd,zd)
if    xsd*zd>=0
      Re=0; d=1;
else  Re=50;d=0;
End
```

The MATLAB code used in chapter IV to plot and analyze all signals:

```
%% Reg Suspension Testing
%% Constants
clc;clear;close all
Ts=5e-5; % Sampling time; Sampling freq=20 KHz
Vi=0.8;
Li=0.0015;
Ri=1.565;
C=68e-6;
fpwm=1000; %PWM driving freq
Tpwm=1/fpwm;
RB=100;
% Suspension Constants
ms=2.299;
mus=2.278;
k=1521;
kw=15600;
c=70;
cw=50;
% Input data file from the test
%             [R_des   ii      ii_a    Vi   Vo
%               Xs     Xsd    Xsdd     z    zd
%              dabc   Xusdd    e      Rcon  dc];
%% Sim 3-phase With Conv
% this closed-loop reults from the Sim ch4
clc;clear;close all
[t,R_des,ii,ii_a,Vi,Vo,Xs,Xsd,Xsdd,z,zd,dabc,Xusdd,e,Rcon,dc]=trial('wi
thcon');
R_des(R_des>50)=50;
dabc(R_des>10)=0;dabc(R_des<10)=1;

%m=[R_des;ii;ii_a;Vi;Vo;Xs;Xsd;Xsdd;z,;zd;dabc;Xusdd;e;Rcon;dc];
m=[R_des,ii,ii_a,Vi,Vo,Xs,Xsd,Xsdd,z,zd,dabc,Xusdd,e,Rcon,dc];
m=m';
figure();myplot2(t,m(1,:),1,2,1,1);myplot2(t,m(2,:),2,2,1,2);
figure();myplot2(t,m(3,:),3,2,1,1);myplot2(t,m(4,:),4,2,1,2);
figure();myplot2(t,m(5,:),5,2,1,1);myplot2(t,m(6,:),6,2,1,2);
figure();myplot2(t,m(7,:),7,2,1,1);myplot2(t,m(8,:),8,2,1,2);
figure();myplot2(t,m(9,:),9,2,1,1);myplot2(t,m(10,:),10,2,1,2);
figure();myplot2(t,m(11,:),11,2,1,1);myplot2(t,m(12,:),12,2,1,2);
figure();myplot2(t,m(13,:),13,2,1,1);ylim([-5
5]);myplot2(t,m(14,:),14,2,1,2);ylim([-100 200])
figure();myplot2(t,m(15,:),15,2,1,1);


function
[t,R_des,ii,ii_a,Vi,Vo,Xs,Xsd,Xsdd,z,zd,dabc,Xusdd,e,Rcov,dc]=trial(fil
ename)
y=load(filename)
t=y.noconv.R_des.Time;
R_des=y.noconv.R_des.Data;
ii=y.noconv.ii.Data;
```

```
ii_a=y.noconv.ii_a.Data;
Vi=y.noconv.Vi.Data;
Vo=10*y.noconv.Vo.Data;
Xs=y.noconv.Xs.Data;
Xsd=y.noconv.Xsd.Data;
Xsdd=y.noconv.Xsdd.Data;
z=y.noconv.z.Data;
zd=y.noconv.zd.Data;
dabc=y.noconv.dabc.Data;
Xusdd=y.noconv.Xusdd.Data;
e=y.noconv.e.Data;
Rcov=y.noconv.Rcov.Data;
dc=y.noconv.dc.Data;
end


function [y]=myplot(t,x1,s,r,c,n)
 if isempty(r);r = 1;end
 if isempty(c);c = 1;end
 if isempty(n);n = 1;end

cR_des= {'','time[s]','R_{des}',''};
cii= {'','time[s]','i_i','Generators Current (i)'};
cii_a= {'','time[s]','i_ia','Generators Avg. Current (i)'};
cVi= {'','time[s]','V_i',''};
cVo= {'','time[s]','Vo[v]','Output Voltage[V]'};
cXs= {'','time[s]','Sprung mass disp.(m)','Sprung mass disp.(m)'};
cXsd= {'','time[s]','Sprung mass Vel.(m/s)','Sprung mass Vel.(m/s)'};
cXsdd= {'','time[s]','Sprung mass Acc.(m/s^2)','Sprung mass
Acc.(m/s^2)'};
cz= {'','time[s]','Relative Disp.(m)','Relative Disp.(m)'};
czd= ;
cdabc= {'','time[s]','d_abc',''};
cXusdd= {'','time[s]','Unsprung mass Acc.(m/s^2)',''};
ce= {'','time[s]','e',''};
cRcon= {'','time[s]','R_{con}',''};
cdc= {'Duty-ratio','time[s]','d_c',''};

InVec=[cR_des;cii;cii_a;cVi;cVo;cXs;cXsd;cXsdd;cz;czd;cdabc;cXusdd;ce;
cRcon;cdc];
w=InVec(s,:);

subplot(r,c,n);
y=plot(t,x1,'LineWidth',1);xlabel(w{2});grid
on;set(gca,'FontSize',14);title(w{1});
    ylim('Auto');;ylabel(w{3});
     xlim('Auto')
    legend(w{4},'Location','northeast')

end
```

B.2 Chapter IV Experiments Files

This section is dedicated to show the details for implementing the regenerative controller in the experiment. Details of the subsystem and is also shown in Figures 104, 105 and 106.

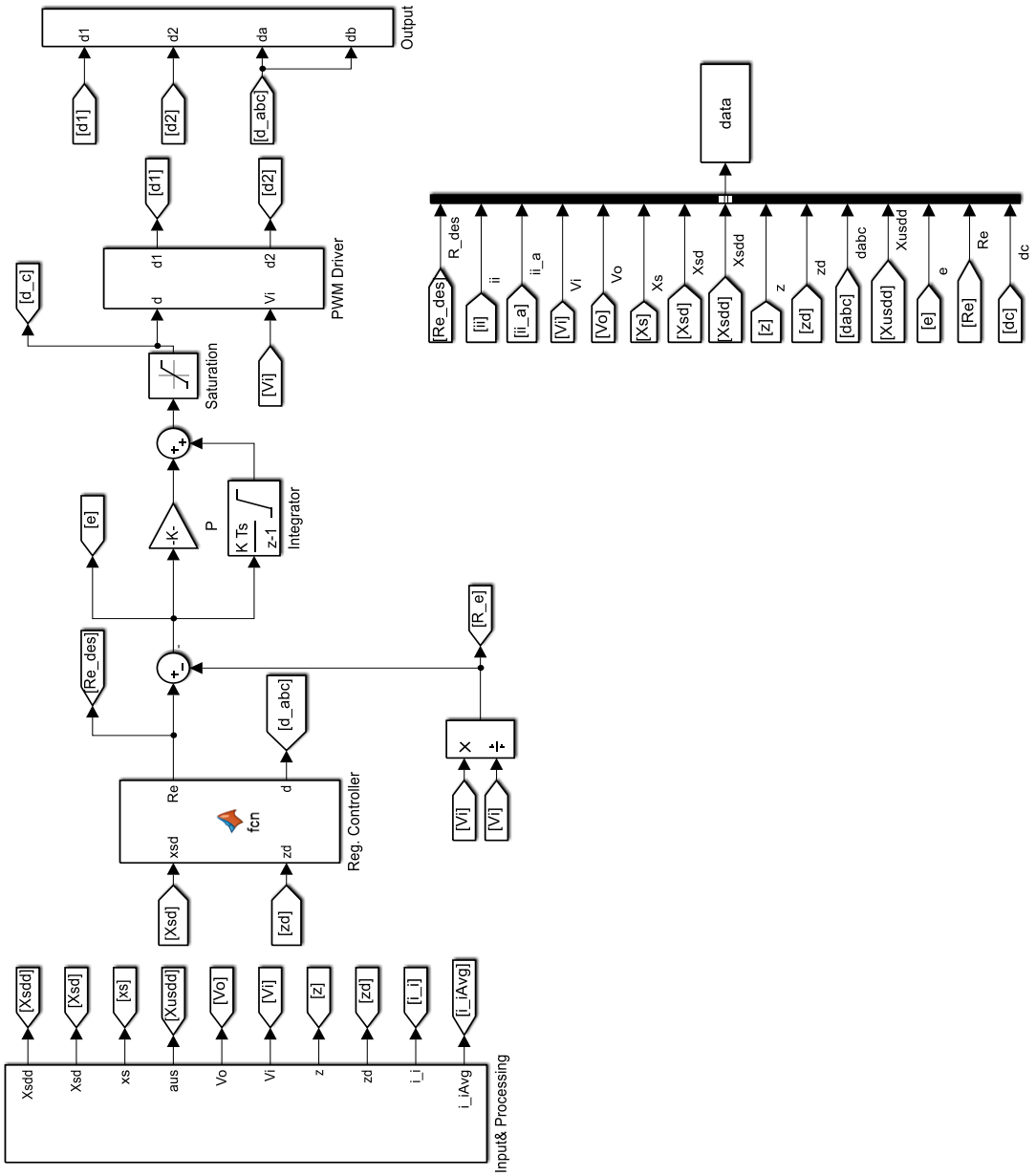

Figure 103. Experiment regenerative control of suspension system.

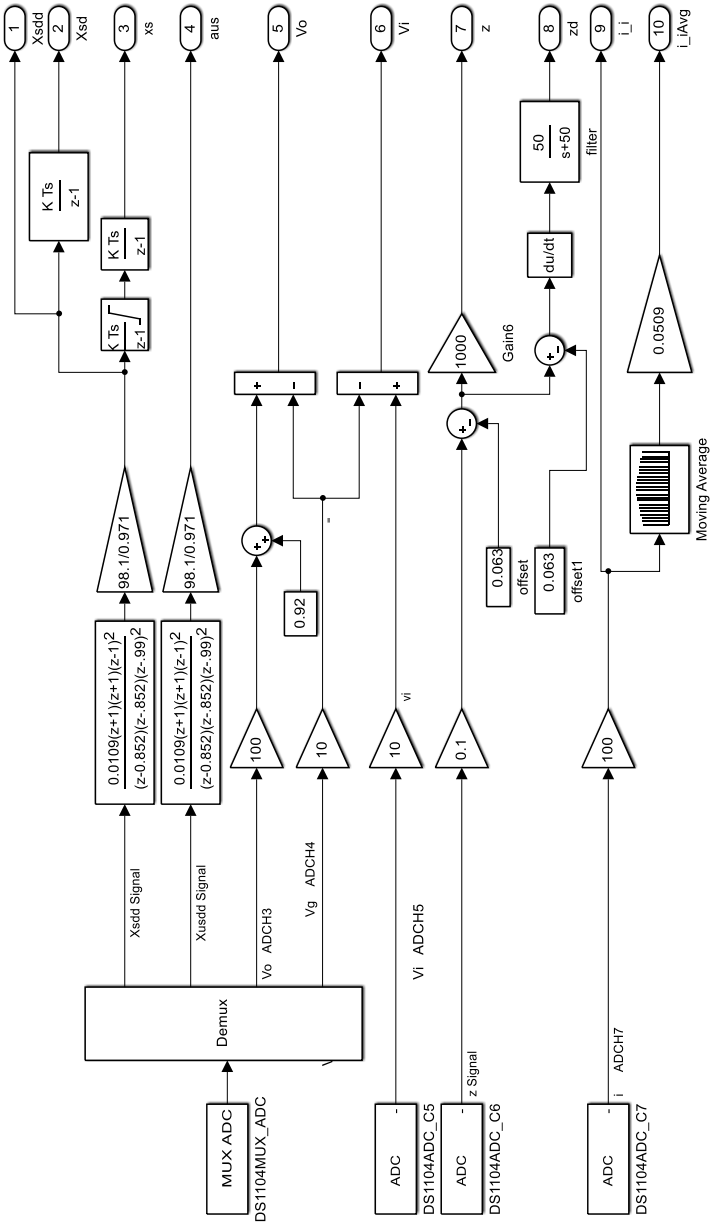

Figure 104. Reading and filtering sensors signals

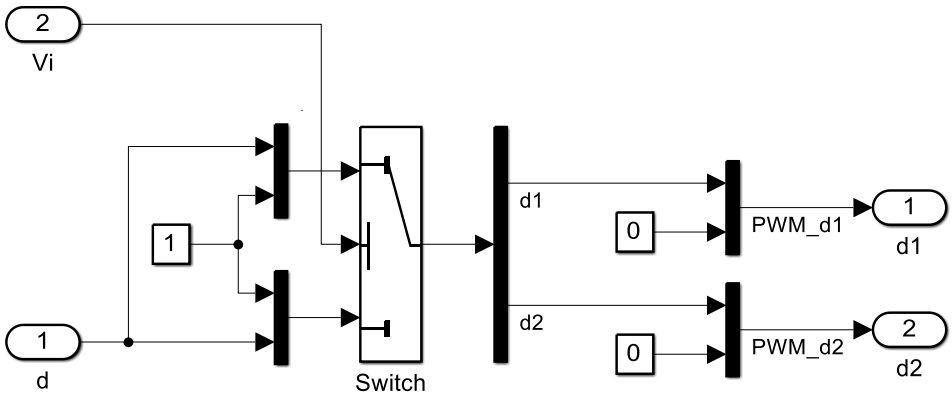

Figure 105. PWM generation

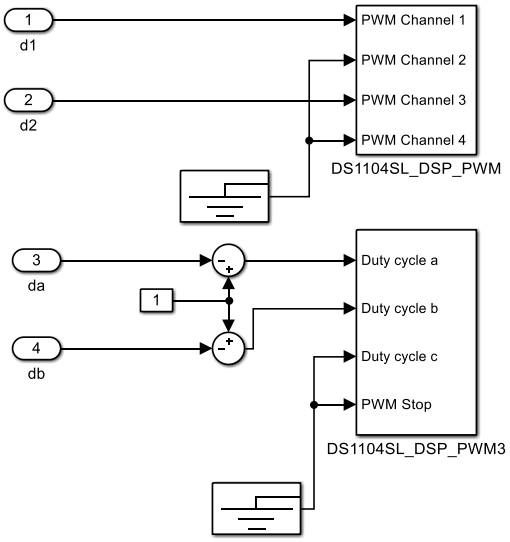

Figure 106. Sending PWM signals to dSPACE hardware.